UNIVERSIDADE D
COIMBRA

Inês Ramos Rego

The role of the mitochondrial chaperone TRAP1 in the retinal pigment epithelium

Dissertação no âmbito do Mestrado em Biologia Celular e Molecular orientada pelo Doutor Celso Henrique Freitas Alves e pelo Professor Doutor Paulo Fernando Martins dos Santos e apresentada ao Departamento de Ciências da Vida da Faculdade de Ciências e Tecnologia da Universidade de Coimbra.

Julho de 2023

UNIVERSIDADE D
COIMBRA

Inês Ramos Rego

THE ROLE OF THE MITOCHONDRIAL CHAPERONE TRAP1 IN THE RETINAL PIGMENT EPITHELIUM

Dissertação no âmbito do Mestrado em Biologia Celular e Molecular orientada pelo Doutor Celso Henrique Freitas Alves e pelo Professor Doutor Paulo Fernando Martins dos Santos e apresentada ao Departamento de Ciências da Vida da Faculdade de Ciências e Tecnologia da Universidade de Coimbra.

Julho de 2023

This research was funded by National Funds via Fundação para a Ciência e Tecnologia (FCT), through the Strategic Project UIDB/04539/2020, Strategic Project UIDP/04539/2020 (CIBB), CEECIND/00886/2017, CEECIND/00041/2022 and Centro 2020 Regional Operational Programme (CENTRO-01-0145-FEDER-000008: BrainHealth 2020). The funding sources had not been involved in the research activities and in the preparation of this Master Thesis.

A todos a quem amo…

"Para ser grande, sê inteiro: nada
Teu exagera ou exclui.
Sê todo em cada coisa. Põe quanto és
No mínimo que fazes.
Assim em cada lago a lua toda
Brilha, porque alta vive."

In Odes de Ricardo Reis, Fernando Pessoa
Lisboa, Ed. Ática, 1946

Agradecimentos

Ao terminar mais uma etapa em que cresci imenso a nível profissional e, sobretudo, pessoal, não poderia deixar de agradecer a todos os que me acompanharam nesta caminhada.

Começo por agradecer ao Doutor Henrique Alves pela orientação desta dissertação. Agradeço todo o empenho, disponibilidade e por alargar imenso os meus horizontes ao possibilitar um enriquecedor estágio laboratorial nos Países Baixos. Agradeço especialmente por estimular o meu pensamento crítico, a minha resiliência enquanto cientista e por me dar a possibilidade de realizar trabalho de forma independente.

Agradeço ao Professor Doutor Paulo Santos pela disponibilidade em ser coorientador desta tese e pelos valiosos conselhos e sugestões quanto à parte experimental e escrita deste trabalho.

Agradeço ao Professor Doutor Francisco Ambrósio, investigador principal do Grupo *Retinal Dysfunction and Neuroinflammation Lab* por me ter recebido no seu Laboratório, proporcionando todas as condições necessárias para o desenvolvimento deste projeto. Agradeço também toda a disponibilidade, compreensão e a confiança para participar na implementação de novas técnicas e para integrar projetos do seu Grupo de Investigação.

Agradeço também a todos os restantes investigadores que participaram no projeto de estudo da proteína TRAP1 e que colaboraram em algumas das técnicas experimentais. Agradeço ao Doutor Paulo Oliveira, ao Doutor José Teixeira, ao Doutor Hugo Fernandes, à Mestre Sandra Mimoso Pinhanços, à Doutora Rosa Fernandes, à Doutora Mónica Zuzarte, à Mestre Beatriz Neves, aos membros do laboratório do Doutor Peter Quinn e do Doutor Stephen Tsang e às alunas Daniela Silvério, Maria Isabel Eufrásio, Ângela Soares e Beatriz Cruz.

Agradeço a todos os membros do *Retinal Dysfunction and Neuroinflammation Lab* pelo apoio, orientação e pela disposição em partilharem os vossos conhecimentos.

Um agradecimento especial às minhas colegas Ângela Soares e Rita Pais. Muito obrigada por todas as nossas conversas, por todos os bons momentos partilhados, pela boa disposição, pelas gargalhadas, pela criatividade musical e pelo apoio nos momentos mais difíceis.

Um agradecimento muito especial à Doutora Elisa Campos pela amizade, apoio, carinho, preocupação e partilha de conhecimento a todos os níveis.

Muito obrigada à Sara Oliveira por toda a ajuda, pela confiança e pelo ombro amigo em todos os momentos.

Agradeço aos meus colegas de Mestrado em Biologia Celular e Molecular, Marta Silva e Tiago Torres, por todas as conversas, desabafos, pelo apoio e pela força nas épocas difíceis em que as aulas e os trabalhos pareciam não ter fim.

Agradeço imenso à minha querida Carolina Santos, por todo o amor, pelo carinho, pela amizade, pela força e motivação.

Um grande agradecimento à Mafalda Penetra, por todo o apoio ao longo de todos estes anos, pela amizade, pela força, pelas longas conversas e desabafos, pelos inúmeros lanches e passeios.

Agradeço imenso à minha amiga Raquel Nossa, por todo o carinho, pela amizade, pelas conversas, pela motivação e por tornar a Figueira da Foz ainda mais bonita. Não é uma amizade desde sempre, mas é para sempre.

Agradeço imenso à Família Serrano, os meus grandes amigos. Agradeço à Isabel e ao Joaquim Serrano toda a amizade, apoio, carinho e encorajamento desde sempre. Agradeço ao Simão Serrano e à Rosa Carvalho por todo o amor, carinho e pelo ombro amigo. Agradeço à fofinha Lia Serrano por tornar os nossos dias mais bonitos com o seu sorriso. Muito obrigada por serem família de coração.

Agradeço agora às pessoas mais importantes da minha vida, que me amam incondicionalmente e que me apoiam sempre em todos os capítulos da minha vida. Ao vosso lado todos os sonhos são possíveis! Um enorme e muito especial agradecimento aos meus Pais, os magníficos Sofia e Francisco Rego. Obrigada por estarem sempre presentes, pelo carinho, pelo apoio e amor incondicional e por me terem transmitido os valores que me permitem ser a pessoa que sou hoje. Agradeço imenso à minha querida Mãe pelo amor, pelos ensinamentos, pelas longas conversas, pela força, pelo apoio, pela motivação e por nunca deixar de acreditar em mim e nas minhas capacidades. Muito obrigada ao meu querido Pai pelo amor, pela orientação, pelo carinho, pelo incentivo e pela paciência em aceitar que nunca me vou levantar à hora que o despertador toca. Agradeço aos meus Pais, sobretudo, por me ensinarem a valorizar o que é mais importante na vida.

Agradeço ao meu querido Avô Manuel Ramos Catarino (*in memoriam*) por todo o carinho e pelo amor incondicional. Sei que tinhas muito orgulho em mim e que te faria muito feliz celebrares mais uma conquista do teu cordeirinho. Agradeço à minha querida Avó Maria Adélia Toscano por todo o apoio, amor, carinho e por patrocinar pastéis de nata e outros lanches saudáveis sempre que a jornada académica se torna mais difícil.

Agradeço ao meu querido Avô António Rego pelo carinho, apoio, compreensão, por nunca deixar de acreditar nas minhas capacidades e por acompanhar sempre as novidades tecnológicas. Agradeço à minha querida Avó Fátima Varandas (*in memoriam*) pelo carinho e amor, sei que terias muito orgulho na pessoa em que me tornei. Agradeço à minha querida Tia Carla Rego pelo carinho, pela dedicação e pelo amor demonstrado ao longo de toda esta minha jornada.

Muito obrigada a todos os que, de alguma forma, fizeram parte desta linda etapa de aprendizagem em Coimbra e que me acompanharam nesta caminhada. Que venham novos projetos e se abram novos horizontes.

Querida Família e Amigos, a todos vós dedico este trabalho, tornando-o nosso.

Inês Ramos Rego

Statement of Originality

This Master Thesis includes adapted material from a review and an experimental original article, in which I am the first author, that have been previously published in a peer reviewed journal and are referred below:

> **Ramos Rego, Inês *et al.*** "TRAP1 in Oxidative Stress and Neurodegeneration." *Antioxidants* vol. 10, 1829. Published 19 Nov. 2021.
>
> **Ramos Rego, Inês *et al.*** "TRAP1 Is Expressed in Human Retinal Pigment Epithelial Cells and Is Required to Maintain their Energetic Status." *Antioxidants* vol. 12, 381. Published 4 Feb. 2023.

It is also important to refer that, except for the data represented in the "Figure 6. TRAP1 is expressed in human RPE cells" (page 53), all the experimental data presented in this thesis was obtained during the School Year 2022/2023 within the scope of the subject "Dissertation in Biomedicine" from the Master Programme in Cellular and Molecular Biology. Moreover, both the text and the figures contained in this thesis were modified, completed, adapted, and updated after the publication of the articles, at the time of writing this thesis, to avoid any plagiarism issues. Additionally, the last part of the Results section is not published or submitted, and it is reported for the first time in this dissertation.

I certify that the intellectual content of this thesis (conceptualization, methodology, experimental design, investigation, data analysis and interpretation) is product of my own work, performed by me during my registration as graduate student in the Master Programme in Cellular and Molecular Biology at the Faculty of Sciences and Technology of the University of Coimbra. Furthermore, all assistance received in preparing this thesis, resources and funding have been acknowledged. I declare that, to the best of my knowledge, my thesis does not infringe upon anyone's copyright nor violate any proprietary rights and that any material from the work of other people included in my thesis is fully acknowledged in accordance with the standard referencing practices.

I declare that this is a true copy of my thesis, as approved by my supervisors, and that this thesis has not been submitted to any other University or Institution.

Inês Ramos Rego

Index

Abstract

Age-related macular degeneration (AMD) is the leading cause of severe vision loss and blindness in elderly people worldwide. Vision loss caused by advanced stages of AMD has profound human and socioeconomic consequences in all societies. This degenerative disease affects the central macula (fovea) compromising central visual acuity in advanced stages, which impairs one's ability to drive, read and recognize faces. The oxidative stress-induced damage of the retinal pigment epithelium (RPE) is thought to play a key role in the onset and progression of AMD. The hallmarks of the early stages of AMD are the accumulation of macular drusen and pigmentary abnormalities. Progression to late AMD is characterized by the loss of both RPE and photoreceptor cells and abnormal proliferation of choroidal capillaries. The RPE is a monolayer of polarized and pigmented cells located between the photoreceptor cells and the choroid and plays an important role in the maintenance of the retinal homeostasis, and protection against oxidative stress, being suggested as a critical site of AMD pathology. Retinal pigment epithelial cells are particularly susceptible to oxidative stress due to exposure to intense focal light, high metabolic activity, unique phagocytic function, large oxygen gradient from the choroid, and accumulation of oxidized lipoproteins with aging. Since oxidative stress-induced RPE damage results from the excessive accumulation of reactive oxygen species (ROS), produced mainly in mitochondria, mitochondrial function homeostasis is critical for maintaining ROS at physiological levels.

Tumour necrosis factor receptor-associated protein 1 (TRAP1), also known as heat shock protein 75 (HSP75), is a mitochondrial molecular chaperone that supports protein folding and contributes to the maintenance of mitochondrial integrity even under cellular stress. TRAP1 protects against mitophagy, mitochondrial apoptosis and dysfunction by decreasing the production and accumulation of ROS, thus, reducing oxidative stress. Previous studies also determined that downregulation of TRAP1 expression impacts cellular function, resulting in lower mitochondrial membrane potential, increased intracellular ROS production and increased cell death.

In the context of AMD, oxidative stress-induced damage to the RPE occurs due to the excessive accumulation of ROS, primarily produced in mitochondria under pathological conditions. Maintaining mitochondrial function homeostasis is crucial for keeping ROS at physiological levels and preventing the metabolic dysfunction observed in AMD pathology. Therefore, it is important to investigate proteins that are not yet related as being involved in oxidative stress mechanisms within the RPE in the context of AMD.

Considering the functions of TRAP1 described in other cell types, we propose that TRAP1 modulates mitochondrial metabolism in the RPE and plays a role in preventing the onset and progression of AMD. We hypothesize that TRAP1 can mediate protection against oxidative stress in the RPE and therefore be a potential treatment target for AMD.

The objective of this study was to assess the presence and function of TRAP1 in the human RPE and investigate whether TRAP1 provides protection against oxidative stress in RPE cells. To test our hypothesis, we aimed to study the cellular functions of TRAP1 in the RPE, using the Human Adult Retinal Pigment Epithelial-19 (ARPE-19) cell line as *in vitro* model. We also aimed to optimize and implement an experimental protocol for the differentiation of RPE cells from human induced pluripotent stem cells (iRPE) to access the presence of TRAP1. Using the ARPE-19 cell line, we evaluated the effect of *TRAP1* ablation on cell viability, cell proliferation, cell mass and protein content. Then, we assessed the impact of TRAP1 loss on intracellular ROS production and superoxide anion production. Mitochondrial morphology and network were also analyzed. Moreover, the effect of *TRAP1* silencing on mitochondrial respiration was determined. Finally, we have evaluated the impact of *TRAP1* ablation in the localization and levels of TRAP1 upon hydrogen peroxide-induced oxidative stress.

Our findings reveal that TRAP1 is expressed in human adult RPE cells and primarily localized in the mitochondria. Additionally, silencing TRAP1 expression increased ROS production in human RPE cells and led to a quiescent metabolic state. The successful establishment of the iRPE model will also allow to perform key experiments in the future, using a more complex human RPE *in vitro* model, that better replicates the characteristics of primary RPE. These results provide valuable insights into the development of new therapeutical strategies for AMD.

Keywords: Age-related macular degeneration (AMD); Mitochondria; Oxidative stress; Retinal pigment epithelium (RPE); Tumor necrosis factor receptor-associated protein 1 (TRAP1).

Resumo

A degenerescência macular da idade (DMI) é a principal causa de perda severa de visão e de cegueira em pessoas idosas em todo o mundo. A perda de visão nas fases avançadas da DMI tem consequências profundas a nível humano e socioeconómico. Esta doença degenerativa afeta a parte central da mácula (fóvea) comprometendo a acuidade visual central em fases avançadas, impedindo os indivíduos de realizar tarefas do quotidiano, como conduzir, ler e reconhecer rostos. O dano no epitélio pigmentado da retina (RPE) induzido por *stress* oxidativo desempenha um papel fulcral no desenvolvimento da DMI. Nas fases iniciais, a DMI causa a acumulação de lipoproteínas oxidadas e anomalias a nível dos pigmentos. A progressão para a DMI avançada é caracterizada pela morte das células do RPE e dos fotorreceptores, além da proliferação anormal de capilares da coróide. O RPE é uma camada única de células polarizadas e pigmentadas localizada entre os fotorreceptores e a coróide e desempenha um papel importante na manutenção da homeostasia da retina e na proteção contra o *stress* oxidativo, sendo sugerido como um local crítico da patologia da DMI. As células do RPE são particularmente suscetíveis ao *stress* oxidativo devido à elevada exposição à luz, alta atividade metabólica, função fagocítica, exposição a elevado gradiente de oxigénio e acumulação de lipoproteínas oxidadas. Visto que o dano do RPE induzido pelo *stress* oxidativo resulta da acumulação excessiva de espécies reativas de oxigénio (ROS), produzidas principalmente na mitocôndria, a homeostasia da função mitocondrial é fundamental para manter as ROS em níveis fisiológicos.

A proteína 1 associada ao recetor do fator de necrose tumoral (TRAP1), também conhecida como proteína de choque térmico 75 (HSP75), é um *chaperone* molecular mitocondrial que contribui para a manutenção da integridade mitocondrial, através do seu efeito antioxidante. A TRAP1 inibe a mitofagia, apoptose e disfunção mitocondrial, diminuindo a produção e acumulação de ROS e, consequentemente, reduzindo o *stress* oxidativo. Estudos reportados na literatura também determinaram que a redução da expressão de TRAP1 afeta a função celular, resultando numa redução do potencial de membrana mitocondrial, aumento da produção intracelular de ROS e aumento da morte celular.

No contexto da DMI, o dano do RPE induzido por *stress* oxidativo ocorre devido à acumulação excessiva de ROS, produzidas principalmente na mitocôndria em condições patológicas. Assim, manter a homeostasia da função mitocondrial é crucial para manter as ROS em níveis fisiológicos e prevenir a disfunção metabólica observada na patologia da DMI. Portanto, é importante investigar proteínas que ainda não foram relacionadas como estando envolvidas em mecanismos de *stress* oxidativo no RPE no contexto da DMI.

Considerando as funções da TRAP1 descritas em outros tipos de células, propomos que a TRAP1 é capaz de modular o metabolismo mitocondrial no RPE, desempenhando um papel importante na prevenção da progressão da DMI. A nossa hipótese é que a TRAP1 tem uma função protetora contra o *stress* oxidativo no RPE e, portanto, pode ser um potencial alvo terapêutico para a DMI.

O presente estudo pretendeu avaliar a presença e função da TRAP1 no RPE humano e investigar se a TRAP1 confere proteção contra o *stress* oxidativo em células do RPE. Para testar a nossa hipótese, estudámos as funções celulares da TRAP1 no RPE, utilizando uma linha celular de epitélio pigmentado de retina humana adulta (ARPE-19) como modelo *in vitro*. Também otimizámos e implementámos um protocolo experimental para a diferenciação de células do RPE a partir de células estaminais pluripotentes induzidas humanas (iRPE) para verificar a presença de TRAP1. Utilizando a linha celular ARPE-19, avaliámos o efeito da redução de TRAP1 na viabilidade celular, proliferação celular, massa celular e conteúdo proteico. Em seguida, avaliámos o impacto da perda de TRAP1 na produção intracelular de ROS e de aniões superóxido. A morfologia e a rede mitocondrial também foram analisadas. Além disso, determinámos o efeito do silenciamento de TRAP1 na respiração mitocondrial. Por fim, avaliámos o impacto da redução de TRAP1 na localização e nos níveis de TRAP1 após a indução de *stress* oxidativo através de peróxido de hidrogénio.

Neste estudo demonstramos que a TRAP1 é expressa nas células do RPE humano, estando localizada principalmente na mitocôndria. Além disso, o silenciamento da expressão de TRAP1 aumentou a produção de ROS em células do RPE humano e conduziu a um estado metabólico quiescente. O sucesso na implementação do modelo iRPE também permitirá a realização de experiências importantes no futuro, utilizando um modelo *in vitro* mais complexo e que replique melhor as características das células primárias do RPE humano. Em suma, os nossos resultados fornecem informações valiosas para o desenvolvimento de novas estratégias terapêuticas para a DMI.

Palavras-chave: Degenerescência macular da idade (DMI); Epitélio pigmentado da retina (RPE); Mitocôndria; Proteína 1 associada ao recetor do fator de necrose tumoral (TRAP1); *Stress* oxidativo.

Abbreviations

A2E - Bis-retinoid N-retinyl-N-retinylidene ethanolamine

AMD - Age-related Macular Degeneration

ARPE-19 - Adult Retinal Pigment Epithelial-19

ATP - Adenosine Triphosphate

BER - Base Excision Repair

C3 - Complement Component 3

cDNA - Complementary Deoxyribonucleic Acid

CFH - Complement Factor H

CFI - Complement Factor I

CO_2 - Carbon Dioxide

CRALBP - Cellular Cetinaldehyde-binding Protein

CRC - Colorectal Cancer

CRISPR/Cas9 - Clustered Regularly Interspaced Short Palindromic Repeats/Cas9 Protein

c-Src - Proto-oncogene Tyrosine-protein Kinase

CTD - C-terminal Domain

CTM - Chetomin

CypD - Cyclophilin D

CytC - Cytochrome C

dd - Differentiation Day

DHE - Dihydroethidium

DMEM - Dulbecco's Modified Eagle Medium

DMSO - Dimethyl Sulfoxide

DNA - Deoxyribonucleic Acid

Drp1 - Dynamin-related protein 1

ECAR - Extracellular Acidification Rate

ERK1/2 - Extracellular Signal-regulated Protein Kinases 1 and 2

ETC - Electron Transport Chain

FBS - Fetal Bovine Serum

FCCP - Carbonyl Cyanide p-trifluoro-methoxyphenyl Hydrazone

GRP94 - Glucose-regulated Protein 94

GzmM - Granzyme M

H_2O_2 - Hydrogen Peroxide

HBSS - Hank's Balanced Salt Solution

HIF1α - Hypoxia-inducible Factor 1α

hiPSC - Human Induced Pluripotent Stem Cells

HSP27 - Heat Shock Protein 27

HSP75 - Heat Shock Protein 75

HSP90 - Heat Shock Protein 90

HtpG - High Temperature Protein G

iRPE - Human Induced Pluripotent Stem cell-derived retinal pigment epithelium

iRPE-AMD - Human Induced Pluripotent Stem cell-derived RPE from AMD donors

K_m - Michaelis Constant

MAP1LC3 - Microtubule-associated Protein 1A/1B-light chain 3

MD - Middle Domain

MEF – Mouse Embryonic Fibroblasts

Mff - Mitochondrial Fission Factor

MFI - Mean Fluorescence Intensity

Mfn1/2 - Mitofusin 1/2

MiD51 - Mitochondrial Dynamics of 51 kDa Protein

MIEF1- Mitochondrial Elongation Factor 1

mPTP - Mitochondrial Permeability Transition Pore

mRNA - Messenger Ribonucleic Acid

mtDNA - Human Mitochondrial Deoxyribonucleic Acid

mtHsp70 - Mitochondrial Heat Shock Protein 70

mtUPR - Mitochondrial Unfolded Protein Response

NADPH - Nicotinamide Adenine Dinucleotide Phosphate

NEEA - Nonessential Amino Acids

NIC - Nicotinamide

NTD - N-terminal Domain

OCR - Oxygen Consumption Rate

OPA - Optic Atrophy Protein

OXPHOS - Oxidative Phosphorylation

PBS - Phosphate-buffered Saline

PCR - Polymerase Chain Reaction

PFA - Paraformaldehyde

PGC-1α - Peroxisome proliferator-activated receptor-gamma coactivator-1α

PINK1 - PTEN Induced Kinase 1

POS - Photoreceptor Outer Segments

PQ - Paraquat

PQC - Protein Quality Control

PTM - Post-translational Modifications

PVDF - Polyvinylidene Difluoride

RIPA - Radioimmunoprecipitation

RNA - Ribonucleic Acid

ROS - Reactive Oxygen Species

RPE - Retinal Pigment Epithelium

RPE DM - Retinal Pigment Epithelium Differentiation Medium

RPE65 - Retinal Pigment Epithelium-specific Protein of 65 kDa

rRNA - Ribossomal Ribonucleic Acid

SAM50 - Sorting and Assembly Machinery Protein-50

SDH - Succinate Dehydrogenase

SDS-PAGE - Sodium Dodecyl Sulfate-Polyacrylamide Gel Electrophoresis

SEM - Standard Error of the Mean

shRNA - Short Hairpin Ribonucleic Acid

shTRAP1 - Short Hairpin Ribonucleic Acid Specific for TRAP1

siCTL - Scramble Control Small Interfering Ribonucleic Acid

siRNA - Small Interfering Ribonucleic Acid

siTRAP1 - Small Interfering Ribonucleic Acid Specific for TRAP1

SOD - Superoxide Dismutase

SRB - Sulforhodamine B

TBST - Tris Buffered Saline with 0.1% Tween 20

TCA - Tricarboxylic Acid

TEM - Transmission Electron Microscopy

TMRM - Tetramethylrhodamine Methyl Ester

TNF-α - Tumour Necrosis Factor-α

TRAP1 - Tumour Necrosis Factor Receptor-associated Protein 1

tRNA - Transfer Ribonucleic Acid

UQCRC2 - Ubiquinol-cytochrome-c Reductase Complex Core Protein 2

VEGF - Vascular Endothelial Growth Factor

WT - Wild-type

ZO-1 - Zonula Occludens-1

ΔΨm - Mitochondrial Membrane Potential

List of Figures

1. Introduction

1. Introduction

1.1. Age-related Macular Degeneration

Age-related macular degeneration (AMD) is the leading cause of severe vision loss and blindness in elderly people worldwide, affecting over 30 million people (Deng et al., 2021). Vision loss caused by advanced stages of AMD has profound human and socioeconomic consequences in all societies (Guymer & Campbell, 2023).

The hallmarks of the early stages of AMD are pigmentary abnormalities and the accumulation of macular drusen, yellowish deposits mainly composed of lipofuscin, proteins, and lipids (Algvere et al., 2016). According to the basic clinical classification, early AMD is defined by the presence of medium-sized drusen (63-125 μm) **(Fig. 1)** while intermediate AMD is defined by the presence of extensive medium drusen or at least one large druse (>125 μm), and retinal pigmentary changes (hyperpigmentation or hypopigmentation) in the macular region (Mitchell et al., 2018). The presence of intermediate and large drusen often indicates a higher risk of developing advanced stages of AMD. Progression to late AMD can have different clinical manifestations **(Fig. 1)**. Geographic Atrophic AMD (dry AMD/non-exudative AMD) is characterized by degeneration and loss of both retinal pigment epithelium (RPE) and photoreceptor cells (Holz et al., 2014; Datta et al., 2017; Fleckeinstein et al., 2018) **(Fig. 1C)**. This degeneration might also involve the choroid and the Bruch´s membrane (Holz et al., 2014). Neovascular AMD (wet AMD/exudative AMD) is characterized by the abnormal proliferation of choroidal capillaries (Algvere et al., 2016; Mitchell et al., 2018) **(Fig. 1D)**. In this advanced form of the disease, the abnormal growth of blood vessels under the retina often leads to fluid leakage and/or hemorrhage into the intraretinal, subretinal or sub-RPE space (Santarelli et al., 2015) **(Fig. 1D)**. Stress or damage in the RPE and the associated immune responses are believed to promote the production of pro-angiogenic factors, such as vascular endothelial growth factor (VEGF), thereby driving choroidal neovascularization (Ambati et al., 2012). Abnormal neovascularization can also result in fibrotic scar formation, destroying the architecture of the overlying RPE and outer retina, resulting in permanent central vision loss (Ambati et al., 2012).

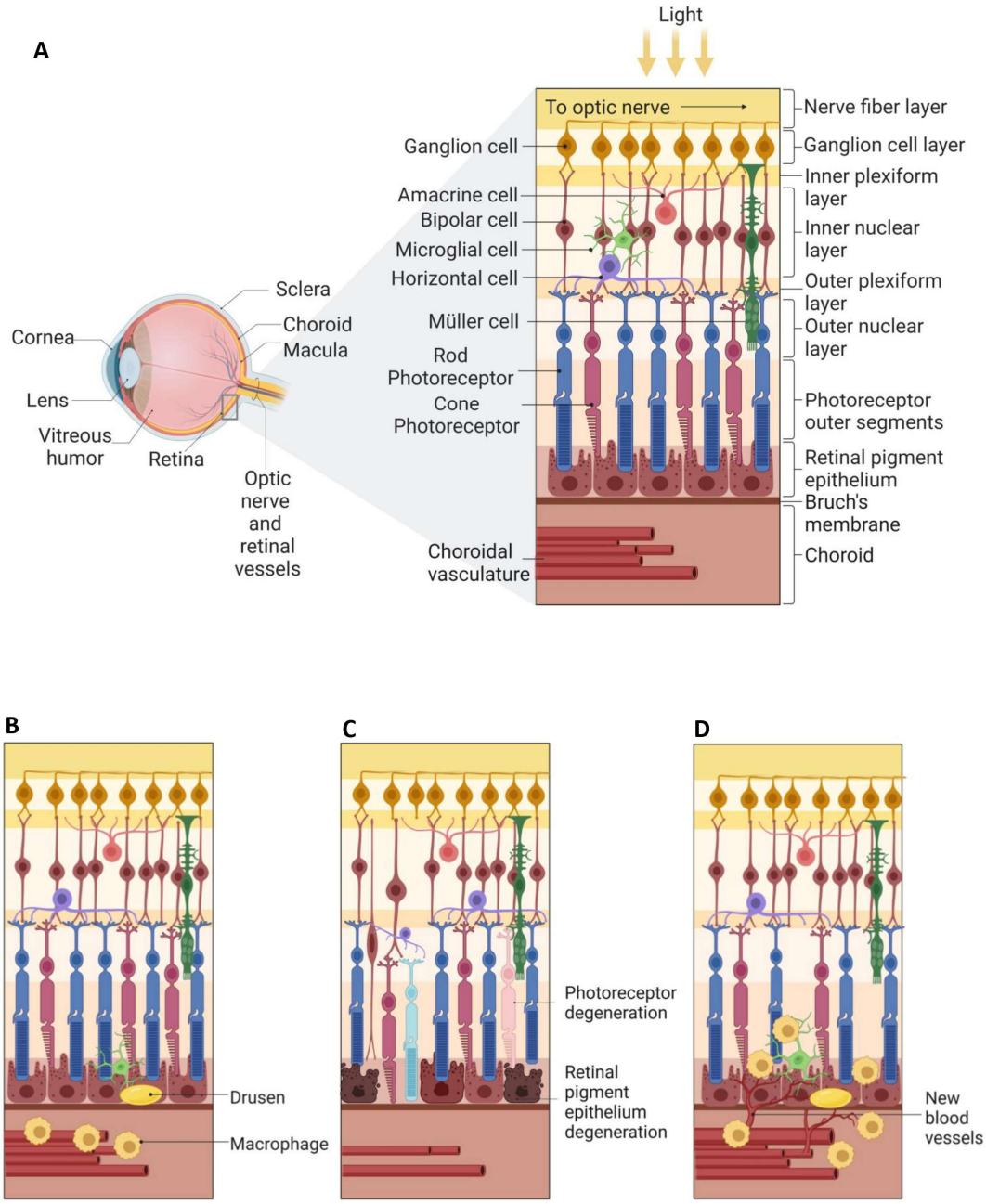

Figure 1. Retinal anatomy in health and disease. (A) A cross-section of the human eye shows the localization of some of the eye components, namely, the cornea, sclera, choroid, lens, vitreous humor, retinal vessels, optic nerve, macula and retina. A cross-section of the retina shows that the retinal anatomy is composed of several layers. Normal retinal architecture comprises (from anterior to posterior) retinal ganglion cells, resident retinal microglia, bipolar cells, horizontal cells, Müller glial cells, photoreceptors, the retinal pigment epithelium (RPE), the Bruch´s membrane and a choroidal vascular network **(B)** Early or intermediate stages of age-related macular degeneration (AMD) are associated with the accumulation of subretinal drusen and microglia and of choroidal macrophages, accompanied by a thickened Bruch membrane. **(C)** Progression to advanced forms of atrophic AMD is characterized by confluent regions of

RPE and photoreceptor degeneration as well as constriction of choroidal blood vessels. **(D)** Progression to late neovascular AMD is characterized by the invasion of abnormal, leaky choroidal blood vessels and accompanying macrophages into the retina through breaks in the Bruch membrane, which leads to photoreceptor degeneration. Illustration created with *BioRender*.

Concerning therapeutical approaches, VEGF inhibitors can be used to treat two important complications of retinal dystrophies related with AMD: choroidal neovascularization and macular edema. For the exudative form of neovascular AMD, therapies based in intravitreal injections of anti-VEGF molecules, including ranibizumab, bevacizumab, aflibercept, and brolucizumab, have revolutionized the treatment of AMD. Monthly administration of these drugs has consistently demonstrated significant improvement in visual acuity in approximately 30% of patients with neovascular AMD (Ambatti et al., 2012; Amoaku et al., 2015; Parodi et al., 2020; Mettu et al., 2021). However, the nonexudative form of AMD can continue to progress to macular atrophy, apparently independent of the exudative process, resulting in progressive and irreversible loss of visual function as the area of macular atrophy enlarges (Wykoff et al., 2021). In the past month of May 2023, the United States Food and Drug Administration approved intravitreal pegcetacoplan as the first treatment for geographic atrophy, developed by the Apellis Pharmaceuticals under the commercial name of Syfovre (Bakri et al., 2023). Intravitreal injection of 15 mg pegcetacoplan, an inhibitor of complement component 3 (C3) cleavage, demonstrated a statistically significant 20-30% reduction in the enlargement rate of geographic atrophy lesions after monthly treatment compared with sham treatment. The phase 2 FILLY trial (NCT02503332) also revealed reduced thinning of photoreceptor layers and slower macular atrophy progression after twelve months of pegcetacoplan treatment (Liao et al, 2020; Wykoff et al., 2021; Pfau et al., 2022; Nittala et al., 2022; Bakri et al., 2023).

1.2. Retinal Pigment Epithelium

The retinal pigment epithelium (RPE) is a monolayer of polarized and pigmented cells located between the photoreceptor cells and the choroid, and an essential component of the outer blood-retinal barrier (Alves et al., 2020; Fields et al., 2020). The apical membrane of the RPE faces the photoreceptor outer segments while the basolateral membrane faces Bruch's membrane (Fields et al., 2020). The polarity of retinal pigmented cells is crucial to ensure differential expression of ion channels on the apical or basal membrane, enabling transepithelial transport, maintaining homeostasis in the subretinal space (Fields et al., 2020). The RPE also plays a major role in the maintenance of overlying photoreceptor cells by performing crucial functions such as phagocytosis of photoreceptor outer segments (POS) and reisomeration of all-trans-retinal and transport of retinoids in the visual cycle (Lakkaraju et al., 2020; Fields et al., 2020). Additionally,

the RPE has an important secretory activity of several growth factors and extracellular matrix components, that help maintaining the structural integrity of choriocapillaris endothelium and photoreceptors. The RPE also plays an important role in establishing the immune privilege of the eye by secreting immunosuppressive factors (Lakkaraju et al., 2020). Degeneration and impaired clearance mechanisms of RPE contribute to increased accumulation of lipofuscin, a yellowish aggregate of oxidized proteins and lipids, the main constituent of drusen. Therefore, RPE structure and function are essential to normal vision and to the maintenance of the eye as a site of relative immune privilege. Therefore, RPE has been suggested as a critical site of AMD pathology (Feher et al., 2006; Nordgaard et al., 2008; Wang et al., 2009; Karunama et al., 2010; Mitter et al., 2014; Holz et al., 2014; Kitagishi et al., 2017; Fleckeinstein et al., 2018; Fleckeinstein et al., 2021).

1.2.1 Mitochondrial dysfunction in the RPE and its association with AMD pathology

Mitochondrial dysfunction in the RPE has been suggested as a crucial factor in AMD development. In fact, several studies have been shedding light into the association between AMD and alterations in mitochondrial structure, function and cellular communication (Nordgaard et al., 2006; Ferrington et al., 2017; Golestaneh et al., 2017). A study by Feher *et al.* using transmission electron microscopy (TEM) analysis of human donor eyes affected by AMD showed a reduction in the number of mitochondria and loss of cristae and matrix density in the mitochondria of aging human RPE. These changes were more pronounced in individuals with AMD, when compared with age-matched controls with no AMD pathology (Feher et al., 2006).

Since mitochondria encoded genes are involved in oxidative phosphorylation (OXPHOS), mitochondrial damage leads to impaired OXPHOS metabolism and to the further increase in reactive oxygen species (ROS) production, causing mitochondrial damage (Datta et al., 2017). In fact, a study by Golestaneh *et al.* supported this theory by reporting that human induced-pluripotent stem cells (hiPSC) derived from AMD patients and differentiated into RPE cells not only were highly susceptible to oxidative stress but also used glycolysis as the primary source of ATP rather than OXPHOS, which resulted in reduced adenosine triphosphate (ATP) production. Indeed, these cells presented damaged mitochondria and enhanced glycolytic metabolism (Golestaneh et al., 2016). In AMD, when mitochondrial function is disrupted, the mitochondria of the RPE rely on glycolysis to produce ATP, reducing the available glucose to photoreceptors, thereby starving the neural retina and causing cell death (Kanow et al., 2017).

In a proteomic analysis of the RPE performed by the Ferrington´s research team, changes in the expression of proteins involved in mitochondrial refolding and trafficking in RPE were reported in AMD patients as compared with non-AMD subjects (Nordgaard et al., 2008). The

proteomic study of the RPE affected by AMD pathology also highlighted a decrease in the level of the mitochondrial heat shock protein 70 (mtHsp70), a molecular chaperone that regulates the ATP-dependent import of nuclear-encoded proteins into the mitochondrial matrix mitochondrial calcium regulation (Nordgaard et al., 2006, Nordgaard et al., 2008). Therefore, decreased mtHsp70 levels could be detrimental to overall mitochondrial function and limit energy production in AMD (Kaarniranta et al., 2019; Kaarniranta et al., 2020).

Summing up, several experimental approaches by different research groups using cultures of RPE cells provided direct evidence that ATP production and mitochondrial function are impaired in AMD (Ferrington et al., 2017; Golestaneh et al., 2017). Besides impairing bioenergetics, damage to the mitochondria of RPE cells associated with AMD also disrupted intracellular calcium homeostasis and mitochondria-nuclear signaling, thereby having a more global impact on cell health (Rottenberg and Hoek, 2017; Fisher and Ferrington, 2018). Taken together, these results strengthen the hypothesis that mitochondrial damage and dysfunction may be involved in AMD pathology.

1.2.2. Mitochondrial DNA damage in the RPE and its role in AMD pathophysiology

Human mitochondrial DNA (mtDNA) contains 13 intron-less polypeptide-encoding genes and several shorter genes coding for functional ribonucleic acid (RNA), including 12S and 16S ribosomal RNA (rRNA) and 22 transfer RNA (tRNA). Since the mitochondria of the RPE cells are especially susceptible to oxidative stress-induced damage, the mitochondrial genome is also a particularly susceptible target (Karunadharma et al., 2010; Lin et al., 2011; Ao et al., 2018; Mehrzadi et al., 2020; Ferrington et al., 2021). In fact, due to its proximity the inner mitochondrial membrane and to the lack of protective histones, proteins associated with deoxyribonucleic acid (DNA), the mtDNA is a more vulnerable target to oxidative damage than nuclear DNA (nDNA) (Lin et al., 2011). The existence of many intronless regions with high transcription rates also increases predisposition of mtDNA to oxidative damage and increases the probability of having mtDNA damage localized in a coding sequence (Ao et al., 2018). Since many coding sequences in the mtDNA are related to genes encoding for subunits of the electron transport chain (ETC), their damage can have a serious deleterious effect in cellular metabolism (Ao et al., 2018). The interaction of ROS with mtDNA also leads to DNA damage and impaired synthesis of proteins involved in several pathways, such as proteins involved in the ETC. This contributes to additional ROS generation and further mtDNA damage, which induces a vicious cycle of oxidative damage disrupting mitochondrial function (Mehrzadi et al., 2020).

There is increasing evidence of mtDNA damage in age-related diseases such as AMD (Karunadharma et al., 2010; Terluk et al., 2015; Kaarniranta et al., 2020). A study by Karunadharma *et al.* that compared mtDNA damage in the RPE from age matched human donor samples reported that, although the aging process was associated with an increase in the common deletion region in mtDNA, AMD-related mtDNA damage was more pronounced and distributed throughout the mitochondrial genome (Karunadharma et al., 2010). This suggests that AMD pathology involves disease-specific changes that are superimposed on a background of typical age-related changes. Based on the analysis of two nuclear genes, the authors noticed that mtDNA accumulated about eight times more damage than its nuclear counterpart. These authors concluded that damage in mtDNA may be an important element of AMD pathogenesis, as they may underline RPE dysfunction, crucial for AMD (Karunadharma et al., 2010). Terluk *et al.* have also shown that mtDNA damage is especially pronounced in the RPE, which might point to a crucial role of mtDNA damage as an early event in AMD progression (Terluk et al., 2015). This study showed that mtDNA damage affects regions required for transcription and replication of mitochondrial proteins, and in region of the mitochondrial genome that encode for the complex I and II subunits of the ETC, which may have an impact in ATP production (Terluk et al., 2015). Besides compromised energy production, cells displaying mtDNA damage can also present an imbalance in apoptotic signals, leading to RPE dysfunction and cell death, hallmarks of AMD pathogenesis (Kanda et al., 2007; Kinnunen et al., 2012; Kaarniranta et al., 2019; Kaarniranta et al., 2020).

Recent studies have been focusing on the role of mtDNA haplogroups, specific sets of genetic differences. A recent study by Panvini *et al.* (Panvini et al., 2022) compared the effects of mtDNA haplogroups H and J, two of the most prevalent in the European population (Herrnstadt et al., 2002), on transcriptome regulation and cellular resilience to oxidative stress in human RPE cytoplasmic hybrid (cybrid) cell lines *in vitro*. Adult Human Retinal Pigment Epithelium-19 (ARPE-19) cybrid cell lines containing mtDNA haplogroups H and J were exposed to a stimulus of 300 μM hydrogen peroxide (H_2O_2) to mimic oxidative stress conditions. Following exposure to oxidative stress, the J cybrids showed increased mitochondrial swelling, disturbed fission/fusion events, increased calcium uptake, and higher secreted levels of tumor necrosis factor-α (TNF-α) and VEGF, compared to the H cybrids. Thirteen genes involved in mitochondrial complex I and V function, antioxidant defenses, and inflammatory responses, were significantly downregulated. Their results show that a group of important genes controlling both mitochondrial and cellular functions showed differences in expression levels between mtDNA haplogroups H and J (Panvini et al., 2022). The authors also suggest that the J mtDNA haplogroup, which as previously associated with AMD progression (Mueller et al., 2012; Kenney et al., 2013), can have strong regulatory influence on the RPE transcriptome, implying respective

mutations that can control nuclear responses to the environmental stress, increasing cellular susceptibility to stress and retinal degenerations (Panvini et al., 2022). A previous study by Bao *et al.* (Bao et al., 2021) assessed the response of AMD ARPE-19 cybrids with several mtDNA haplogroups, including the J haplogroup, to treatment with a mitochondria-targeting PU-91 cytoprotective drug that upregulates peroxisome proliferator-activated receptor-gamma coactivator-1alpha (PGC-1α), a primary regulator of the mitochondrial biogenesis pathway. Their study reinforced the idea that mtDNA haplogroups contribute to the differential responses of AMD cybrid cells to PU-91 drug *in vitro*. These findings also suggest that mtDNA haplogroups may influence responses of AMD patients to drug treatment.

1.2.3 Susceptibility of the RPE to oxidative stress

Retinal pigment epithelial cells are particularly susceptible to oxidative stress (Jarrett et al., 2008; Mitchell et al., 2018). The RPE cells are exposed not only to intense focal light but also to a highly oxidative environment due to the large oxygen gradient from the underlying capillaries of the choroid, across the RPE to the outer retina (Jarrett et al., 2008). The unique phagocytic function of the RPE also provides additional oxidative burden. An abundance of ROS, such as singlet oxygen, superoxide anion, and hydroxyl radicals, is generated in the visual cycle as peroxidation products of photoreceptor polyunsaturated fatty acids and in nicotinamide adenine dinucleotide phosphate (NADPH) oxidase-mediated reactions in the phagocytosis of the outer segments of the photoreceptors (Jarrett et al., 2008; Mitchell et al., 2018).

To meet the high energetic demands, the mitochondrial population of the RPE exhibits robust metabolic activity, with increased OXPHOS. The metabolic process of OXPHOS produces energy in the form of ATP, in a mechanism that involves the transfer of electrons between the subunit complexes of the ETC coupled with the reduction of oxygen. However, the reduction of oxygen is incomplete, leading to production of anion superoxide, generating high local concentrations of ROS (Bilbao-Malavé et al., 2021). Additionally, the decrease in mitochondrial membrane potential facilitates the leakage of ROS into the cytoplasm. With aging, the capacity to neutralize mitochondrial-derived ROS is highly decreased and might result in the loss of mitochondrial homeostasis, impact cytoplasmic processes and overall cellular health (Bilbao-Malavé et al., 2021).

Another source of oxidative-stress induced damage in the RPE is the accumulation of oxidized lipoproteins with aging (Mitter et al., 2014). In healthy conditions, lipofuscin and other heterogeneous complexes of oxidized lipids and proteins are efficiently cleared from the RPE by targeting for lysosomal degradation. However, with aging, the autophagy and lysosomal pathways are impaired and waste materials start accumulating in the cytoplasm and eventually suffer oxidation, producing free radicals and becoming toxic to the RPE cells (Mitter et al., 2014).

1.2.4. Defense mechanisms of the RPE against oxidative stress

To ensure protection from oxidative stress-induced damage, the RPE has several defense mechanisms. One of the first lines of defense are the melanosomes, that synthetize and store melanin (Kwon et al., 2022). The pigment melanin absorbs and filters harmful light, particularly of lower wavelength, decreasing the photo-oxidation of lipofuscin, that tends to accumulate with aging and phagocytic activity (Ao et al., 2018). It has also been reported that melanin is able to display antioxidative properties by scavenging free oxygen radicals (Kwon et al., 2022). Interestingly, melanin density is higher in the central macula, the most affected region in AMD pathology. However, with aging, the melanin density suffers a significative decrease. The RPE also possesses an intrinsic antioxidant defense system that involves both enzymatic, such as superoxide dismutase (SOD), hemeoxygenase-1 and catalase, and non-enzymatic antioxidants such as α-tocopherol, β-carotene and ascorbate (Ao et al., 2018). Another molecule with an important antioxidant activity is glutathione, that contributes to the maintenance of ascorbate in its reduced form and to the detoxification of reactive products of lipid peroxidation (Minasyan et al., 2017). The sophisticated base excision repair (BER) exonuclease activity of DNA polymerases existent in the RPE is also very important to prevent the damage resultant from overproduction of ROS. (Burke et al., 2011).

The antioxidant response induced in the RPE by oxidative stress has been linked to the activation of autophagy (Wang et al., 2014; Johansson et al., 2015), a protective mechanism responsible for the removal of dysfunctional or deleterious cellular components including the ones generated by oxidative damage. Compromised autophagy might lead to dysfunctional RPE (Wang et al., 2009; Mitchell et al., 2018), having a role in the development of AMD pathology. As reported by Yao *et al.,* the deletion of the autophagy inducer RB1CC1 results in degeneration of the RPE, inducing an AMD-like phenotype in mice (Yao et al., 2015). In fact, mitochondrial homeostasis depends in a process where damaged mitochondria are sequestered and then degraded. Afterwards, the damaged mitochondrial fragments are selectively removed by mitophagy, a specialized type of autophagy (Westermann et al., 2010). Moreover, if the

mitochondrial membrane potential (ΔΨm) is affected and consequently decreased, the PTEN induced kinase 1 (PINK1) remains on the mitochondrial surface, where it phosphorylates a wide range of proteins, such as Parkin. Phosphorylated Parkin in turn ubiquitinates proteins of the outer mitochondrial membrane. This eventually results in lysosomal degradation mediated by the microtubule-associated protein 1A/1B-light chain 3 (MAP1LC3), leading to removal of affected mitochondria, thus, having a protective role in the RPE (Lazarou et al., 2015; Rub et al., 2017; Quinn et al., 2019; Alves et al., 2020). However, deficient mitophagy processes can result in elevated mitochondrial ROS, impaired mitophagy and mitochondrial dynamics in the RPE, described to be implicated in early stages of AMD pathology (Karunadharma et al., 2010; Kitagishi et al., 2017).

1.2.5. Cell culture models to study RPE-related pathogenesis in AMD

Several distinct features of AMD pathophysiology present numerous challenges for *in vitro* disease modelling. The diverse hallmark RPE phenotypes, such as morphology, pigmentation, and polarization, varies significantly across different models and culture conditions, directly impacting the suitability of these models for investigating different features of AMD biology (reviewed in Bharti et al., 2022).

Despite these difficulties, an increasing body of evidence suggests that it is possible to develop and employ cellular models for studying specific aspects of AMD pathogenesis. In this context, *in vitro* models of the RPE have gained prominence. These models include a range of options, including spontaneously formed cell line ARPE-19 (Dunn et al., 1996), immortalized cell lines such as hTERT-RPE1 (Bodnar et al., 1998; Jiang et al., 1999), RPE-J (Nabi et al., 1993), and D407 (Davis et al., 1995), as well as primary human (fetal or adult) (Hu and Bok, 2001; Maminishkis et al., 2006; Sonoda et al., 2009) or animal (mouse and pig) RPE cells (Gibbs et al., 2003; Toops et al., 2014; Fernandez-Godino et al., 2016; Klingeborn et al., 2017). Furthermore, RPE derived from embryonic or human induced pluripotent stem cells (hiPSC) have also been explored in these models (Maroutti et al., 2015; Sharma et al., 2019; Smith et al., 2019).

1.2.5.1. Adult Human Retinal Pigment Epithelium-19 (ARPE-19) Cell Line

The Adult Human Retinal Pigment Epithelium-19 (ARPE-19) cell line is the most widely used RPE cell line (reviewed in Klettner, 2020). It arose spontaneously from a 19-year-old donor and was selected for its epithelial phenotype (Davis et al., 1995; Dunn et al., 1996). The original cell line was pigmented, able to differentiate into a semi-polarized phenotype with a

relatively low transepithelial resistance and expressed several RPE markers such as CRALBP and RPE65 (Dunn et al., 1996). ARPE-19 cells have already been used to study many characteristics of AMD, including epithelial-to-mesenchymal transition (Yang et al., 2021), inflammation (Tseng et al., 2013), phagocytosis defects (Xu et al., 2012), and complement activation (Chung et al., 2017; Fernandez-Godino et al., 2018). However, this cell line has an abnormal karyotype, with a deletion in the long arm of chromosome 9 and an addition in the long arm of chromosome 19, with an otherwise normal karyotype (Davis et al., 1995; Dunn et al., 1996; Fasler-Kan et al., 2018; Hazim et al., 2019).

Since expression patterns of ARPE-19 cells depend on culture conditions (Hu et al., 2001; Tian et al., 2004; Samuel et al., 2017), a relative high degree of differentiation can be achieved when cells are cultured under conditions that promote differentiation in mature RPE (Lynn et al., 2018). Indeed, ARPE-19 cells are able to mimic many characteristics of primary human RPE, such as pigmentation, polarization and expression of RPE-specific differentiation markers. (Ahmado et al., 2011; Hazim et al., 2019; Pfeffer and Fliesler, 2022). Improved conditions to enhance the differentiation of ARPE-19 cells involve incorporating specific media additives that influence cellular metabolism and utilizing a porous Transwell® filter enabling an oxygen gradient to promote polarization. One approach involves culturing ARPE-19 cells at low passages in low-serum media (1% fetal bovine serum) containing high glucose and pyruvate for up to four months (Samuel et al., 2017). The ARPE-19 cells cultured for four months developed strong pigmentation, a phenotype characteristic of native RPE, and expressed RPE-specific differentiation markers, an arrangement resembling cobblestones, polarized protein expression, abundant microvilli, the ability to perform phagocytosis, and the secretion of VEGF (Samuel et al., 2017; Ahmado et al., 2011). A more recent method incorporates the use of 10 mM nicotinamide (NIC) instead of pyruvate, resulting in the rapid differentiation of ARPE-19 cells. When NIC is present, the cells develop a tightly packed, cobblestone-like appearance within one week and form a well-polarized epithelium within four weeks (Hazim et al., 2019).

Despite the limitations in the use of RPE cell lines, the use of validated lines and in the appropriate culture conditions to promote a differentiated epithelium, make the ARPE-19 cell line useful for various types of RPE studies. In fact, ARPE-19 cells are a simple and economic model system to study research questions related with AMD cell biology. They combine ease of access and usability with rapid readouts capability. ARPE-19 cells provide great advantages in conducting high-throughput testing, particularly when achieving a substantial yield is necessary (Aboul Naga et al., 2015). Additionally, ARPE-19 cell line serves as a valuable tool for fast and efficient drug screening and biocompatibility testing. Toxicity studies can also be easily performed with this cell line, as there are many assays and methods for fast and efficient screening

on the market, such as cell viability and apoptosis assays (Spitzer et al., 2007, Spitzer et al., 2011; Schnichels et al., 2012; Schnichels et al., 2013; Susskind et al., 2016; Hurst et al., 2017). Moreover, the ARPE-19 cell line is particularly valuable since it displays a genetic profile similar to primary RPE cells (Faby et al., 2014; Finnemann et al., 1997; Wang et al., 2016). Importantly, ARPE-19 cells have been successfully utilized in gene editing, as evidenced by the generation of a mutant line through *EFEMP1* gene editing, which is associated with dominant macular degeneration (Fernandez-Godino et al., 2018).

1.2.5.2. Primary Human RPE Cell Cultures

Primary human RPE cell cultures, when cultured under specific conditions, exhibit characteristics that resemble the RPE tissue. Primary human RPE cultures can be generated from fetal human RPE (Maminishkis et al., 2006; Sonoda et al., 2009) or from the adult human RPE monolayers derived from donor eyes (Ferrington et al., 2017). The establishment of adult primary RPE cultures directly obtained from AMD donors is particularly valuable to identify alterations underlying AMD development such as autophagic defects, mitochondrial dysfunction, secretion of specific proteins, and patterns of epigenetic modifications, when compared to cultures established from healthy donors (Ferrington et al., 2016, Ferrington et al., 2017; Zhang et al., 2020).

However, the use of primary human RPE cultures is very challenging due to the limited availability of donor tissue, preferably collected shortly after death. Additionally, after three or four passages, primary RPE cells undergo dedifferentiation and lose pigmentation, acquiring a fibroblastic morphology that differs from their natural cobblestone-like appearance (Hazim et al., 2019).

1.2.5.3. Human induced pluripotent stem cells-derived RPE (iRPE)

In the last years, human induced pluripotent stem cells-derived RPE (iRPE) have emerged as additional source for the generation of fully mature and functional RPE cells (Ferrer et al., 2014; Maroutti et al.; 2015; Smith et al., 2019; Sharma et al., 2019; Sharma et al., 2020; Miyagishima et al., 2021; Bharti et al., 2022). In fact, the use of iRPE cells offers a promising alternative for further studies (Smith et al., 2019), enabling a better disease modelling. One significant concern with the differentiation of human induced pluripotent stem cells (hiPSC) into RPE is the current lack of standardized protocols for differentiating and maintaining iRPE. Several factors, including substrate surface, plating density, feeding medium and frequency, and

culture duration, along with the source of donor tissue and individual donor characteristics, are likely to influence the phenotype, function and gene expression profile of iRPE (Sorkio et al., 2014). There is a clear need to establish standardized methods that can be universally employed for hiPSC differentiation. It is also crucial to perform functional validation of iRPE across different laboratories to enable direct comparisons of results obtained using a given patient cell line. In the last twenty years, researchers have developed multiple iterations of RPE differentiation protocols (reviewed in Sharma et al., 2020). Notably, directed or guided differentiation approaches (Idelson et al., 2009; Osakada et al., 2009; Sharma et al., 2019) have emerged as significant advancements in RPE differentiation methods. These approaches involve the targeted administration of specific growth factors at defined time points to control the developmental path of hiPSC towards the RPE cell lineage. In the protocol by Sharma *et al*., the hiPSC are cultured in vitronectin coated wells and uses 10 mM nicotinamide (NIC), 150 ng/ml Activin A and a cocktail of growth factors to direct differentiation (Sharma et al., 2019). This protocol yields fully mature and functional RPE cells, significantly enhances the efficiency of differentiation when compared to the spontaneous differentiation and improves the reproducibility of the experimental procedures across multiple hiPSC lines (Sharma et al., 2019). However, the use of growth factors increases the cost of iRPE differentiation. Moreover, these highly efficient established protocols use biologic products derived from animal cells or bacteria, thus presenting potential clinical challenges. The alternative use of non-biological products such as small molecules not only limit the risk of infection or immune rejection, but also offer a cost-effective alternative. To address this issue, Maroutti *et al*. developed an approach by identifying novel RPE differentiation-promoting factors using a high-throughput quantitative polymerase chain reaction (PCR) screen analysis (Maroutti et al., 2015). They identified chetomin (CTM), a dimeric epidithiodiketopiperazine metabolite of the fungus *Chaetomium cocliodes* and *Chaetomium seminudum* species, as a strong inducer of RPE differentiation. The authors also found that the CTM cellular toxicity can be prevented throughout the combination with the previously known neural inducer NIC. Single passage of the whole culture yielded a highly pure iRPE cell population that displayed many of the morphological, molecular, and functional characteristics of native RPE (Maroutti et al., 2015; Smith et al., 2019).

Compared to cell sources discussed in the previous sections, the RPE differentiation process from hiPSC is time-consuming and involves many economic resources. However, the iRPE cells offer key advantages, allowing the generation of fully mature and functional RPE cells (Maroutti et al.; 2015; Smith et al., 2019; Sharma et al., 2019; Miyagishima et al., 2021). The iRPE cell cultures offer both diversity and accessibility, as hiPSC can be obtained through reprogramming of fibroblasts derived from skin biopsies or peripheral blood mononuclear cells obtained through blood withdrawal. This allows the derivation of patient-specific iRPE cells,

enabling comparative analysis between diseased and healthy cells and the correlation of cellular characteristics with patient phenotypes and genotypes (Sharma et al., 2020; Miyagishima et al., 2021; Bharti et al., 2022). The obtention of unlimited high-quality iRPE cells has been explored by several research groups worldwide to investigate the potential of these iRPE cells as a source for patient transplantation, already in clinical trials for geographic atrophic AMD (NCT01344993; NCT02590692) (Sharma et al., 2022; Cabral de Guimaraes et al., 2022).

In fact, several authors have shown that iRPE cells can be used to model AMD *in vitro*, providing an unprecedented opportunity to understand the evolution of disease processes and to identify novel therapeutics (Garcia et al., 2015; Golestaneh et al., 2016; Saini et al., 2017; Dalvi et al., 2019; Peters et al., 2022). Golestaneh *et al.*, demonstrated that iRPE derived from AMD human donors exhibit the disease relevant cellular phenotype and is a valuable tool for *in vitro* disease modelling in AMD (Golestaneh et al., 2016). In this study, the authors generate hiPSC from RPE cells and skin fibroblasts of AMD donors and age-matched healthy donors. Then, the hiPSC are differentiated into RPE cells (iRPE). In comparison with healthy iRPE, the iRPE derived from AMD donors (iRPE-AMD) show increased susceptibility to oxidative stress and present higher levels of cell death when exposed to a 48-hour stimuli of 0.4 mM H_2O_2 that mimics oxidative stress conditions. The iRPE-AMD cells also produce significantly higher levels of ROS under oxidative stress conditions, when compared to healthy iRPE. Moreover, unlike healthy iRPE cells, iRPE-AMD cells are unable to increase SOD expression as an antioxidant defense when under oxidative stress conditions. Additionally, PGC-1α, a master regulator of mitochondrial biogenesis and function, is repressed in iRPE-AMD cells. Phenotypic analysis also showed that the iRPE-AMD present disintegrated mitochondria, increased number of autophagosomes, higher levels of cytoplasmic lipid accumulation and presence of lipid droplets, when compared to normal iRPE (Golestaneh et al., 2016). Another study using iRPE derived from AMD donors, showed significantly increased expression of a panel of transcripts comprising a subset of complement and inflammatory proteins, including complement component 3 (C3), complement factor I (CFI) and complement factor H (CFH), which have been reported in drusen deposits (Saini et al., 2017). A recent study also reported deficient cholesterol efflux and increased intracellular lipid accumulation in iRPE under hypoxia, an environmental risk factor for AMD (Peters et al., 2022). Since oxidative stress in RPE cells is an important player in AMD pathogenesis, Garcia *et al.*, generated an *in vitro* model of chronic oxidative stress in the iRPE. The authors exposed healthy iRPE cells to paraquat (PQ), a known chemical inducer of oxidative stress that reacts with oxygen and generates superoxide radicals and, over time, hydrogen peroxide and hydroxyl radicals. Their study showed that 160 μM PQ can be used to generate a model of chronic oxidative stress environment in iRPE, mimicking one of AMD disease hallmarks (Garcia et al., 2015). Taken together, these findings indicate the utility of iRPE as a disease model

to shed light on the mechanism of AMD progression, AMD risk factors and for screening of potential therapeutic targets.

1.3. Tumor Necrosis Factor Receptor-Associated Protein 1 (TRAP1)

Tumor necrosis factor receptor-associated protein 1 (TRAP1), also known as heat shock protein 75 (HSP75), belongs to the heat shock protein 90 (HSP90) chaperone family and is mainly located in the mitochondria. In humans, the HSP90 family consists of three additional isoforms: HSP90α and HSP90β in the cytosol and glucose-regulated protein 94 (GRP94) in the endoplasmic reticulum (Serapian et al., 2021). The prototypic member of the HSP90 family has three structural domains: an N-terminal domain (NTD) responsible for ATP binding, a middle domain (MD) crucial for client protein binding, and a C-terminal domain (CTD) responsible for dimerization. Similarly to other chaperones, HSP90 family members play essential roles in the folding of client proteins and in the degradation of misfolded proteins (Faienza et al., 2020; Dekker et al., 2021).

TRAP1 has been extensively studied in the field of oncology due to its selective upregulation in several human tumors, which correlates with malignant progression, metastatic potential, and resistance to chemotherapy (reviewed in Faienza et al., 2020). Consequently, TRAP1 has emerged as a potential therapeutic target, and researchers are working on developing specific inhibitors. In addition to its role in tumor cells, mitochondrial TRAP1 acts as a cellular regulator of oxidative stress-induced cell death (Xiang et al., 2010; Amoroso et al., 2014; Wang et al., 2015; Masgras et al., 2017a; Amoroso et al., 2017; Purushottam Dharaskar et al., 2020; Standing et al., 2020; Sanchez-Martin et al., 2020), mitochondrial homeostasis and bioenergetics (Guzzo et al., 2014; Matassa et al., 2018; Sima et al., 2018; Liu et al., 2020; Cannino et al., 2022; Chen et al., 2022), and mitochondrial unfolded protein response (mtUPR) in the endoplasmic reticulum (ER) (Takemoto et al., 2011; Amoroso et al., 2012). However, the understanding of the role of TRAP1 in central nervous system cells, both in physiological and pathological conditions, remains limited.

1.3.1 TRAP1 Molecular Structure

The human *TRAP1* gene locus resides on chromosome 16p13. The gene spans 60 kb and consists of 18 exons. The main TRAP1 transcript is composed of 2112 bp, encoding a protein of 704 amino acids (Rasola et al., 2014). The protein comprises three major domains: NTD, MD, and CTD (Kang et al., 2012; Faienza et al., 2020; Dekker et al., 2021; Ramos Rego et al., 2021) **(Fig. 2A).** The N-terminal 59 amino acid sequence acts as a mitochondrial targeting signal, which is cleaved upon translocation to the mitochondria (Kang et al., 2012; Hoter et al., 2018) **(Fig. 2B).**

TRAP1 is expressed in various tissues, including the central nervous system (https://www.proteinatlas.org/ENSG00000126602-TRAP1/tissue; accessed on 6 June 2023) (Song et al., 1995; Felts et al., 2000; Guo et al., 2003).

Unlike other HSP90 paralogs, both TRAP1 and its bacterial homolog chaperone high temperature protein G (HtpG) (Shiau et al., 2006) lack a charged linker between the MD and CTD (Cechetto et al., 2000) and do not require any co-chaperones (Zuehlke et al., 2010; Elnatan et al., 2018). TRAP1 has an extended N-terminal β-strand that spans between monomers in the closed state, acting as a thermal regulator of protein function (Rasola et al., 2014). It also exhibits an asymmetric conformation due to reconfigurations in the interface between MD and CTD, which is critical for client binding (Masgras et al., 2021). Notably, TRAP1 can form tetramers, consisting of dimers of dimers (Joshi et al., 2020). While TRAP1 has a comparable ATP turnover rate to other HSP90 paralogs (Sima et al., 2018), its affinity for ATP is one order of magnitude higher (Leskovar et al., 2008). The Michaelis constant (K_m) for ATP binding by TRAP1 is 14.3 μM, much lower than the average K_m of 127 μM for other HSP90 paralogs (Leskovar et al., 2008). TRAP1 regulates substrate influx and takeover through the ATPase cycle, following a distinct mechanism from other HSP90 chaperones (Matassa et al., 2013).

Research on the ATPase cycle of TRAP1 has revealed that both protomers of TRAP1 undergo structural alterations during the process of ATP binding, hydrolysis, and release (Leskovar et al., 2008; Lavery et al., 2014; Sung et al., 2016; Masgras et al., 2017a; Masgras et al., 2017b). These conformational changes induced by ATP can have an impact on the conformation of the client protein that is bound to TRAP1 (Verba et al., 2016). Throughout its ATPase cycle, TRAP1 can adopt three distinct conformations: an open state, an intermediate coiled-coil state with closely positioned N-terminal domains, and a closed state where the N-terminal extends between protomers (Masgras et al., 2017a). When ATP binds to TRAP1, in the absence of co-chaperones, a significant structural transformation takes place, resulting in a closed and asymmetric conformation (Leskovar et al., 2008; Lavery et al., 2014; Sung et al., 2016; Masgras et al., 2017a; Masgras et al., 2017b) **(Fig. 2C, D).**

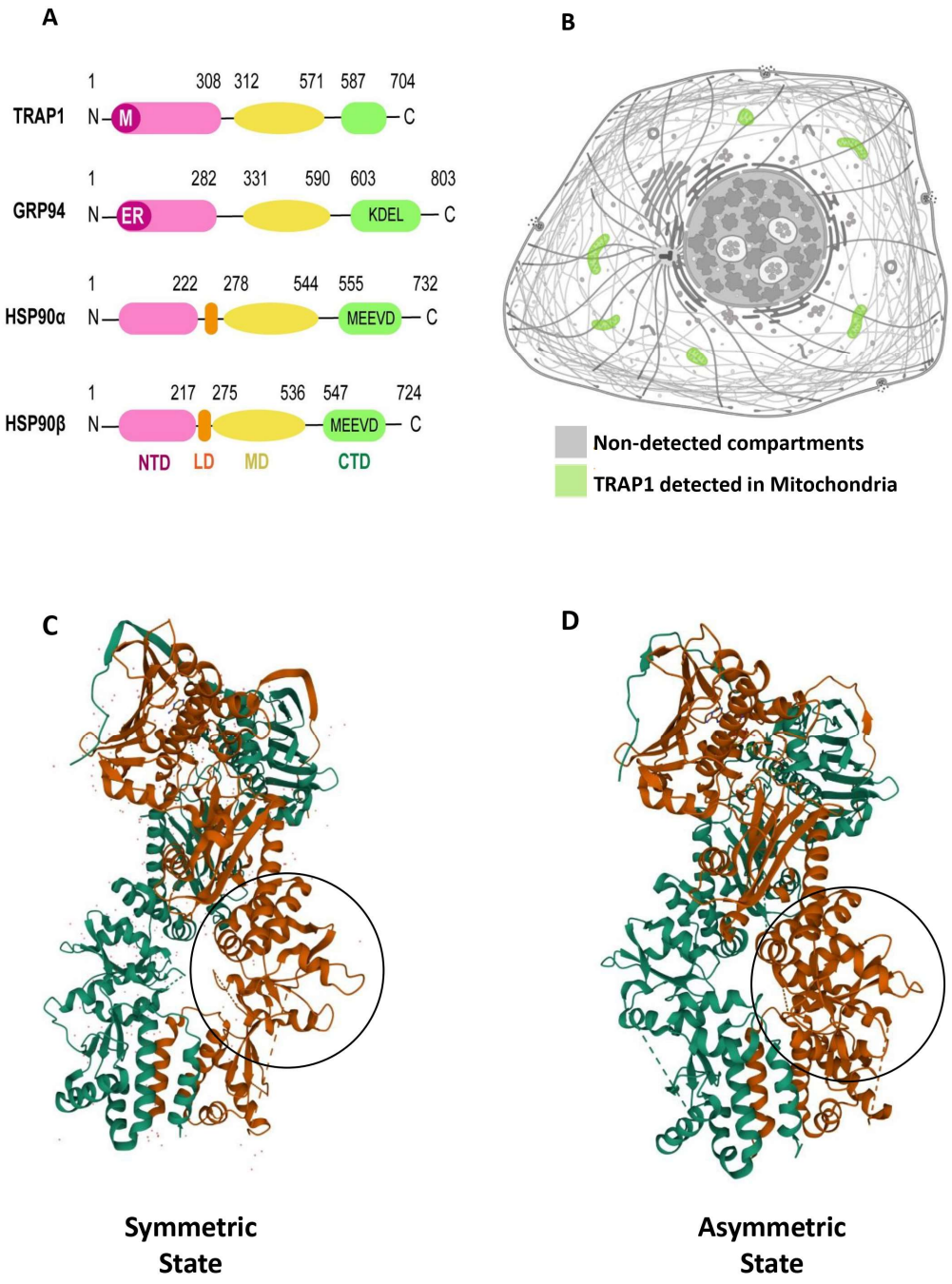

Figure 2. TRAP1 molecular structure. (A) Prototypic HSP90 family member contains three structural domains, an N-terminal domain (NTD) responsible for ATP binding, a middle domain (MD) which is important for client binding, and a C-terminal domain (CTD) responsible for dimerization. GRP94 contains also a KDEL motif. While HSP90α and HSP90β contain a MEEVD motif and a linker domain (LD). Mitochondrial signal sequence present in TRAP1 is indicated with "M" and endoplasmic reticulum signal sequence present in GRP94 is indicated with "ER". Lengths of TRAP1, GRP94, HSP90α and HSP90β are 704, 803, 732 and 724 amino acids, respectively. **(B)** TRAP1 is primarily located in mitochondria. TRAP1

detection in cell mitochondria is highlighted in green (image available at v20.proteinatlas.org/ENSG00000126602-TRAP1/cell; accessed on 6 June 2023). **(C)** 3D structures of TRAP1 dimer in different nucleotide states, with each protomer in a different color. Symmetric state of TRAP1 in fully hydrolyzed state of protein (PDB code 5TVX; image available at https://www.rcsb.org/3d-view/5TVX/1; accessed on 6 June 2023) (Elnatan et al., 2016; Elnatan et al., 2017; Liu et al., 2020; Senhal et al., 2021). Asymmetric state of TRAP1 in double ATP state (PDB code 6XG6; image available at https://www.rcsb.org/3d-view/6XG6/1; accessed on 6 June 2023) (Elnatan et al., 2017; Liu et al., 2020; Senhal et al., 2021). Black circle highlights substructure in middle domain that undergoes rearrangement upon nucleotide hydrolysis. Figure adapted from Ramos Rego *et al.*, 2021.

1.3.2 TRAP1 Functions and Signaling Pathways
Role of TRAP1 in the Mitochondria

1.3.2.1 TRAP1 and Energetic Metabolism Regulation

The mitochondrial chaperone TRAP1 plays a crucial role in regulating mitochondrial energy metabolism, including the processes of oxidative phosphorylation (OXPHOS) (Rasola et al., 2014; Masgras et al., 2017a; Yoshida et al., 2013; Sciacovelli et al., 2013). TRAP1 interacts with proteins within the mitochondrial electron transport chain (ETC), such as succinate dehydrogenase (SDH) and cytochrome oxidase, also known as complex II and complex IV, respectively. **(Fig. 3)**. Additionally, TRAP1 is a crucial modulator of protein quality control (PQC) (Rasola et al., 2014; Masgras et al., 2017a; Joshi et al., 2020; Dekker et al., 2021). Mitochondrial metabolism can also be impacted when TRAP1 undergoes post-translational modifications (PTM). A specific PTM, known as O-GlcNAcylation, is reported to reduce the ATPase activity of TRAP1, leading to an increase in mitochondrial metabolism. The effect of O-GlcNAcylation on mitochondrial metabolism is dependent on the presence of TRAP1 and plays a crucial role in providing regulatory feedback. Importantly, TRAP1-O-GlcNAcylation acts as a metabolic regulatory mechanism by reversibly attenuate the chaperone activity of TRAP1, reducing the binding of TRAP1 to ATP and its interaction with the client protein SDH (Kim et al., 2022).

The interaction between TRAP1 and the mitochondrial proto-oncogene tyrosine-protein kinase (c-Src) results in the downregulation of cytochrome oxidase activity (Miyazaki et al., 2003; Ogura et al., 2012; Yoshida et al., 2013). Furthermore, TRAP1 influences the ability of mitochondrial c-Src to stimulate OXPHOS (Miyazaki et al., 2003; Ogura et al., 2012). Another interaction of TRAP1, specifically with subunit A of SDH, inhibits SDH activity, resulting in a reduction of ROS generation (Guzzo et al., 2014; Dekker et al., 2021) **(Fig. 3)**. This inhibition is enhanced by the phosphorylation of TRAP1 dependent on extracellular signal-regulated protein

kinases 1 and 2 (ERK1/2), leading to antioxidant and antiapoptotic effects in tumor cells. Furthermore, the inverse correlation between TRAP1 expression and SDH activity in human osteosarcoma SAOS-2 cells supports the inhibitory relationship between TRAP1 and SDH, as reported by Sciacovelli *et al.* (Sciacovelli et al., 2013) **(Fig. 3)**. Notably, TRAP1 stabilizes the hypoxia-inducible factor 1α (HIF1α), a transcription factor crucial for tumor cell growth (Masgras et al., 2017a; Sciacovelli et al., 2013; Laquatra et al., 2021). Importantly, TRAP1-dependent stabilization of HIF1α (Sciacovelli et al., 2013; Bruno et al., 2022) occurs independently of oxygen availability, prompting a complex transcriptional program that orchestrates a metabolic shift towards aerobic glycolysis while repressing OXPHOS (Bhattacharya et al., 2016; Singh et al., 2017; Zhang et al., 2018; Laquatra et al., 2021).

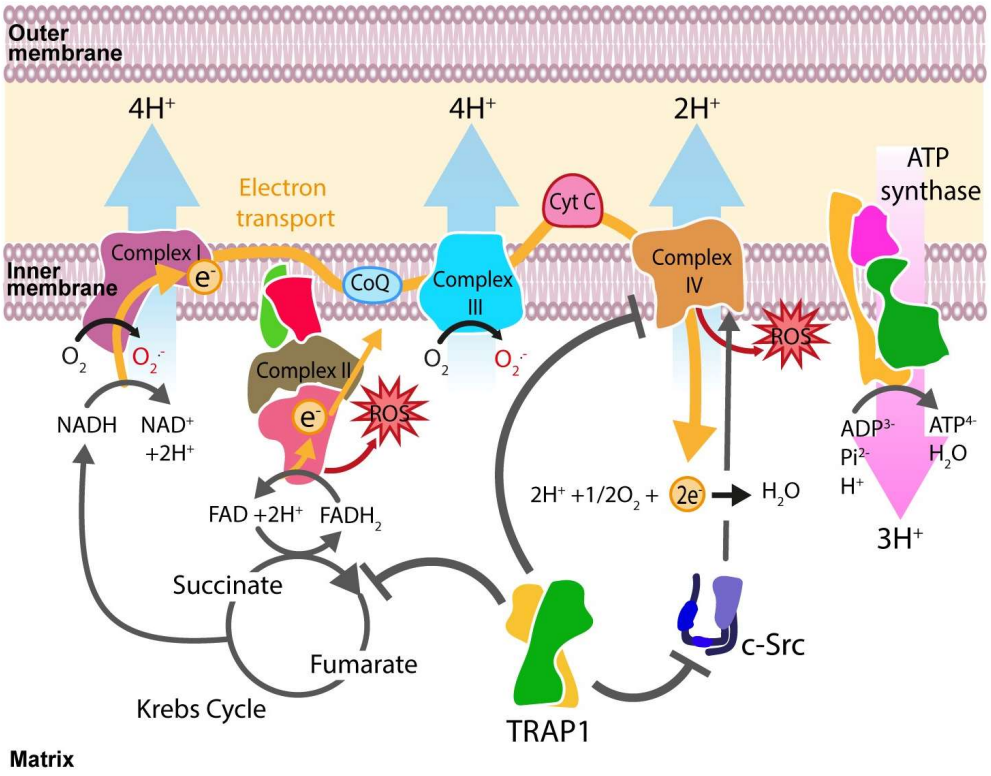

Figure 3. Role of TRAP1 in energetic metabolism regulation. TRAP1 modulates oxidative phosphorylation (OXPHOS) by interacting with proteins of mitochondrial electron transport chain (ETC), namely succinate dehydrogenase (SDH) and cytochrome oxidase, also known as complex II and complex IV, respectively. TRAP1 inhibits proto-oncogene tyrosine-protein kinase (c-Src) downregulating cytochrome oxidase activity. TRAP1 also inhibits SDH activity, resulting in less electron funneling and lower reactive oxygen species (ROS) generation as a side-reaction of ETC. Figure adapted from Ramos Rego *et al.*, 2021.

Multiple studies indicate that TRAP1 plays a role in upregulating glycolysis while suppressing OXPHOS, resulting in reduced ROS production, which is associated with the Warburg effect (Amoroso et al., 2012; Sciacovelli et al., 2013; Bhattacharya et al., 2016). OXPHOS is crucial for maintaining organelle function and plays a central role in cellular energy metabolism, offering higher energy efficiency compared to glycolysis. Consequently, downregulation of OXPHOS leads to decreased mitochondrial respiration. Additionally, this downregulation increases the availability of NADPH, an important ROS scavenger, further reducing ROS levels (Dekker et al., 2021). Consequently, the decrease in OXPHOS is linked to enhanced mitochondrial tolerance to oxidative stress and protection against apoptosis (Constantino et al., 2009; Chae et al., 2012; Masgras et al., 2017a; Matassa et al., 2018). Human colorectal cancer (CRC) HCT116 cells express higher levels of TRAP1 compared to neighboring healthy cells, indicating a predominant Warburg phenotype (Sciacovelli et al., 2013) that could provide advantages in terms of cellular survival and proliferation. In a recent study using HCT116 cells, Matassa *et al*. also reported that TRAP1 is able to regulate the metabolic switch depending on nutrient availability. In these cells, TRAP1 regulates mitochondrial complex III activity through binding to ubiquinol-cytochrome-c reductase complex core protein 2 (UQCRC2), a core component of complex III. This decreases respiration rate during basal conditions but allows sustained OXPHOS in conditions of glucose deprivation (Matassa et al., 2022).

To further investigate the role of TRAP1 in adaptive responses to oxygen deprivation, Bruno *et al*. used the HCT116 cell line under conditions of hypoxia. The findings of the study demonstrated that TRAP1 plays a significant role in the stabilization of HIF1α and in the regulation of the glycolytic metabolism during hypoxia. Moreover, the expression of glucose transporter 1, glucose uptake, and lactate production were found to be partially impaired in CRC cells with silenced TRAP1 under hypoxic conditions. According to the authors, TRAP1 is a crucial factor in maintaining the genetic and metabolic program induced by HIF1α during hypoxia, thereby presenting a promising target for innovative metabolic therapies (Bruno et al., 2022).

To clarify the regulatory role of TRAP1 in energetic metabolism, researchers generated a *Trap1* knockout mouse (*Trap1*$^{-/-}$) (Lisanti et al., 2014). Interestingly, mouse embryonic fibroblasts (MEF) lacking *Trap1* exhibited impaired mitochondrial function, accompanied by significantly increased ROS production and increased sensitivity to oxidative damage compared to wild-type (WT) cells. The homozygous deletion of *Trap1* also led to decreased expression of SDH, indicating a loss of protein-folding quality control within the mitochondria (Lisanti et al., 2014). *Trap1*$^{-/-}$ mice showed a reduced occurrence of age-associated pathologies, including inflammatory tissue degeneration and spontaneous tumor formation. Furthermore, the

homozyguous deletion of TRAP1 resulted in a global reprogramming of cellular bioenergetics, with compensatory upregulation of both oxidative phosphorylation and glycolysis transcriptomes. This resulted in impaired mitochondrial respiration and cell proliferation and increased susceptibility to oxidative stress. This adaptation was accompanied by increased mitochondrial accumulation of cytoprotective chaperones, namely HSP90 and heat shock protein 27 (HSP27), and a shift towards glycolytic metabolism *in vivo* (Lisanti et al., 2014).

1.3.2.2 TRAP1 and Redox Homeostasis

Protection against Oxidative Stress and Apoptosis

Mitochondrial dysfunction and disruption of redox homeostasis primarily result from oxidative stress triggered by the accumulation of ROS generated as a side reaction product of the ETC (Wang et al., 2013; Gaki et al., 2014; Avolio et al., 2020). TRAP1 plays a protective role in mitigating mitochondrial dysfunction by reducing ROS production and accumulation, thus reducing oxidative stress (Amoroso et al., 2014; Masgras et al., 2017a; Purushottam Dharaskar et al., 2020; Standing et al., 2020; Sanchez-Martin et al., 2020). *TRAP1* overexpression leads to a decrease in ROS accumulation (Hua et al., 2007; Im et al., 2007; Zhang et al. 2015), whereas *TRAP1* silencing increases susceptibility to oxidative stress, indicating an inverse relationship between TRAP1 expression and overall cellular ROS levels (Hua et al., 2007; Im et al., 2007; Montesano et al., 2007; Matassa et al., 2013; Yoshida et al., 2013). The antioxidant activity of TRAP1 is closely linked to its regulation of respiratory complexes in the ETC, such as SDH and cytochrome oxidase (Yoshida et al., 2013; Sciacovelli et al., 2013; Laquatra et al., 2021).

Accumulation of ROS can trigger the release of cytochrome C (CytC), initiating caspase-mediated apoptosis, an essential process of programmed cell death for maintaining cellular and tissue equilibrium (Baines et al., 2005). The association between TRAP1 and apoptosis was initially identified by Hua *et al*., who demonstrated the protective role of TRAP1 against granzyme M (GzmM)-mediated apoptosis (Hua et al., 2007). The protease GzmM induces cell death by cleaving client proteins, inducing ROS generation and CytC release, which subsequently leads to mitochondrial swelling and a decline in mitochondrial transmembrane potential (Hua et al., 2007). This activates caspase-mediated apoptosis, initiating the mitochondrial apoptotic machinery. The same study also reported that silencing *TRAP1* through interference RNA results in increased ROS accumulation and increased GzmM-mediated apoptosis, whereas TRAP1 overexpression mitigates both ROS production and GzmM-induced apoptosis (Hua et al., 2007).

The regulation of the mitochondrial permeability transition pore (mPTP), which controls the transition between an open and closed state, relies on the Ca^{2+} content in the mitochondrial matrix (Kroemer et al., 2007; Rasola et al., 2007; Tsujimoto et al., 2007; Xie et al., 2021). An excessive accumulation of Ca^{2+} in the matrix triggers the opening of the mPTP, although other factors that play a partial role in induction of pore opening remain only partially understood (Rasola et al., 2007). Maintaining mPTP regulation is crucial for preserving mitochondrial homeostasis since the opening of the pore leads to loss of the mitochondrial inner membrane potential, membrane rupture, and apoptosis (Baines et al., 2005; Montesano et al., 2007; Kang et al., 2012; Dekker et al., 2021). One of the key regulators of the mPTP is a mitochondrial matrix protein called cyclophilin D (CypD) (Rasola et al., 2007; Amoroso et al., 2014; Matassa et al., 2018). Indeed, CypD-deficient mitochondria produce fewer ROS and are less prone to mitochondrial swelling and permeability transition caused by Ca^{2+} overload. Moreover, the absence of CypD protects neurons from cell death induced by oxidative stress (Matassa et al., 2018; Laquatra et al., 2021).

Activated CypD increases the sensitivity of the mPTP to opening, resulting in mitochondrial swelling and depolarization. This leads to ruptures in the outer membrane, which causes the release of CytC into the cytosol and, eventually, cell death (Kang et al., 2007; Kang et al., 2012; Siegelin et al., 2013). PTEN-induced kinase 1 (PINK1) depletion leads to CytC release, which correlates with a decrease in the phosphorylation of TRAP1 by PINK1 (Pridgeon et al., 2007). Counteracting the CypD effect, TRAP1 inhibits the formation of the mPTP (Siegelin et al., 2013) **(Fig. 4)**. Additionally, through a competitive binding to F-ATP synthase, TRAP1 reverses the induction of mPTP by CypD, effectively opposing mPTP-dependent mitochondrial depolarization and cell death (Cannino et al., 2022).

Overexpression of TRAP1 effectively blocks the apoptotic cascade mediated by mitochondria and the subsequent activation of caspase-3 (Kang et al., 2007; Wang et al., 2015). Indirect inhibition of mPTP opening can also be achieved through the modulation of ROS concentration (Amoroso et al., 2014; Matassa et al., 2018)

Using a hypoxic model of cardiomyocytes, Xiang *et al.* discovered that TRAP1 silencing induces the mPTP opening (Xiang et al., 2010), the release of CytC from mitochondria into the cytosol, and increased activation of caspase-3, ultimately resulting in apoptosis (Xiang et al., 2019). While upregulation of TRAP1 had the opposite effect (Xiang et al., 2010; Xiang et al., 2019).

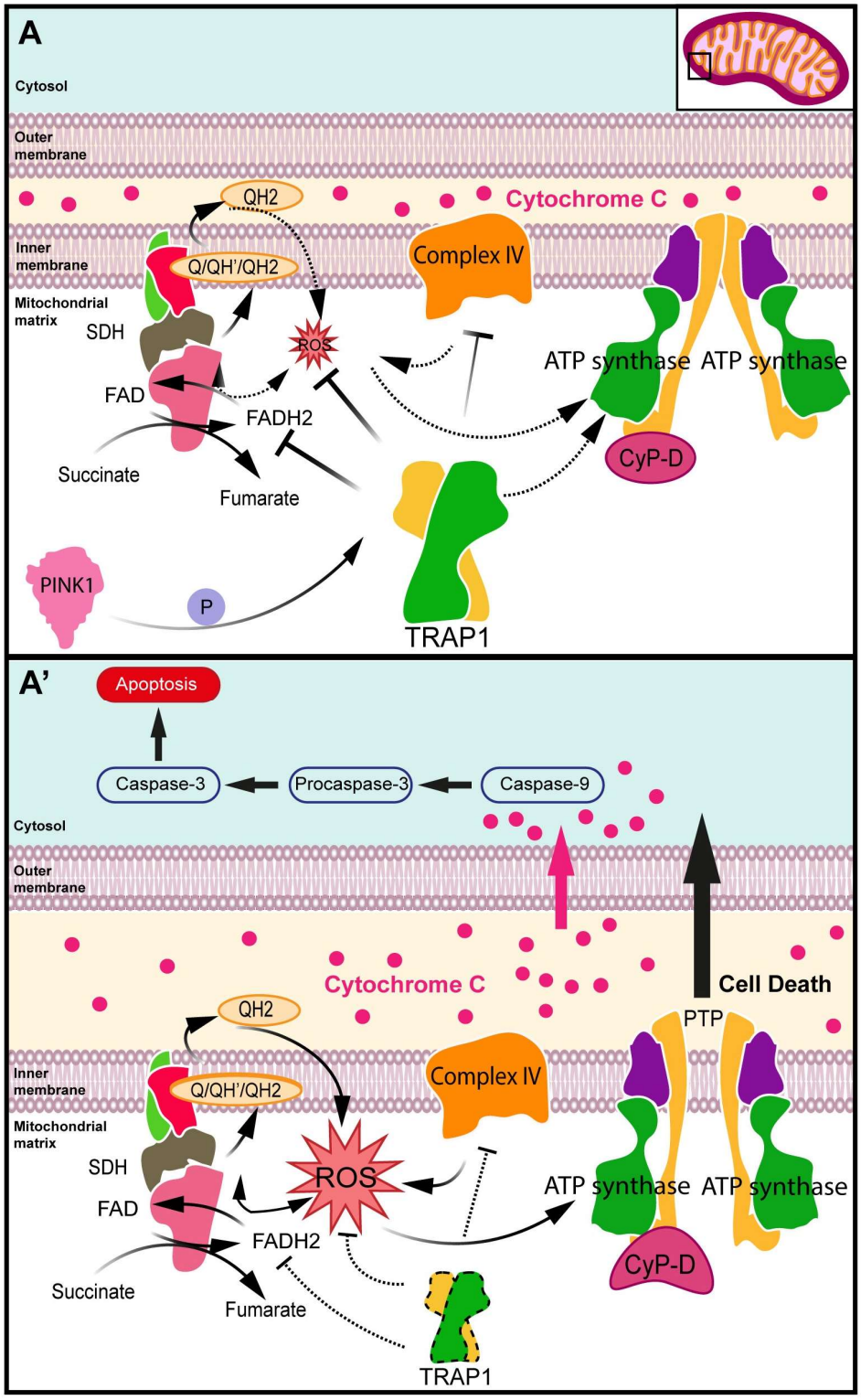

Figure 4. Role of TRAP1 in redox homeostasis. (A) TRAP1 inhibits reactive oxygen species (ROS) accumulation by controlling respiratory complexes of electron transport chain (ETC), namely, succinate dehydrogenase (SDH) and cytochrome oxidase. Counteracting the effect of cyclophilin D (CypD) and

through its interaction and with F-ATP synthase, TRAP1 inhibits mitochondrial permeability transition pore (mPTP) formation. Overexpression of TRAP1 blocks mitochondria-mediated apoptotic cascade and ensuing caspase-3 activation. **(A')** PTEN-induced kinase 1 (PINK1) depletion leads to cytochrome C (CytC) release, which correlates with reduction in TRAP1 phosphorylation by PINK1. Activated CypD sensitizes mPTP to opening, leading to mitochondrial swelling and depolarization, with outer membrane ruptures causing release of CytC into cytosol and eventually cell death. Figure adapted from Ramos Rego *et al.*, 2021.

To investigate the protective role of TRAP1 through inhibition of mPTP opening, Guzzo *et al.* conducted a whole-cell Ca^{2+} retention capacity assay, which allows a quantitative assessment of mPTP induction. They reported that *Trap1* knockdown increased the sensitivity of mPTP to Ca^{2+} in cancer cells, while *Trap1* overexpression inhibited mPTP opening in MEF cells. This protection against mPTP opening was also observed in SAOS-2 and MEF cells under starvation conditions (Guzzo et al., 2014). Notably, TRAP1 was found to inhibit mPTP opening not only in tumor cells (Guzzo et al., 2014; Sima et al., 2018) and hypoxic cellular models (Xiang et al., 2010; Xiang et al., 2019) but also in NRK-52E kidney cells exposed to high glucose conditions causing oxidative stress (Liu et al., 2020), in H9C2 myocardial cells exposed to extracellular acidification (Zhang et al., 2019; Zhang et al., 2020), and in C17.2 neural stem cells (Wang et al., 2015).

Guzzo and colleagues also reported that the *Trap1* knockdown using short hairpin RNA (shRNA) for TRAP1 (shTRAP1) in SAOS-2 and human cervix carcinoma HeLa cells led to a constant increase in intracellular ROS levels and mitochondrial superoxide anion levels (Guzzo et al., 2014). When TRAP1 expression was rescued in shTRAP1 cells, both global ROS and mitochondrial superoxide levels returned to their basal values. Assessment of mitochondrial superoxide levels using the MitoSOX probe in SAOS-2 and MEF cells through cytofluorimetric analysis revealed that TRAP1 expression reduced intracellular ROS levels, providing protection against oxidative stress-induced cell death in conditions of serum and glucose depletion (Guzzo et al., 2014). Importantly, *Trap1* overexpression in non-transformed MEF resulted in a decrease in intracellular ROS and mitochondrial superoxide anion levels (Guzzo et al., 2014). These findings highlight the pathophysiological significance of TRAP1 in maintaining mitochondrial and redox homeostasis during specific stress conditions (Masgras et al., 2021), such as oxidative stress damage, and its role in protection against mitophagy and apoptosis.

1.3.3. TRAP1 Role in Neurodegeneration

Several *Drosophila* transgenic strains were created to examine the function of TRAP1 in neuronal degeneration (Butler et al., 2012; Zhang et al., 2013; Costa et al., 2013; Baqri et al., 2014; Kim et al., 2016). Ablation of *Drosophila Trap1* increased the susceptibility to stress induced by heat, paraquat, rotenone, or antimycin (Costa et al., 2013; Baqri et al., 2014). It also increased the production of mitochondrial ROS in the optic lobes of young adult fly brains (Baqri et al., 2014) and in the flight muscles in fly thoraces (Kim et al., 2016). However, another study demonstrated that mutation or knockdown of *Trap1* substantially improved *Drosophila* survival during oxidative stress caused by paraquat or rotenone (Kim et al., 2016). A recent study using RNA sequencing and quantitative proteomic analysis of IMR-32 human neuroblastoma cells suggested that cells overexpressing TRAP1 exhibit enhanced mitochondrial functions and improved TCA cycle functions (Dharaskar et al., 2023a). Another study from the same authors also reported that TRAP1 maintains mitochondrial integrity and augments glutamine metabolism upon glucose deprivation to meet the cellular energy demand (Dharaskar et al., 2023b) **(Fig. 5)**. Depletion of TRAP1 induces the mitochondrial unfolded protein response (mtUPR), which is a protective pathway involving communication between mitochondria and the nucleus activated in response to a mitochondrial stress signal (Kim et al., 2016; Lopez-Crisosto et al., 2021).

As already mentioned, TRAP1 plays a crucial role in the PINK1/Parkin signaling pathways, as it undergoes phosphorylation and activation by PINK1 (Pridgeon et al., 2007). However, the expression of *Trap1* fails to rescue the decreased ATP levels in the thorax, impaired mitochondrial integrity, and reduced levels of complex I subunits in *Parkin* mutant flies (Zhang et al., 2013). The same researchers have also demonstrated that TRAP1 is unable to rescue mitochondrial fragmentation and dysfunction when Parkin is silenced using small interfering RNA (siRNA) in human neuronal SH-SY5Y cells (Zhang et al., 2013). The expression of *Trap1* appears to be sufficient for reversing the phenotype observed in *Pink1* mutant flies, with motor impairment, reduced lifespan, and mitochondrial dysfunction (Costa et al., 2013). On the other hand, other studies have shown that inhibiting TRAP1 genetically and pharmacologically, rather than overexpressing it, in *Drosophila* significantly improves the survival rate during oxidative stress. This inhibition also rescues mitochondrial dysfunction and the loss of dopaminergic neurons caused by *Pink1* mutation (Kim et al., 2016). The specific expression of *Trap1* in neurons seems to be sufficient for suppressing neurodegeneration and reverse the respiratory deficit present in *Pink1* null or mutant flies (Cechetto et al., 2000; Masgras et al., 2021) **(Fig. 5B)**.

In Parkinson's disease models, decreased *Trap1* expression in flies expressing [A53T]α-synuclein exacerbates the loss of dopaminergic neurons and increases sensitivity to oxidative stress (Butler et al., 2012; Zheng et al., 2021). Interestingly, the overexpression of TRAP1 counteracts mitochondrial stress induced by [A53T]α-synuclein in flies, rat primary neurons, and SH-SY5Y human neuronal cells. The study also suggests that the ATPase domain of TRAP1 is essential for its protective effects (Buter et al., 2012).

Several studies have investigated the effects of TRAP1 ablation or knockdown *in vitro*, primarily utilizing the SH-SY5Y neuroblastoma cell line (Kubota et al., 2009; Chien et al., 2011; Takamura et al., 2012; Zhang et al., 2013). Knockdown of *TRAP1* in SH-SY5Y cells resulted in abnormal mitochondrial morphology, characterized by a decrease in fragmented mitochondria and an increase in connectivity. This effect was achieved through a nontranscriptional mechanism that led to reduced levels of dynamin-related protein 1 (Drp1) and mitochondrial fission factor (Mff), two proteins involved in mitochondrial fission. However, the expression levels of other fission proteins (Fis1 and mitochondrial dynamics of 51 kDa protein (MiD51)/mitochondrial elongation factor 1 (MIEF1)) and fusion proteins (mitofusin 1/2 (Mfn1/2) and optic atrophy protein (OPA)) remained unchanged. This suggests that TRAP1 plays a role in mitochondrial fusion/fission processes, which ultimately impact mitochondrial and cellular function (Takamura et al., 2012) **(Fig. 5A)**.

The Giffard laboratory conducted studies using *in vitro* and *in vivo* models of ischemic injury, which revealed a protective effect mediated by TRAP1 (Volobouéva et al., 2008; Xu et al., 2009). In primary astrocyte mouse cultures, TRAP1 overexpression resulted in decreased production of ROS, preserved mitochondrial membrane potential during glucose deprivation, and maintained ATP levels and cell viability during oxygen-glucose deprivation (Volobouéva et al., 2008). Moreover, *in vivo* overexpression of TRAP1 in neurons and astrocytes, through DNA transfection, significantly improved mitochondrial function, increased preservation of ATP levels in the brain, and a reduction in free radical generation and lipid peroxidation (Xu et al., 2009). Recently, in a study conducted on primary cultures of motor neurons from mice, it was observed that the overexpression of TRAP1 had a protective effect on these cells by preventing the loss of mitochondrial membrane potential, reducing the production of ROS, and rescuing neurons from death induced by oxidative stress. On the other hand, TRAP1 knockdown resulted in a decrease in mitochondrial membrane potential under basal conditions, but it did not exacerbate mitochondrial dysfunction or neuronal death under oxidative stress conditions (Clarke et al., 2022) **(Fig. 5A)**.

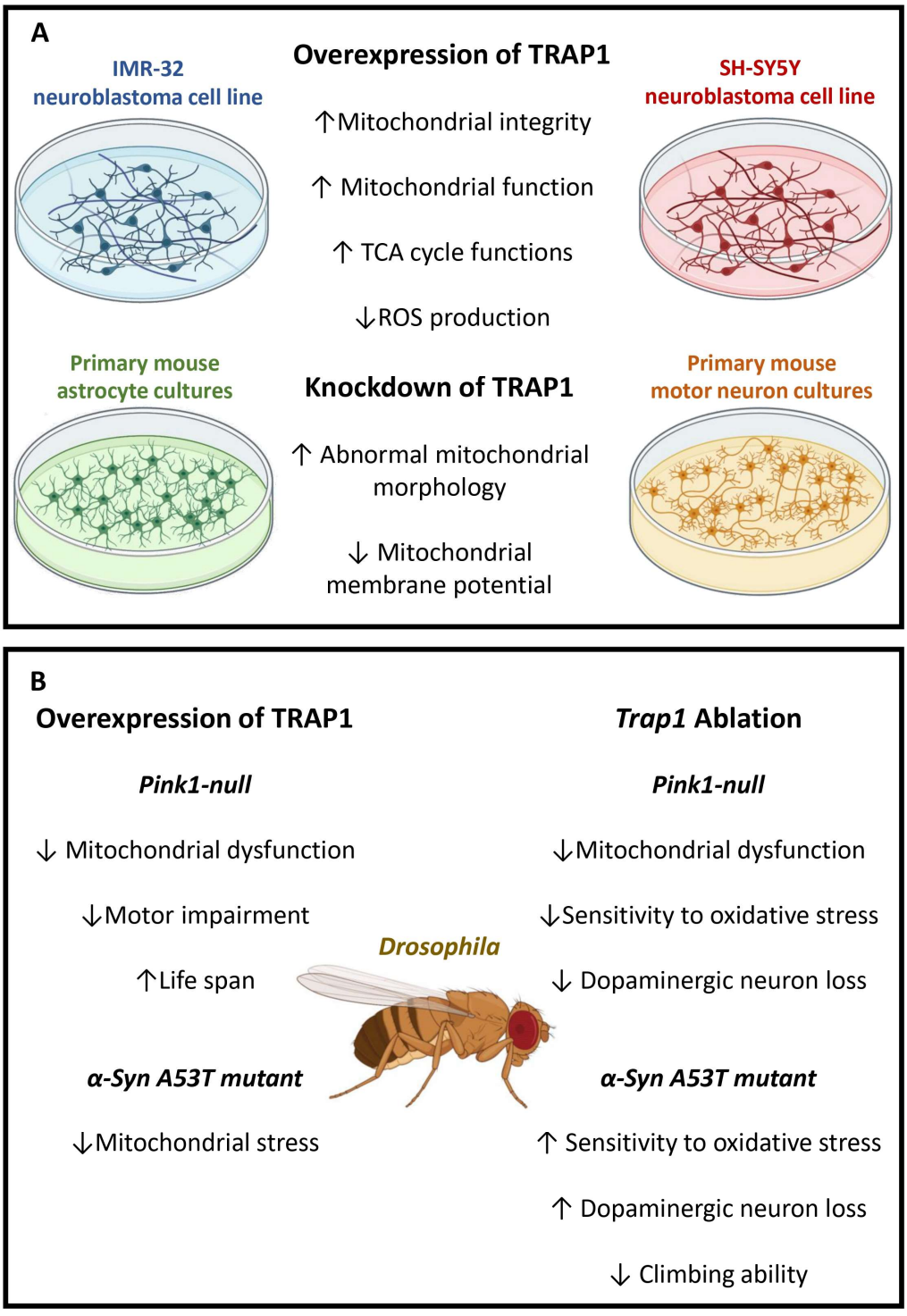

Figure 5. Role of TRAP1 in neurodegeneration. (A) IMR-32 human neuroblastoma cells overexpressing TRAP1 maintain mitochondrial integrity, exhibit enhanced mitochondrial function and improved tricarboxylic acid (TCA) cycle functions. SH-SY5Y neuroblastoma cells lacking TRAP1 show abnormal mitochondrial morphology. Primary mouse astrocyte cultures with TRAP1 overexpression present decreased production of reactive oxygen species (ROS) and significantly improved mitochondrial function.

Primary mouse motor neuron cultures overexpressing TRAP1 have a reduced production of ROS while cells lacking TRAP1 present a decrease in mitochondrial membrane potential. **(B)** In *Drosophila* animal models, overexpression of TRAP1 or *Trap1* ablation in different genetic backgrounds have different outcomes in terms of mitochondrial dysfunction, sensitivity to oxidative stress, survival of dopaminergic neurons, motor ability and life span. Illustration created with *BioRender*.

The important role of TRAP1 in neuroprotection is further supported by studies using TRAP1/HSP90 inhibitors, which have been found to induce neuronal toxicity and lead to visual disorders (reviewed in Ramos Rego et al., 2021). Although the expression of TRAP1 in the RPE has never been described in the literature, both HSP70 and its family member HSP90 have been identified in the retina (Wakakura et al., 1993; Kojima et al., 1996; Dean et al., 2001). In a recent study using a HSP90α murine knockout model, it was reported that HSP90α is essential for the maintenance of rod photoreceptors (Munezero et al., 2023). Furthermore, in human trials, some HSP90 inhibitors, such as 17-DMAG and NVP-AUY922, have caused visual disorders and retinal dysfunction. However, other inhibitors like 17-AAG and NV-HSP990 did not have similar effects (Chen et al., 2014; Bradley et al., 2014; Li et al., 2015; Yamaguchi et al., 2020). These findings related with the TRAP1 family member HSP90 highlights the involvement of TRAP1 in neurodegenerative processes, thereby opening possibilities for new therapeutic approaches focused on modulating this protein for addressing these devastating disorders.

1.4. Objectives of the Work and Hypothesis

In the context of AMD, oxidative stress-induced damage to the RPE occurs due to the excessive accumulation of ROS, primarily produced in mitochondria under pathological conditions. Maintaining mitochondrial function homeostasis is crucial for keeping ROS levels at physiological levels and preventing the metabolic dysfunction observed in AMD pathology. Therefore, it is important to investigate proteins that are novel players in oxidative stress mechanisms within the RPE in the context of AMD.

Considering the functions of TRAP1 described in other cell types, we propose that TRAP1 modulates mitochondrial metabolism in the RPE and plays a role in preventing the onset and progression of AMD. We hypothesize that TRAP1 mediates protection against oxidative stress in the RPE and therefore be a potential treatment target for AMD.

The objective of this study was to assess the presence and function of TRAP1 in the human RPE and investigate whether TRAP1 provides protection against oxidative stress in RPE cells. To test our hypothesis, we studied the cellular functions of TRAP1 in the RPE, using the Adult Human Retinal Pigment Epithelium-19 (ARPE-19) cell line as *in vitro* model. We also aimed to optimize and implement an experimental protocol for the differentiation of human induced pluripotent stem cells into RPE cells (iRPE) to access the presence of TRAP1 in a fully differentiated cell. Moreover, since TRAP1 expression is reported to be upregulated in tumours, it is important to confirm its expression in an RPE *in vitro* model that is not an immortalized or transformed cell line. The establishment of this model will allow us to perform key experiments in the future, using a more complex human RPE *in vitro* model, that better replicate the characteristics of primary human RPE. Using ARPE-19 cell line, we evaluated the effect of *TRAP1* ablation on cell viability, cell proliferation, cell mass, protein content and proliferation. Then, we assessed the impact of TRAP1 loss on intracellular ROS production and superoxide anion production. Mitochondrial morphology and network were also analyzed. Moreover, the effect of *TRAP1* silencing on mitochondrial respiration was determined. Finally, we have evaluated the impact of *TRAP1* ablation in the localization and levels of TRAP1 upon hydrogen peroxide-induced oxidative stress.

2. Materials and Methods

2. Materials and Methods

2.1. Adult Human Retinal Pigment Epithelium Cells (ARPE-19) Maintenance

The adult human retinal pigment epithelial cell line ARPE-19 obtained from the American Type Culture Collection (ATCC® CRL-2302, Manassas, USA) was maintained in Dulbecco's Modified Eagle Medium/Nutrient Mixture F-12 (DMEM/F-12) with GlutaMAX™ (Gibco, Waltham, USA) supplemented with 10% (*v/v*) Fetal Bovine Serum (FBS) (Gibco, Waltham, USA), and antibiotics (100 U/mL penicillin, 100 µg/mL streptomycin) (Gibco, Waltham, USA). The cells (passages 6 to 35) were maintained under a humidified atmosphere of 5% carbon dioxide (CO_2) at 37°C.

2.2. Human Induced Pluripotent Stem Cells (hiPSC) Maintenance

The culture of human induced pluripotent stem cells (hiPSCs) was conducted following the STEMCELL Technologies protocol. Previously validated hiPSC line LUMC0004iCTRL10 (Dambrot et al. 2013) was maintained by clonal propagation on growth factor-reduced Matrigel (Corning, New York, USA) in mTeSR Plus medium (STEMCELL Technologies, Vancouver, Canada) under a humidified atmosphere of 5% CO_2 at 37 °C. Briefly, cells were propagated through clonal propagation with the assistance of the RHO/ROCK pathway inhibitor Y-27632 (Tocris Bioscience, Bristol, United Kingdom) and passaged using Versene Solution (Thermo Fisher Scientific, Waltham, USA) or ReLeSR (STEMCELL Technologies, Vancouver, Canada).

2.3. Differentiation and Characterization of hiPSC-derived RPE Cells (iRPE)

To differentiate iRPE, we employed previously described and validated procedures (Maruotti et al., 2015; Smith et al., 2019) with minor modifications. Briefly, hiPSC were cultured on Matrigel in mTeSR Plus medium (STEMCELL Technologies, Vancouver, Canada) at a density of 20,000 cells per cm^2. Once the cells reached the desired confluence, approximately 5 days after passage, the mTeSR Plus medium was replaced with RPE differentiation medium (RPE DM) consisting of Dulbecco's Modified Eagle's Medium: Nutrient Mixture F-12 (DMEM/F12) (Invitrogen, Waltham, USA), 15% Knockout Serum (Invitrogen, Waltham, USA), 2 mM Glutamine (Invitrogen, Waltham, USA), 1× Nonessential amino acids (NEEA) (Invitrogen, Waltham, USA), 0.1 mM β-mercaptoethanol (Sigma-Aldrich, St. Louis, USA), and 1× Antibiotic-Antimycotic (Invitrogen, Waltham, USA). After 24 hours, the RPE DM was supplemented with 10 mM nicotinamide (NIC) (Sigma-Aldrich, St. Louis, USA) and 50 nM chetomin (CTM) (Sigma-Aldrich, St. Louis, USA), and the cells were further cultured for 13 days, with the culture medium being refreshed daily. Then, the cells were cultured in RPE DM medium supplemented

only with 10 mM NIC, with the culture medium being refreshed every other day. Subsequently, the cells were split on day 28 and cultured in RPE Medium, consisting of 70% DMEM (Invitrogen, Waltham, USA), 30% Ham's F-12 Nutrient Mix (Invitrogen, Waltham, USA), 1× B27 (Invitrogen, Waltham, USA), and 1× Antibiotic-Antimycotic (Invitrogen, Waltham, USA). The cells were split at day 56 and maintained in RPE Medium until day 84, with the culture medium being refreshed every other day. After the end of the differentiation protocol, the characterization of hiPSC-RPE cells were performed in passages 2 to 4 of cells cultured in RPE Medium. A detailed protocol is available at the Supplementary Material Section Nº 1.

2.4. Immunofluorescence

ARPE-19 cells were cultured in DMEM/F-12 supplemented with GlutaMAX™ (Gibco, Waltham, USA), 1% FBS (Gibco, Waltham, USA), and antibiotics (100 U/mL penicillin, 100 µg/mL streptomycin) (Gibco, Waltham, USA) for 24 hours. The cells were seeded on 12 mm glass coverslips in 24-well plates at a density of 60,000 cells/well for 24 hours before treatment. After treatment, ARPE-19 cells were fixed using a solution of 4% Paraformaldehyde (PFA) with 4% sucrose for 10 minutes, followed by washing with phosphate-buffered saline (PBS) and blocking for 1 hour with a solution containing 10% normal goat serum, 3% bovine serum albumin, and 0.3% Triton X-100 in PBS. The iRPE cells were cultured in RPE Medium and seeded in 12 mm glass coverslips coated with Matrigel in 24-well plates at a density of 100,000 cells/well and cultured for 8 days. Then, the hiPSC-RPE cells were fixed using the abovementioned fixing solution. Afterwards, both ARPE-19 and iRPE cells were incubated with primary antibodies at room temperature for 1 hour. The primary antibodies used in this study were TRAP1 (1:200; BD Bioscience, Franklin Lakes, USA), SAM50 (1:200; Sigma-Aldrich, St. Louis, USA), ZO-1 (1:250; Sigma-Aldrich, St. Louis, USA) and Ki67 (1:100, Agilent, Santa Clara, USA). After washing with PBS, the cells were incubated with fluorescent-labeled secondary antibodies, including goat anti-mouse/rabbit Alexa Flour 488 (1:200; Invitrogen, Waltham, USA) and goat anti-mouse/rabbit Alexa Flour 568 (1:200; Invitrogen, Waltham, USA), for 1 hour at room temperature. Finally, the cells were counterstained with DAPI (1:5,000; Invitrogen, Waltham, USA) and mounted using Glycergel mounting medium (Dako Cytomation, Glostrup, Denmark). The resulting images were captured using a confocal microscope (Zeiss LSM510, Carl Zeiss, Oberkochen, Germany).

2.5. Polymerase Chain Reaction

ARPE-19 cells underwent two washes with ice-cold sterile PBS. Total RNA was then extracted using the Trizol® reagent (Life Technologies, Carlsbad, USA) following the manufacturer's protocol. The concentration and purity of the RNA were determined using NanoDrop® (Thermo Fisher Scientific, Waltham, USA). Subsequently, 1 µg of total RNA was reverse-transcribed into complementary DNA (cDNA) using the NZY First-Strand cDNA Synthesis Kit (NZYTech, Lisbon, Portugal) according to the provided instructions. The cDNA was treated with RNase-H for 20 minutes at 37 °C and stored at -20 °C until further analysis. Amplification of the cDNA was carried out utilizing a BioRad T100 Thermal Cycler (Bio-Rad, Hercules, USA) in a 40 µL reaction volume containing MYtaq Red mix (NZYTech, Lisbon, Portugal) and 0.25 mM specific primers for TRAP1: HA29_TRAP1_FW 5'-GCTCTGGGAGTACGACATGG-3' and HA30_TRAP1_RV 5'-CTCCGAGGACACAGAATTGGT-3' (129 bp amplicon). The cycling conditions consisted of a melting step at 95 °C for 1 minute, annealing at 62 °C for 30 seconds, and elongation at 72 °C for 30 seconds, repeated for 35 cycles. PCR products were separated using a 2% (*w/v*) agarose gel.

2.6. Western Blotting

Protein extracts from ARPE-19 and iRPE cells were prepared in ice-cold radioimmunoprecipitation assay (RIPA) buffer containing 1 mM dithiothreitol (Sigma-Aldrich, St. Louis, USA) and a protease inhibitor cocktail (Sigma-Aldrich, St. Louis, USA). The protein concentration was determined using Bradford's assay (Invitrogen, Waltham, USA). A total of 20 µg and 40 µg of protein lysates were separated on a 12% gel from sodium dodecyl sulfate-polyacrylamide gel electrophoresis (SDS-PAGE) and transferred onto a polyvinylidene difluoride (PVDF) membrane. The membranes were then blocked in 5% skim milk for 1 hour at room temperature, followed by overnight incubation at 4°C with primary antibodies against TRAP1 (1:5,000; BD Bioscience, Franklin Lakes, USA), RPE65 (1:500; Thermo Fisher Scientific, Waltham, USA), CRALBP (1:500; Abcam, Waltham, USA) and β-actin (1:5,000; Sigma-Aldrich, St. Louis, USA). After washing three times with Tris Buffered Saline with 0.1% Tween 20 (TBST) for 10 minutes each, the membranes were incubated with the respective secondary antibody (anti-mouse, 1:10,000; Invitrogen, Waltham, USA) at room temperature for 1 hour. The membranes were then washed three times with TBST for 10 minutes each. Subsequently, the membranes were imaged using the ImageQuant LAS 500 system (GE Healthcare Bio-Sciences, Chicago, USA) and WesternBright Sirius™ substrate (Advansta, San Jose, USA). The protein band intensities for the experiments with ARPE-19 cells were quantified using Quantity One software (Bio-Rad, Hercules, USA), with β-actin serving as the loading control.

2.7 TRAP1 Silencing in ARPE-19 Cells

To suppress the expression of TRAP1, we employed 0.1 µM siRNA targeting Human TRAP1 (siTRAP1, NM_016292, SI00115150 A60-SIRNA, Qiagen, Hilden, Germany) (Butler et al., 2012). As a control, we used 0.1 µM scrambled control siRNA (siCTL, Unspecific_AllStars_1 A60-SIRNA SI03650318; Qiagen, Hilden, Germany). ARPE-19 cells were cultured in DMEM/F-12 medium supplemented with GlutaMAX™, 1% FBS, and antibiotics (100 U/mL penicillin, 100 µg/mL streptomycin). On day 0, ARPE-19 cells were seeded in a 96-, 24-, or 6-well plate at densities of 10,000, 60,000, or 115,000 cells/well, respectively, to achieve approximately 80% confluency at the time of transfection. On day 1, 4 hours before transfection, the medium was replaced with Opti-MEM medium (Gibco, Waltham, USA). Subsequently, depending on the well size, 0.5, 2, or 8 µL of the lipofectamine RNAiMAX transfection reagent (Invitrogen, Waltham, USA) was mixed with Opti-MEM medium. The master mix, consisting of siCTL or siTRAP1 at a concentration of 0.1 µM diluted in Opti-MEM medium, was combined with the diluted RNAiMAX in a 1:1 ratio and incubated at room temperature for 5 minutes. Then, depending on the well size, 10, 50, or 250 µL of the resulting solution was added dropwise to the cells. The cells were analyzed 24 or 72 hours after transfection. For the cells cultured for 72 hours, the culture medium was replaced with DMEM/F-12 medium supplemented with GlutaMAX™, 1% FBS, and antibiotics 48 hours after transfection.

2.8. Resazurin Assay

ARPE-19 cells were plated at a density of 10,000 cells per well in flat-bottom 96-well microplates. The cells were cultured in DMEM/F-12 medium with GlutaMAX™, supplemented with 1% FBS and antibiotics (100 U/mL penicillin, 100 µg/mL streptomycin). Subsequently, the ARPE-19 cells were exposed to 31.25, 62.5, 125, 500, 1000, or 2000 µM H_2O_2 (PanReac AppliChem, Ottoweg, Germany) for 24 hours. For the experiments evaluating the impact of TRAP1 loss in ARPE-19 cells, transfection was performed 24 hours after seeding, as previously described. To assess cell metabolic activity, Resazurin (Invitrogen, Waltham, USA) assay was used according to the manufacturer's instructions. The culture medium was replaced with DMEM/F-12 medium containing GlutaMAX™, antibiotics, and resazurin (1 mg/mL). The cells were then incubated at 37 °C for 2 hours, and the fluorescence was measured using a Synergy Multi-Mode Reader (BioTek, Winooski, USA) with excitation/emission wavelengths set at 550/590 nm. Afterwards, the cells were washed twice with PBS and fixed with 4% PFA in PBS for 10 minutes. Subsequently, the cell nuclei were counterstained with DAPI (1/5,000; Invitrogen, Waltham, USA). A high-content fluorescence microscope (INCell Analyzer 2000, GE Healthcare, Chicago, USA) was utilized to count the nuclei automatically. The resulting values were expressed as a percentage relative to the control group, which consisted of non-treated cells.

2.9. Sulforhodamine B Assay

After 72 hours of transfection, the culture medium was removed, and cells were rinsed with 1% PBS. Next, the cells were fixed with ice-cold 1% acetic acid in 100% methanol for 16 hours at -20 °C. The microplates containing the fixed cells were then dried at 37 °C. Following that, the cells were exposed to 0.5% Sulforhodamine B (SRB) (Sigma-Aldrich, St. Louis, USA) in 1% acetic acid for 30 minutes at 37 °C and subsequently rinsed three times with 1% acetic acid. The plates were allowed to dry before adding 10 mM Tris (pH 10), followed by incubation at room temperature for 15 minutes with agitation. Lastly, 200 µL of the solubilized solution was added to each well, and the optical density was measured at 540 nm. The SRB Assay was performed in collaboration with Master Sandra Mimoso Pinhanços and Doctor Hugo Fernandes from the Advanced Therapies Group at the Center for Neuroscience and Cell Biology.

2.10. Dihydroethidium Probe

The presence of superoxide anion was detected using the Dihydroethidium (DHE) probe. ARPE-19 cells were seeded in DMEM/F-12 with GlutaMAX™, supplemented with 1% FBS and antibiotics (100 U/mL penicillin, 100 µg/mL streptomycin), at a density of 60,000 cells/well on 12 mm glass coverslips placed in a 24-well plate. Silencing of TRAP1 was performed as previously described. After 24 or 72 hours of transfection, the cells were incubated with 10 µM Dihydroethidium (Invitrogen, Waltham, USA) diluted in PBS with 5% FBS for 30 minutes at 37 °C in a light-protected environment. Subsequently, the cells were rinsed twice with PBS, fixed with 4% PFA with 4% sucrose for 10 minutes, and permeabilized with PBS containing 1% Triton X-100 for 5 minutes. The cells were then counterstained with DAPI (1:5,000; Invitrogen, Waltham, USA) diluted in PBS containing 10% normal goat serum, 3% bovine serum albumin, and 0.3% Triton X-100. Samples were mounted using Glycergel mounting medium (Dako Cytomation, Glostrup, Denmark) and imaged using a confocal microscope (Zeiss LSM510, Carl Zeiss, Oberkochen, Germany). Mean fluorescence intensity (MFI) and the number of DAPI-positive nuclei were automatically calculated and counted using ImageJ v1.53C, with at least 4 images analyzed for each condition/experiment. The results are presented as MFI per cell.

2.11. Transmission Electron Microscopy

After 72 hours of transfection with siCTL or siTRAP1, ARPE-19 cells were fixed using a solution of 2.5% glutaraldehyde in 0.1 M sodium cacodylate buffer (pH 7.2), supplemented with 1 mM calcium chloride. Sequential post-fixation steps were carried out using 1% osmium tetroxide (Sigma-Aldrich, St. Louis, USA) for 1 hour, followed by contrast enhancement with 1% aqueous uranyl acetate for 90 minutes. Subsequently, the samples were rinsed with distilled water and dehydrated in a series of ethanol solutions ranging from 50% to 100%. They were then

impregnated and embedded using an Epoxy embedding kit (Fluka Analytical, Waltham, USA). Ultrathin sections with 70 nm thickness were mounted on copper grids (300 mesh) and stained with a 0.2% lead citrate solution for 7 minutes. Observations were conducted using an FEI-Tecnai G2 Spirit Bio Twin electron microscope operating at 100 kV. The Transmission Electron Microscopy was performed in collaboration with Doctor Mónica Zuzarte from the Imaging Lab at the Coimbra Institute for Clinical and Biomedical Research.

2.12. Mitochondrial Network

To label the mitochondrial network, Image-iT™ Tetramethylrhodamine Methyl Ester Reagent (TMRM) (Invitrogen, Waltham, USA) was used. At 72 hours post-transfection, ARPE-19 cells were incubated with a diluted solution of 75 nM TMRM Reagent in Hank's Balanced Salt Solution (HBSS) containing Ca^{2+} and Mg^{2+} for 30 minutes at 37 °C. Afterwards, the TMRM Reagent solution was replaced with Opti-MEM medium. Cell images were acquired using a Zeiss LSM710 confocal microscope (Carl Zeiss, Oberkochen, Germany) equipped with an environmental chamber. The acquired images were analyzed using ImageJ v1.53K software (National Institute of Health, USA). Parameters were calculated using the Mito-Morphology ImageJ macro (Dagda et al., 2009). The average area-to-perimeter ratio was used as an indicator of mitochondrial interconnectivity, while inverse circularity was employed to evaluate mitochondrial elongation (Dagda et al., 2009).

2.13. Oxygen Consumption and Extracellular Acidification Rate

The Seahorse XFe96 Extracellular Flux Analyzer Technology (Agilent, Santa Clara, USA) was used to determine the oxygen consumption rate (OCR) and extracellular acidification rate (ECAR) of ARPE-19 cells. ARPE-19 cells, at a density of 10,000 cells per well were seeded in XF96-well plates (Agilent, Santa Clara, USA). After 24 hours, the cells were transfected with siCTL or siTRAP1 and then cultured for an additional 48 hours. Subsequently, the cell culture medium was replaced with 175 µL/well of pre-warmed low-buffered serum-free minimal DMEM medium (Sigma-Aldrich, St. Louis, USA) supplemented with glucose (17.5 mM), L-glutamine (2 mM), and sodium pyruvate (0.5 mM). The pH was adjusted to 7.4, and the cells were incubated at 37 °C in a non-CO_2 incubator for 1 hour to ensure temperature and pH equilibrium before the first-rate measurement. Oligomycin, Carbonyl Cyanide p-trifluoro-methoxyphenyl Hydrazone (FCCP), rotenone, and antimycin A solutions were prepared in DMSO, diluted in low-buffered serum-free DMEM medium, and pre-loaded (25 µL) into the ports of each well in the XFe96 sensor. The XFe96 Extracellular Flux Analyzer was loaded with the sensor cartridge and calibration plate for calibration. Subsequently, 2 µM oligomycin was injected into reagent delivery port A, 1 µM FCCP into port B, and 1 µM rotenone plus 1 µM antimycin A into port C,

followed by mixing. To measure the OCR of the cells, three baseline rate measurements of OCR and ECAR were conducted using a 3-minute mixing and 5-minute measuring cycle. The total protein content in each well was determined using the SRB assay, and the raw data was normalized to the total protein content in each well. The analysis of the results was performed using the Software Version Wave Desktop 2.6 (Agilent, Santa Clara, USA). The Seahorse Assay was performed in collaboration with Doctor José Teixeira and Doctor Paulo Oliveira from the Mitochondria, Metabolism and Disease Group at the Center for Neuroscience and Cell Biology.

2.14. Statistical Analysis

Statistical analysis involved testing the normality of the distribution through the Kolmogorov–Smirnov test. If the data did not follow a normal distribution, statistical significance was calculated using the Mann-Whitney U test; otherwise, an unpaired t-test was used. The mean ± standard error of the mean (SEM) was used to express the values, and p values < 0.05 were considered statistically significant. Unless stated otherwise, at least three independent experiments (n=3) were conducted for analysis. All statistical analyses were performed with GraphPad Prism, version 9.0 (GraphPad Software, Boston, USA).

3. Results

3. Results

3.1. TRAP1 Localizes in the Mitochondria of Human Retinal Pigment Epithelial Cells

The presence of TRAP1 messenger RNA (mRNA) in ARPE-19 cells was confirmed through PCR analysis, using specific primers **(Fig. 6A)**. Additionally, the detection of TRAP1 protein in these cells was demonstrated by Western Blotting and immunocytochemistry **(Fig. 6B, C, D)**. Notably, the expression of TRAP1 protein was found to co-localize with MitoTracker **(Fig. 6C)**, a dye that selectively accumulates in mitochondria (Iacovelli et al., 2011), and with the sorting and assembly protein-50 (SAM50) **(Fig. 6D)**, a mitochondrial protein, suggesting that TRAP1 is located within the mitochondrial compartment.

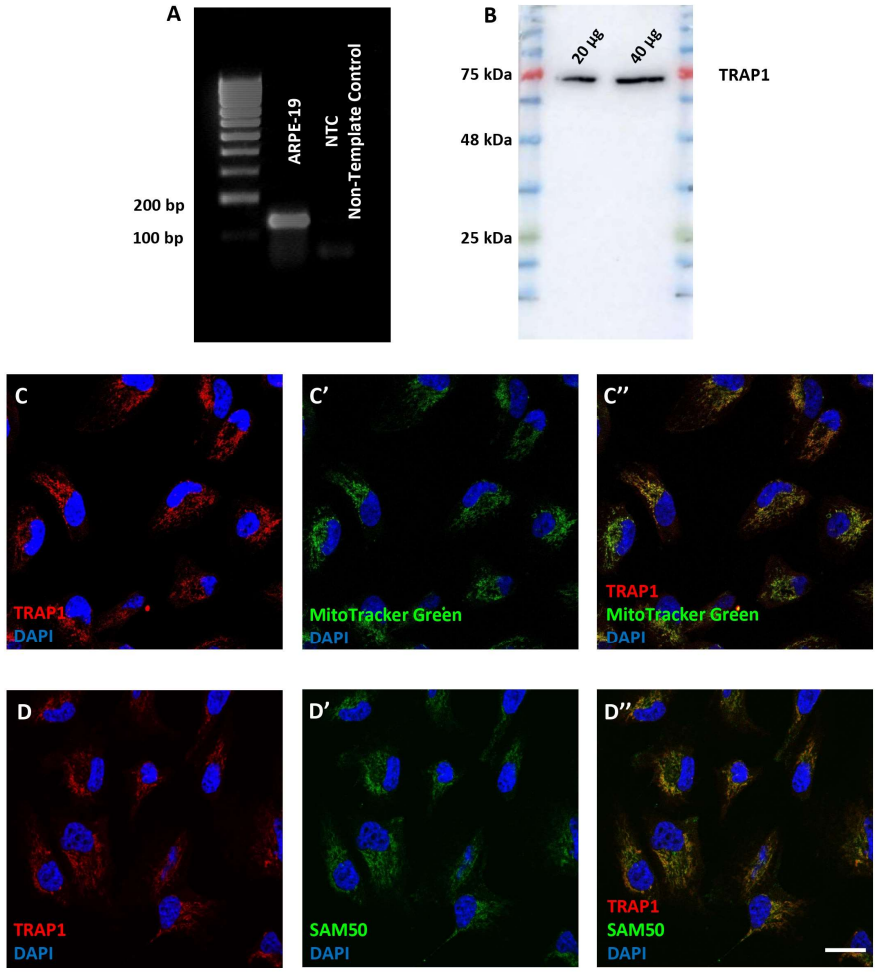

Figure 6. TRAP1 is expressed in human RPE cells. TRAP1 messenger RNA (mRNA) (A) and protein (B) are expressed in ARPE-19 cells. TRAP1 is located mainly in the mitochondria of ARPE-19 cells where it co-localizes with MitoTracker green (C) and the mitochondrial sorting and assembly protein-50 (SAM50) (D). NTC: Non-template control. Scale bars: 10 µm.

3.2. Impact of Oxidative Stress on Cell Viability and TRAP1 Levels

Exposure to hydrogen peroxide (H_2O_2) is commonly utilized as a model to evaluate the susceptibility to oxidative stress and antioxidant activity of retinal pigment epithelial (RPE) cells (Mitter et al., 2014; Aryan et al., 2016; Brown et al., 2019). To determine the optimal concentration and incubation time, ARPE-19 cells were exposed to several concentrations of H_2O_2 for 2 hours **(Fig. 7A)**, 4 hours **(Fig. 7B)**, and 24 hours **(Fig. 7C)**, and cell metabolic activity was assessed using the resazurin assay **(Fig. 7)**.

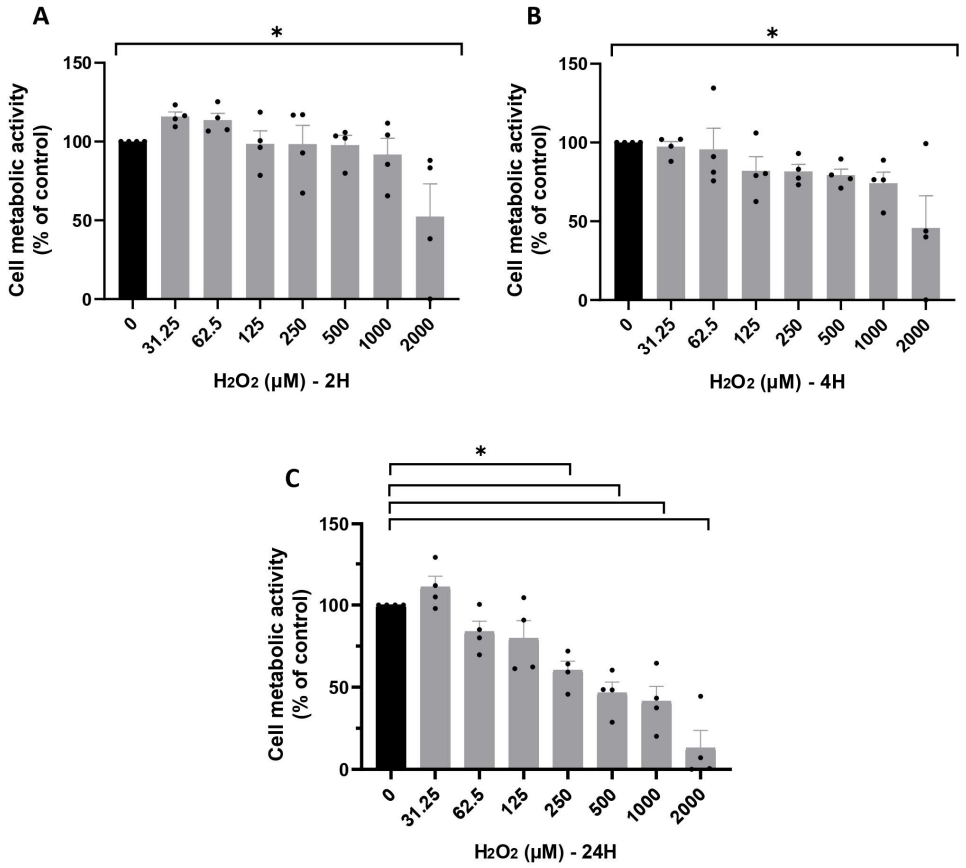

Figure 7. Assessment of cell metabolic activity of ARPE-19 cells upon challenge with hydrogen peroxide. ARPE-19 cells were treated with different doses of hydrogen peroxide (H_2O_2) (0; 31.25; 62.5; 125; 125; 250; 500; 1000 and 2000 µM) for 2 hours (A), 4 hours (B) and 24 hours (C). NS: Non-stimulated (black bars); ST: stimulated with H_2O_2 (grey bars). The values are presented as a percentage of the control (non-treated cells). Cell metabolic activity was assessed using the resazurin assay. Four independent experiments were performed (n=4). Statistical significance was calculated using the Mann-Whitney U test. Statistically significant values: * $p < 0.05$. In the graphs, all values are expressed as mean ± standard error of the mean (SEM).

The viability of ARPE-19 cells decreased in a concentration-dependent manner upon 24-hour exposure to H_2O_2 **(Fig. 2)**. Considering this, for subsequent experiments, a concentration of 500 µM H_2O_2 with a 24-hour incubation period was chosen, as these conditions resulted in a 53.5% ± 6.6% reduction in cell viability compared to the control (non-treated cells; $p = 0.0286$).

To investigate whether the levels and localization of TRAP1 in ARPE-19 cells were altered under oxidative stress, cells were treated with 500 µM H_2O_2 for 24 hours **(Fig. 8)**. Our findings revealed that the localization of TRAP1 remained consistent between non-treated cells **(Fig. 8A)** and treated cells **(Fig. 8B)**. However, western blot analysis demonstrated a decrease in TRAP1 levels (61.4% ± 9.1%) following exposure to 500 µM H_2O_2 for 24 hours **(Fig. 8C,D)**.

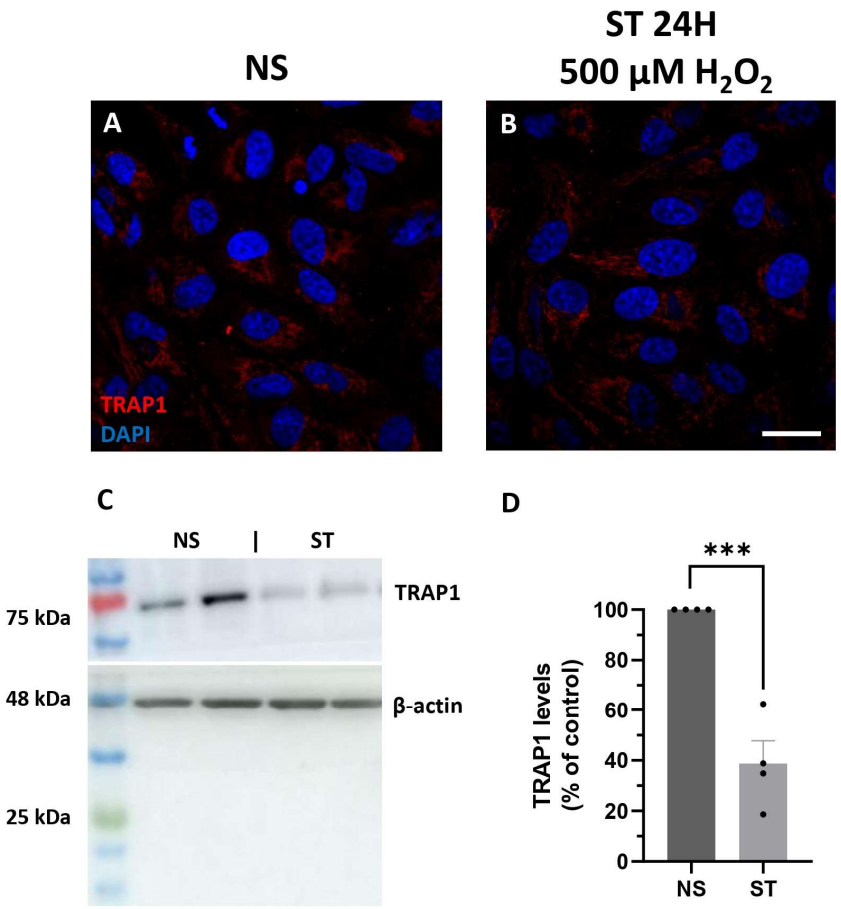

Figure 8. TRAP1 levels decrease upon challenge with hydrogen peroxide. ARPE-19 cells were treated (ST), or not (NS), with 500 µM H_2O_2 for 24 hours. Scale bar in A and B: 20 µm. (D) Exposure to 500 µM H_2O_2 for 24 hours resulted in lower levels of TRAP1. NS: Non-stimulated (dark grey bars); ST: stimulated with H_2O_2 (light grey bars). The values are presented as a percentage of the control (non-treated cells). Four independent experiments were performed (n=4). For the graph D, statistical significance was calculated by

using an unpaired *t*-test. Statistically significant values: * $p < 0.05$, ** $p < 0.01$, *** $p < 0.001$. In the graphs, all values are expressed as mean ± standard error of the mean (SEM).

3.3. TRAP1 Silencing Decreases Cell Metabolic Activity

We aimed to investigate the impact of TRAP1 silencing on cell metabolism (measured as dehydrogenase activity), ROS production, cell proliferation, and cell survival in RPE cells. By using a specific siRNA for TRAP1 (siTRAP1) (Butler et al., 2012), we achieved a reduction of approximately 50% in TRAP1 levels after 72 hours of silencing **(Fig. 9B, C, D, E)**. In contrast, transfection of a scramble control siRNA (siCTL), used as a reference, did not influence TRAP1 levels **(Fig. 9A, B, D, E)**. Following 72 hours of TRAP1 silencing, we observed a 33.8% decrease in cell metabolic activity, as determined by the resazurin assay **(Fig. 9F)**. Notably, TRAP1 silencing did not exacerbate the decline in cell metabolic activity in ARPE-19 cells exposed to 500 μM of H_2O_2 for 24 hours **(Fig. 9G)**. The total number of cell nuclei **(Fig. 9H)**, cell mass quantified through the sulforhodamine B (SRB) assay **(Fig. 9I)**, and the number of proliferating cells indicated by the number of Ki67-positive cells **(Fig. 9J)** remained comparable to the siCTL control. These findings suggest that TRAP1 silencing primarily induces a reduction in cell metabolic activity, rather than promoting cell death or reducing proliferation.

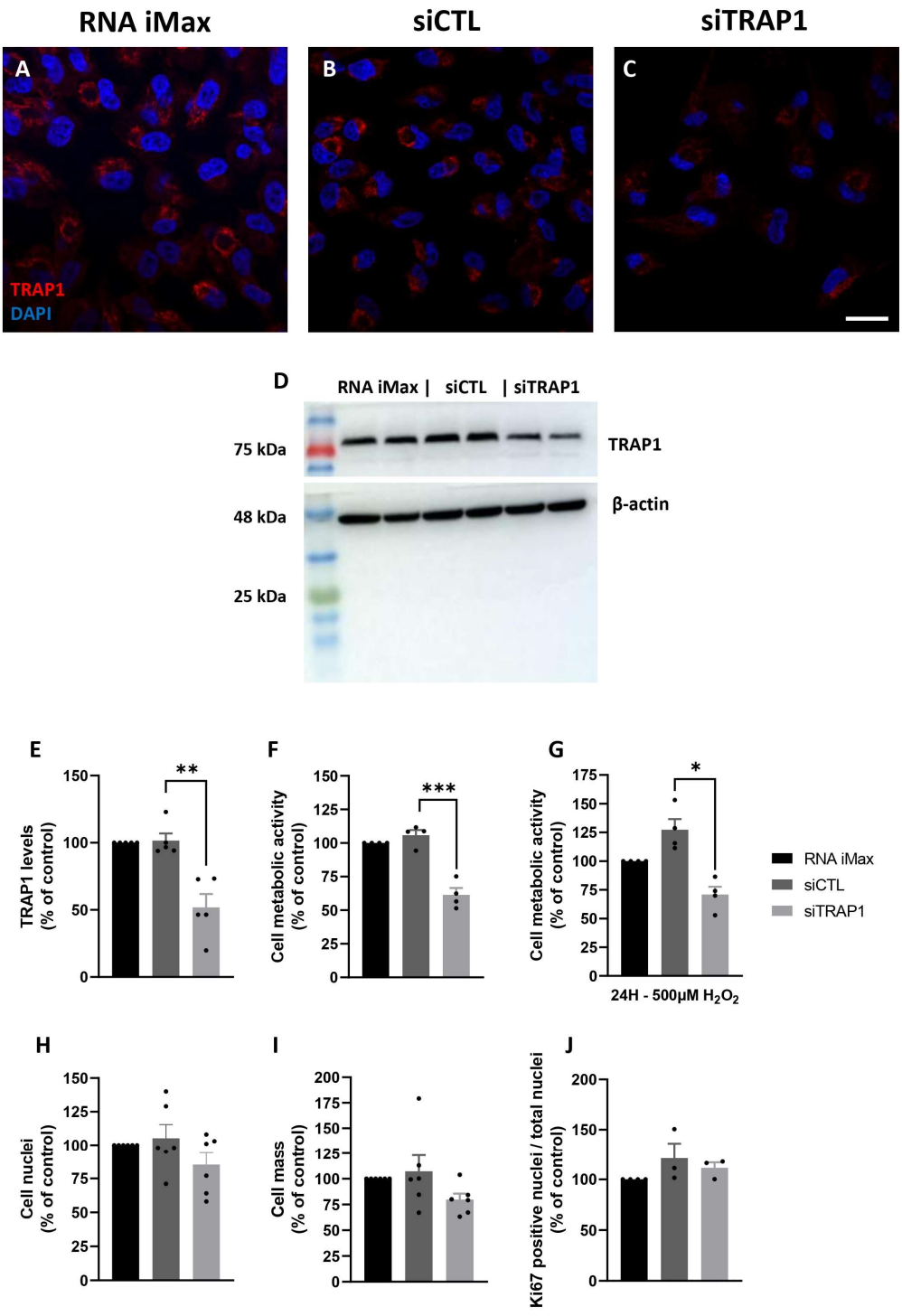

Figure 9. TRAP1 silencing decreases ARPE-19 cellular metabolism. Seventy-two hours after TRAP1 silencing using a specific siRNA (siTRAP1), the levels of TRAP1 were reduced by approximately 50% (A, C, D, E), while the scramble control siRNA (siCTL) did not affect TRAP1 levels (A, B, D, E) compared to the incubation with only the transfection reagent (lipofectamine RNAiMAX) (A, D, E). Scale bars in A-C: 20 µm. TRAP1 siRNA-mediated silencing decreased the cell metabolic activity measured by the resazurin

assay (F). TRAP1 silencing did not further decrease cell metabolic activity upon treatment of cells with 500 µM H_2O_2 for 24 hours (G). The total number of cell nuclei (H), cell mass measured by sulforhodamine B (SRB) assay (I) and the number of proliferating Ki67-positive cells (H) did not change upon TRAP1 silencing. Black bars: cells incubated only with lipofectamine RNAiMAX reagent. Dark grey bars: cells transfected with lipofectamine RNAiMAX reagent and siCTL. Light grey bars: cells transfected with lipofectamine RNAiMAX reagent and siTRAP1. Number of independent experiments: E (n=5); F (n=8); G (n=4); H (n=5); I (n=6); J (n=4). Statistical significance was calculated using the Mann-Whitney U test. Statistically significant values: * $p < 0.05$, ** $p < 0.01$, *** $p < 0.001$. In the graphs, all values are expressed as mean ± standard error of the mean (SEM).

3.4. TRAP1 Silencing Increases Reactive Oxygen Species Production

To investigate the impact of TRAP1 silencing on free radical levels, we evaluated the production of superoxide anions using the dihydroethidium (DHE) assay at 24- and 72-hours following transfection **(Fig. 10)**. Following TRAP1 silencing, we observed an elevation in DHE signal at both 24- and 72-hours post-transfection **(Fig. 10)**. These findings indicate that TRAP1 may play a regulatory role in controlling the levels of superoxide anions in these cells.

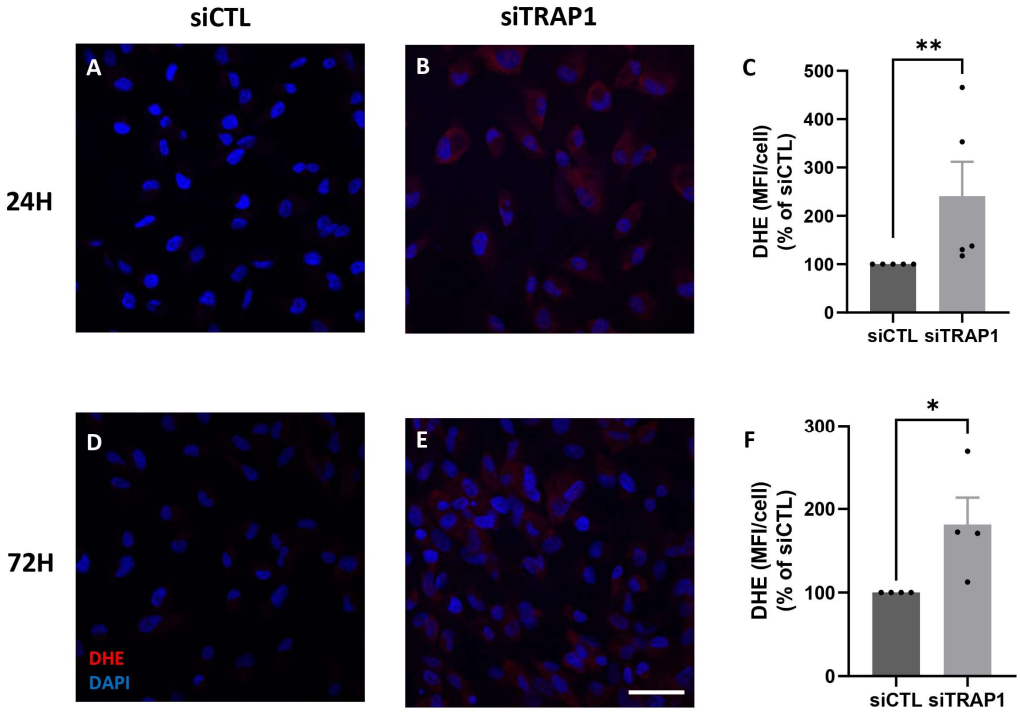

Figure 10. TRAP1 silencing in ARPE-19 cells increase the levels of superoxide anion. Representative confocal microscopy images of fluorescent detection of reactive oxygen species (ROS) by dihydroethidium (DHE) in cells transfected with siCTL (A, D) and siTRAP1 (B, E) for 24 hours (A, B) and 72 hours (D, E). Scale bars: 20 µm. Mean fluorescence intensity (MFI) of at least 4 images per condition/experiment, was

measured using Image J v1.53C, and divided by the number of the DAPI-positive nuclei (MFI/cell) (C, F). Dark grey bars: cells transfected with lipofectamine RNAiMAX reagent and siCTL. Light grey bars: cells transfected with lipofectamine RNAiMAX reagent and siTRAP1. Four independent experiments were performed (n=4). Statistical significance was calculated using the Mann-Whitney U test. Statistically significant values: * $p < 0.05$, ** $p < 0.01$. In the graphs, all values are expressed as mean ± standard error of the mean (SEM).

3.5. TRAP1 Silencing Impairs Mitochondrial Structure

We conducted a comprehensive analysis to examine the impact of TRAP1 silencing on mitochondrial physiology. Initially, we assessed the effect on mitochondrial ultrastructure using transmission electron microscopy (TEM). Silencing of TRAP1 in ARPE-19 cells did not significantly alter the mitochondrial ultrastructure, as clear cristae and membranes were observed **(Fig. 11A, B)**. To complement this analysis, mitochondria were stained with TMRM Reagent and morphological parameters such as mitochondrial interconnectivity and elongation were quantified (Tso et al., 2022). No fragmentation of mitochondria was observed in the siTRAP1 cells compared to the control **(Fig. 11C, D)**. Furthermore, TRAP1 silencing did not affect mitochondrial interconnectivity **(Fig. 11F)** but led to increased mitochondrial elongation **(Fig. 11E)** compared to siCTL cells.

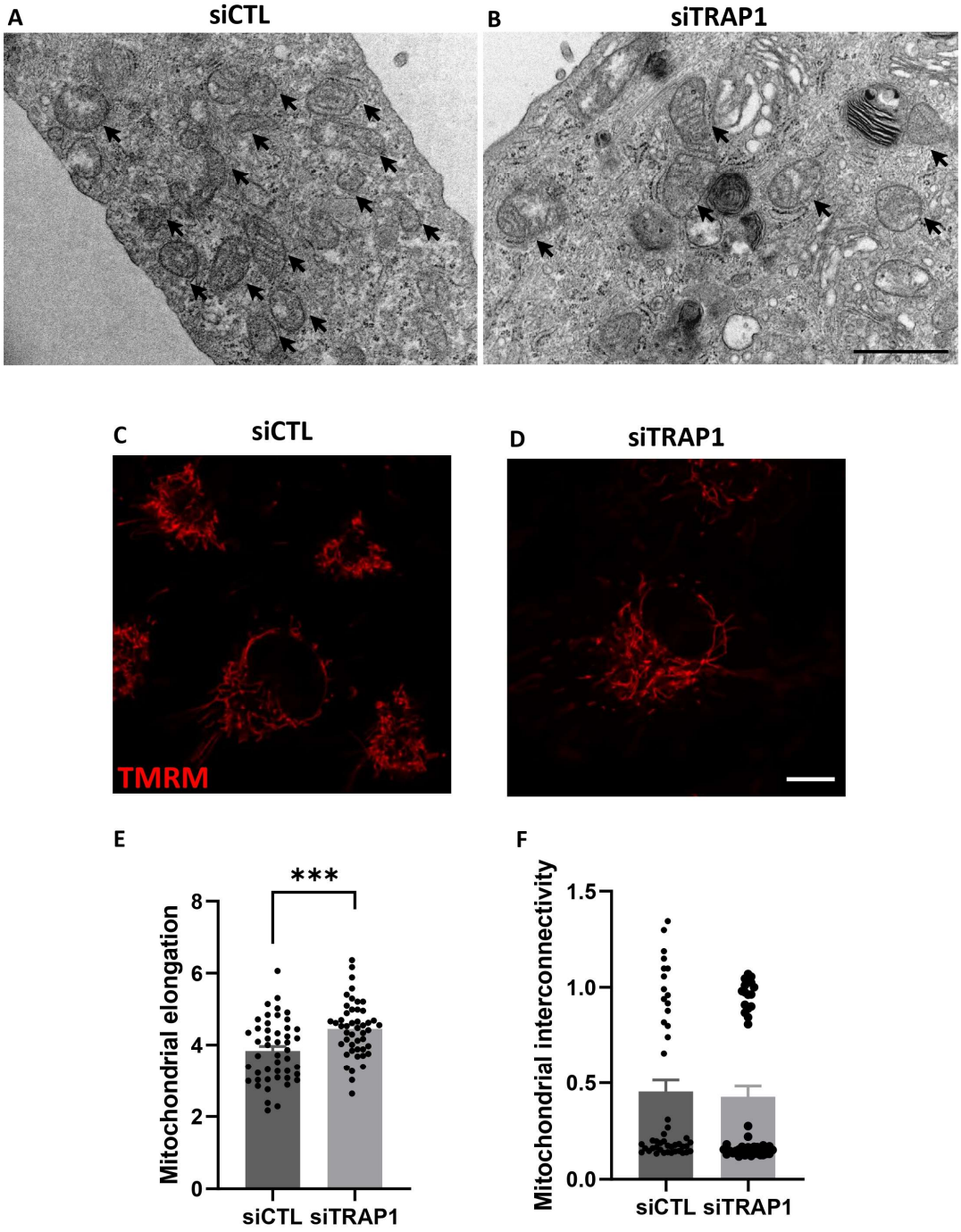

Figure 11. TRAP1 silencing increases mitochondrial elongation without affecting mitochondrial ultrastructure. Transmission electron microscopy (TEM) images of mitochondria from ARPE-19 cells transfected with siCTL (A) or siTRAP1 (B). Representative mitochondria (indicated by black arrows) are presented. Scale bars in A and B: 100 nm. Confocal live imaging microscopy images for mitochondrial labelling in ARPE-19 cells transfected with siCTL (C) or siTRAP1 (D) Scale bars in C and D: 50 µm. siTRAP1 cells showed increased mitochondrial elongation (E). The mitochondrial interconnectivity was similar between the two experimental groups (F). Dark grey bars: cells transfected with lipofectamine

RNAiMAX reagent and siCTL. Light grey bars: cells transfected with lipofectamine RNAiMAX reagent and siTRAP1. Statistical significance was calculated by using an unpaired t-test. Statistically significant values: * $p < 0.05$, ** $p < 0.01$, *** $p < 0.001$. In the graphs, all values are expressed as mean ± standard error of the mean (SEM).

3.6. TRAP1 Silencing Impacts Mitochondrial Energetic Status

We also evaluated the effects of TRAP1 silencing on mitochondrial oxygen consumption rates (OCR) and extracellular acidification rate (ECAR) in ARPE-19 cells **(Fig. 12A)**. TRAP1 silencing resulted in a significant reduction in OCR. TRAP1 silencing resulted in a 60-70% reduction in basal OCR, maximal OCR and ATP production-linked OCR **(Fig. 12C, D, E)** as well as approximately 50% reduction in proton leak-related OCR **(Fig. 12F)**. Additionally, there was a slight decrease in basal extracellular acidification rate (ECAR) **(Fig. 12B)**. Measurement of these two major energy-producing pathways, mitochondrial respiration (represented by OCR) and glycolysis (indirectly measured by ECAR), enables the identification of four bioenergetic phenotypes: quiescent, energetic, aerobic, and glycolytic. Notably, plotting the average data of basal OCR **(Fig. 12C)** against basal ECAR **(Fig. 12B)** revealed that TRAP1 silencing shifted the cellular metabolic profile towards a more quiescent phenotype compared to untreated cells **(Fig. 12B, C)**.

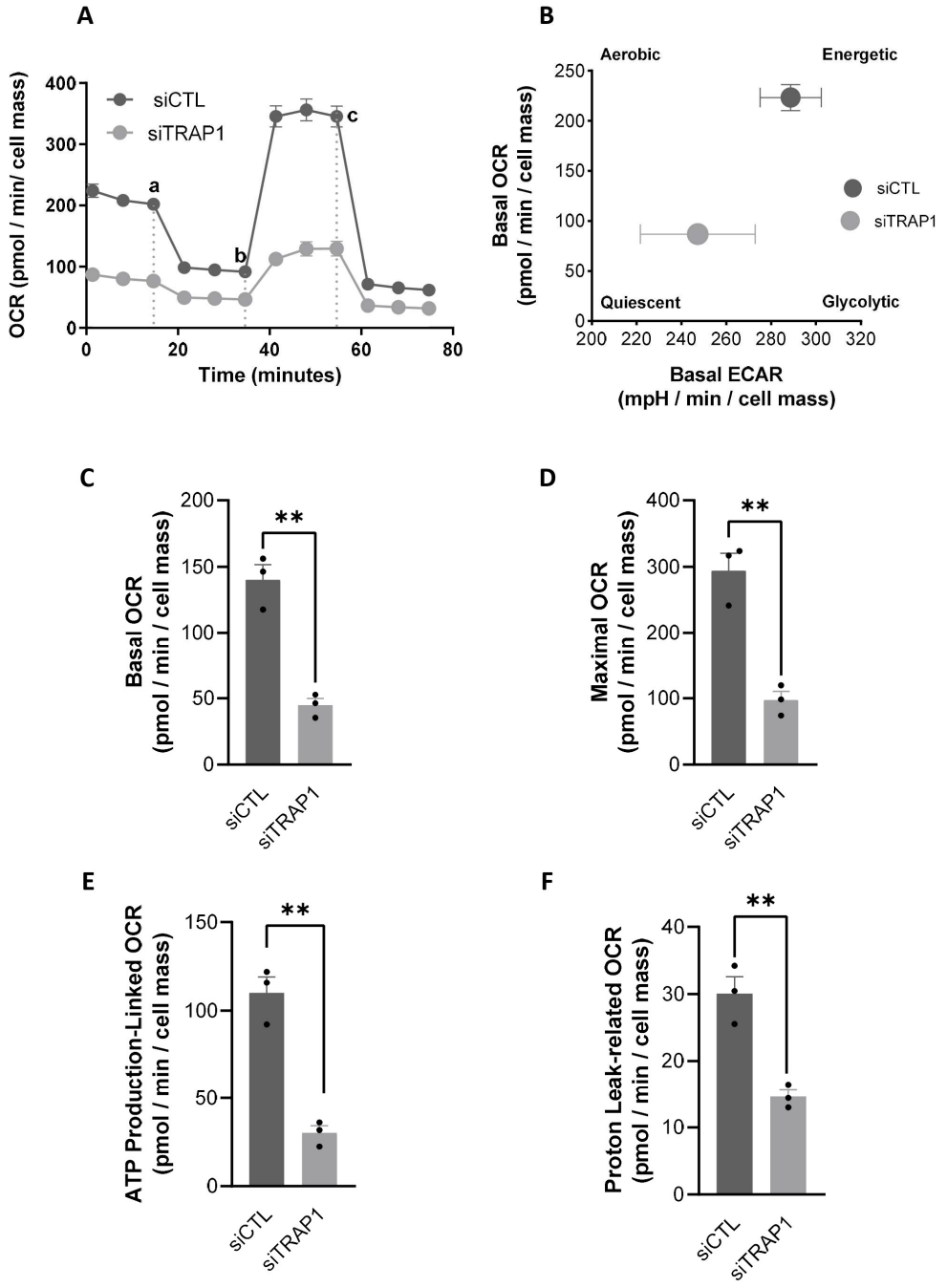

Figure 12. TRAP1 silencing drives a quiescent metabolic state. (A-F) Representative images of oxygen consumption rate (OCR) and extracellular acidification rate (ECAR) measurements using a Seahorse XFe96 Extracellular Flux Analyzer. A shift towards a more quiescent phenotype was observed when the average mitochondrial basal OCR was plotted against the average basal ECAR (B). A decrease in mitochondrial OCR was paralleled by a slight decrease in ECAR (B). siTRAP1 cells presented a decreased basal and maximal OCR when compared to the siCTL cells (C, D). siTRAP1 silencing significantly reduced the ATP production-linked (E) and proton leak-related (F) OCR. Data are the mean ± SEM of 3 independent experiments and show the effects of mitochondrial inhibitors (a) oligomycin (2 µM), (b) FCCP (1 µM) and

(c) antimycin A (1 µM) plus rotenone (1 µM) injected as indicated. The results are expressed as pmol O^2/min/cell mass for OCR and mpH/min/cell mass for ECAR. Dark grey bars: cells transfected with lipofectamine RNAiMAX reagent and siCTL. Light grey bars: cells transfected with lipofectamine RNAiMAX reagent and siTRAP1. Statistical significance was calculated by using an unpaired t-test. Statistically significant values: * $p < 0.05$, ** $p < 0.01$, *** $p < 0.001$. In the graphs, values are expressed as mean ± standard error of the mean (SEM).

3.7. Differentiation and Characterization of iRPE

To differentiate RPE from hiPSC, we used the hiPSC line LUMC0004iCTRL10 **(Fig. 13)**, previously validated as being pluripotent with low levels of somatic variation (Dambrot et al. 2013).

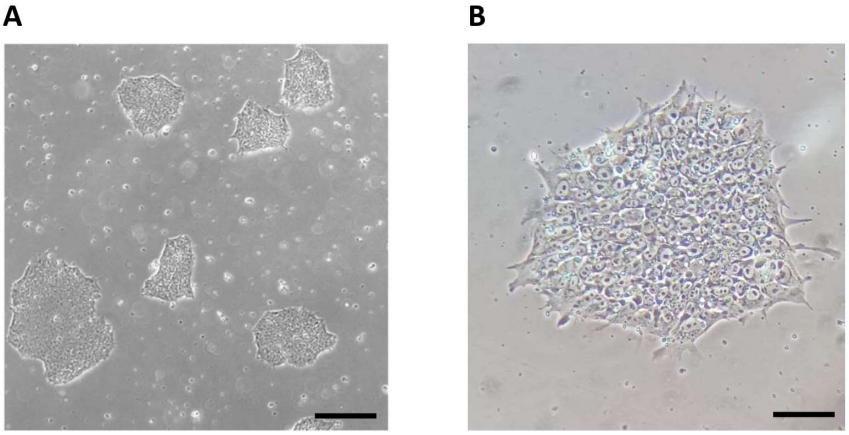

Figure 13. Human induced pluripotent stem cell line LUMC004iCTRL10. Microscopy images of the hiPSC line LUMC004iCTRL10 passage 19. Scale bars: (A) 250 µm, (B) 125 µm. Magnifications: (A) 20X and (B) 40X.

Then, we employed a protocol based in the validated protocols from Maruotti *et al.* and Smith *et al.*, with minor modifications (Maruotti et al., 2015; Smith et al., 2019) **(Fig. 14A)**, altering and adjusting the cell plating densities and the CO_2 levels in the cell culture incubator. During the second month of differentiation, we started to observe some domes and rosette-like structures, as indicated by the black arrows in **Fig. 14H, I**. Cells also formed a very thigh pigmented monolayer. Indeed, at differentiation day (dd) 56, pigmentation was clearly observed in the cell pellet resultant from the splitting and centrifugation of cells **(Fig. 14J, K)**. At dd 84, the final day of the differentiation process, virtually all cells were strongly pigmented **(Fig. 14M, L)**.

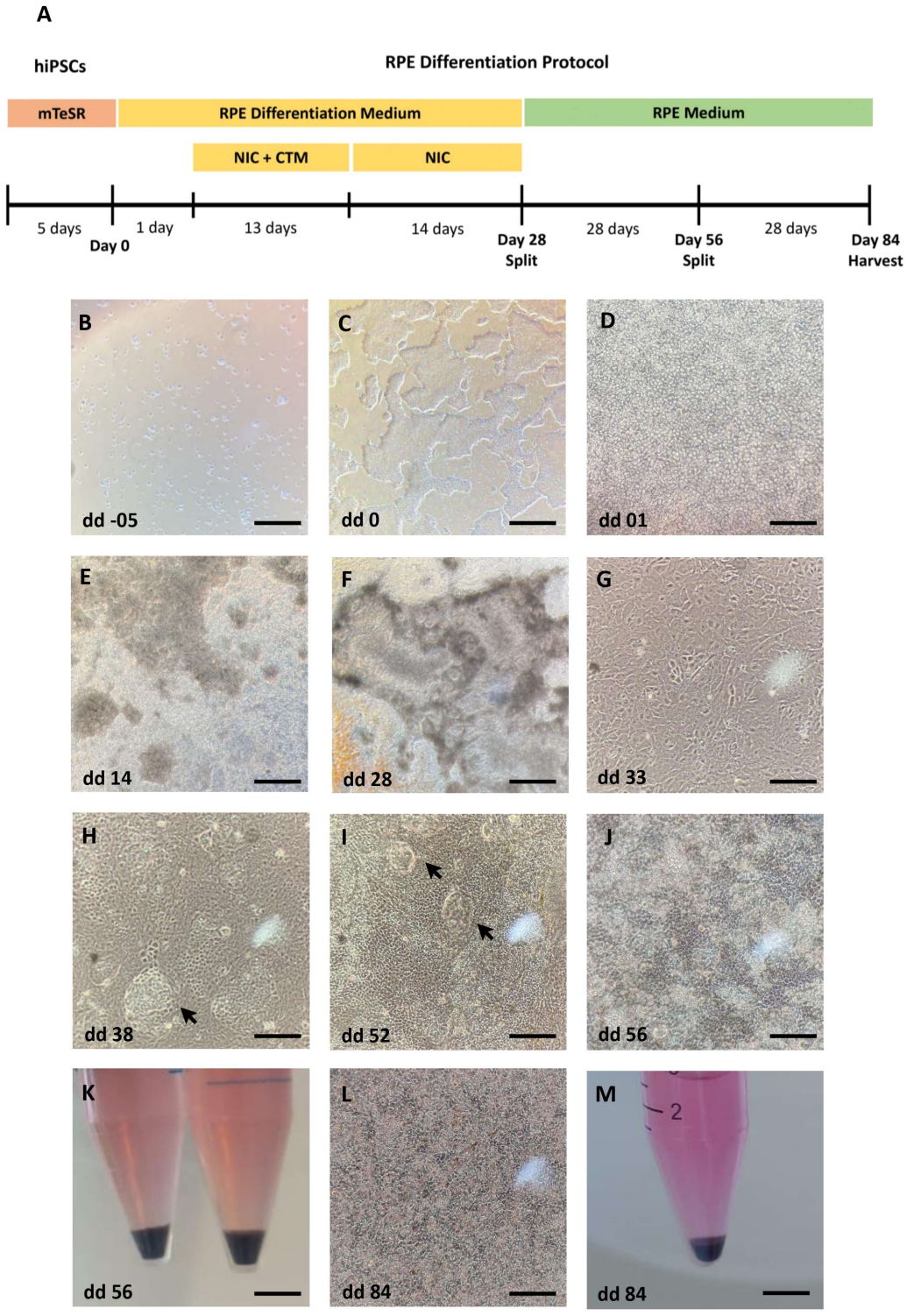

Figure 14. Differentiation of hiPSC into RPE. (A) Schematic protocol of hiPSC differentiation into RPE using a combination of Nicotinamide (NIC) and Chetomin (CTM). (B, C, D, E F, G, H, I, J, L) Microscopy images of the morphology of the differentiating cells through the differentiation process. (B) Cells at

differentiation day (dd) -05, after split and plating at high density. (C) Cells at dd 0 of the differentiation, right after medium change from mTSeR Plus to RPE differentiation medium (RPE DM). (D) Cells at dd 01, the first day with NIC and CTM induction. (E) Cells at dd 14, right after the medium change to RPE DM with NIC induction only. (F) Cells at dd 28, right before splitting and amplification. (H, I) During the second month of differentiation, domes and rosette-like structures were visible, as indicated by the black arrows. (J) Cells have formed a very thigh pigmented monolayer and were ready to split and amplification. (K) Cell pellet resultant from the splitting and centrifugation of cells at dd 56, pigmentation was clearly observed. (L) Cells at dd 84, the final day of differentiation. (M) Cell pellet resultant from the harvesting and centrifugation of cells at dd 84, dark pigmentation was evident. Scale bars: (B, D, L) 500 µm, (C, E, F, J) 250 µm, (G, H, I) 125 µm (K, M) 10 mm. Magnifications: (B, D, L) 10X, (C, E, F, J) 20X and (G, H, I) 40X.

After the end of the differentiation process, we collected the iRPE cells and performed a molecular characterization of the cells to access if they express RPE specific markers. In fact, key RPE markers such as retinal pigment epithelium-specific protein of 65 kDa (RPE65), the cellular retinaldehyde-binding protein (CRALBP) and the tight junction protein zonula occludens 1 (ZO-1) **(Fig. 15)** were expressed in the iRPE cells resultant from our differentiation protocol. Moreover, the cells showed the polarity expected of RPE cells, with ZO-1 showing predominant apical localization **(Fig. 15E, F)**. Finally, we also demonstrated that TRAP1 protein is expressed in the iRPE cells resultant from our differentiation protocol **(Fig. 15G, H, I)**.

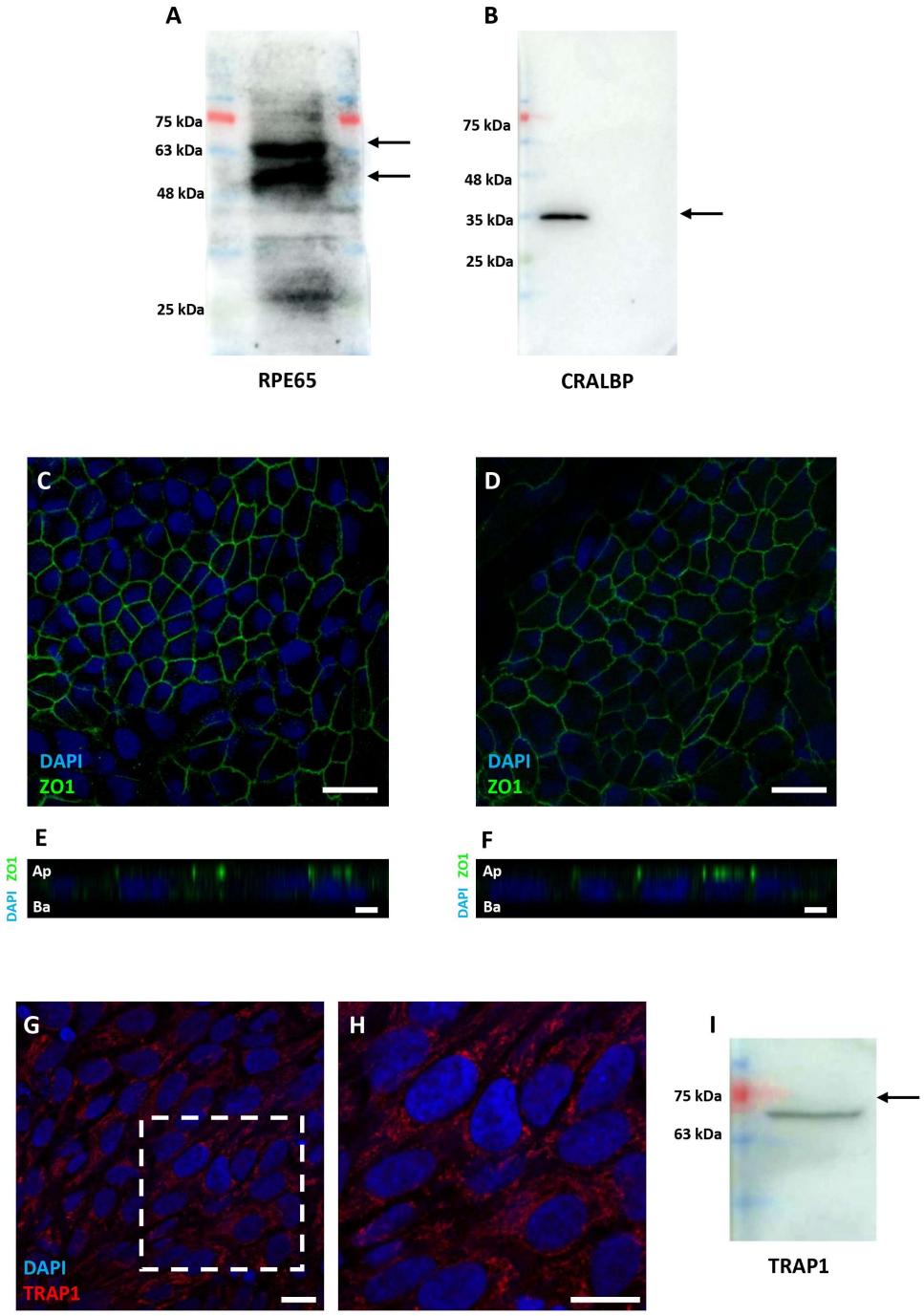

Figure 15. Characterization of the iRPE cells. Western Blotting analysis confirmed that RPE65 (A) and CRALBP (B) protein were expressed by hiPSC-RPE cells. (C, D) Immunocytochemistry analysis also confirmed that these cells express zonula occludens 1 (ZO-1) protein. (E, F) z-stack confocal micrographs showed the typical polarized expression of RPE proteins, with ZO-1 demonstrating apical localization. (G, H) Immunocytochemistry analysis confirmed that TRAP1 was expressed in the iRPE cells. (I) Western Blotting analysis showed the expression of TRAP1 protein. Scale bars: (C, D, G, H) 10 µm, (E, F) 5 µm.

4. Discussion

4. Discussion

Tumor necrosis factor receptor-associated protein 1 (TRAP1) has been found to be expressed in various tissues and cell types (Song et al., 1995; Felts et al., 2000; Yoshida et al., 2013; Sciacovelli et al., 2013; Agorreta et al., 2014; Palladino et al., 2016; Barbosa et al., 2018; Xiao et al., 2021; Bruno et al., 2022; Dharaskar et al., 2023a; Dharaskar et al., 2023b). TRAP1 messenger RNA (mRNA) has been reported to exhibit variable expression in tissues such as the brain, skeletal muscle, heart, kidney, liver, lung, placenta, and pancreas (Song et al., 1995). Previous studies have also identified TRAP1 protein expression in different cell lines, including H1299 human cell lung carcinoma (Barbosa et al., 2018), G361 melanoma (Song et al., 1995), PC-3M prostate carcinoma (Felts et al., 2000), A549 human adenocarcinoma (Agorreta et al., 2014; Palladino et al., 2016) SW480 colorectal adenocarcinoma (Song et al., 1995), HL-60 promyelocytic leukemia (Song et al., 1995), SH-SY5Y neuroblastoma (Yoshida et al., 2013), IMR-32 neuroblastoma (Dharaskar et al., 2023) HCT116 colon cancer (Bruno et al., 2022; Matassa et al., 2022), and human cervix carcinoma HeLa cell lines (Xiao et al., 2021).

Although the expression of TRAP1 in the retinal pigment epithelium (RPE) has never been described in the literature, both HSP70 and its family member HSP90 have been identified in the retina (Kojima et al., 1996; Dean et al., 2001). The important role of TRAP1 is further supported by studies using TRAP1/HSP90 inhibitors, which have been found to induce neuronal toxicity and lead to visual disorders (reviewed in Ramos Rego et al., 2021). Concerning HSP70, a study in a Wistar rat model of retinal ganglion cell degeneration induced by ocular hypertension show that the upregulation of HSP70 supports the survival of injured retinal ganglion cells. The authors also suggest that their findings provide support for translating the HSP70-based cell survival strategy into therapy to protect and rescue injured retinal ganglion cells from degeneration associated with retinal diseases (Park et al., 2001). In a recent study using a HSP90α murine knockout model, it was reported that HSP90α is essential for the maintenance of rod photoreceptors (Munezero et al., 2023). *Hsp90α*$^{-/-}$ mice showed not only a decline in rod photoreceptor function, but also progressive rod photoreceptor degeneration. Photoreceptor nuclei layers were uniformly and progressively reduced on each side of the optic nerve in the retina of the knockout mice. Furthermore, the authors also observed the activation and migration of microglia to the photoreceptor layers, abnormalities in the outer segments and apoptotic nuclei accumulation in *Hsp90α*$^{-/-}$ models (Munezero et al., 2023). Furthermore, in human trials, some HSP90 inhibitors, such as 17-DMAG and NVP-AUY922, have caused visual disorders and retinal dysfunction (Sessa et al., 2013; Yamaguchi et al., 2020). In fact, HSP90 is suggested as a promising therapeutic target in retinal diseases. Indeed, the HSP90 protein family is a fundamental

constituent of a complex defense mechanism that enhances cell survival and regulates homeostasis even under cellular stress and adverse environmental conditions (McClellan et al., 2007; Khong et al., 2011; Zhou et al., 2013; Aguilà et al., 2016; Piri et al., 2016; Fiesel et al., 2017). These findings related with the HSP70 and HSP90 functions highlight the involvement of TRAP1 in neurodegenerative processes and in the function of retinal cells. Further research and clinical studies are needed to validate the therapeutic potential of TRAP1 modulation in retinal diseases, opening possibilities for new therapeutic approaches focused on modulating this protein for addressing devastating disorders such as AMD.

In our study, we demonstrated the presence of TRAP1 in the mitochondria of human RPE cells **(Fig. 6)**. Interestingly, TRAP1 silencing in adult retinal pigment epithelium-19 (ARPE-19) cells in our experiments did not result in reduced cell proliferation **(Fig. 9)**. This contrasts with findings reported by Agorreta *et al.*, Barbosa *et al.* and Palladino *et al.*, who demonstrated that downregulation of TRAP1 inhibits cell proliferation and decreases cell survival in A549 and H1299 lung cancer cell lines and in thyroid carcinoma cells (Agorreta et al, 2014; Palladino et al, 2016; Barbosa et al., 2018). The observed discrepancies may be attributed to the level of TRAP1 suppression or the specific cell types involved.

Furthermore, we investigated whether TRAP1 levels and localization were altered in response to hydrogen peroxide (H_2O_2)-induced damage. We observed that TRAP1 levels were decreased 24 hours after exposure to 500 μM of H_2O_2, while the localization of the protein remained unaffected **(Fig. 7,8)**. However, other studies have shown that TRAP1 expression is upregulated following treatment with H_2O_2 (300 μM) for 24 hours in a neuroblastoma cell line (SH-SY5Y) (Yoshida et al., 2013). The discrepancy in the effect of H_2O_2 treatment on TRAP1 levels could be attributed to the specific cell type, as numerous studies indicate that the role of TRAP1 may differ depending on the cell type (Barbosa et al., 2018; Agorreta et al., 2014; Xiao et al., 2021).

Our findings reveal that silencing of TRAP1 leads to an increase in reactive oxygen species (ROS) production in RPE cells, suggesting its crucial role in regulating ROS levels **(Fig. 9, 10)**. Similar observations of elevated ROS production upon TRAP1 silencing have been reported in HCT116 colon cancer cells (Bruno et al., 2022), lung cancer cells (Barbosa et al., 2018), and HeLa cells exposed to H_2O_2 (Xiao et al., 2021). Furthermore, we investigated the impact of TRAP1 silencing on mitochondrial morphology. We observed that TRAP1 silencing resulted in enhanced mitochondrial elongation while maintaining mitochondrial interconnectivity **(Fig. 11)**. Previous studies conducted in MRC-5 cells showed that reduced TRAP1 levels did not affect mitochondrial morphology compared to control cells, displaying a complex and interconnected mitochondrial network (Barbosa et al., 2018). However, the same authors

demonstrated that TRAP1 silencing in A549 cells led to reduced mitochondrial elongation and interconnectivity (Barbosa et al., 2018).

TRAP1 is known to regulate mitochondrial energy metabolism, particularly oxidative phosphorylation (OXPHOS), through its interaction with proteins in the mitochondrial electron transport chain (ETC), such as complex II and complex IV (Yoshida et al., 2013; Sciacovelli et al., 2013; Rasola et al., 2014; Masgras et al., 2017). Additionally, we assessed the impact of TRAP1 on the metabolic profile and capabilities of ARPE-19 cells. Our data revealed that decreased TRAP1 levels led to an overall decline in respiratory capacity, driving the cells into a quiescent state **(Fig. 12)**. Similarly, other studies demonstrated decreased oxygen consumption without alterations in glycolytic rates in A549 siTRAP1 cells (Barbosa et al., 2018). In contrast, TRAP1 knockout in murine fibroblast cells displayed higher basal oxygen consumption rates and significantly higher maximum respiratory capacity than control cells (Agorreta et al., 2014). Recently, Xiao *et al.* demonstrated that TRAP1 overexpression, rather than TRAP1 ablation, increased maximal respiration and ATP production in cancer-associated fibroblasts (Xiao et al., 2021).

In summary, our study highlights that silencing of TRAP1 leads to increased ROS production in human RPE cells and induces a quiescent metabolic state **(Fig. 10, 12)**. Considering that oxidative stress-induced RPE damage and mitochondrial dysfunction are prominent features of age-related macular degeneration (AMD) (Brown et al., 2019), TRAP1 might play a role in AMD pathology, presenting new avenues for the development of therapeutic approaches targeting TRAP1 modulation. Therefore, future experiments are needed to evaluate the efficacy of TRAP1 gene therapy in more complex models, that better mimic the characteristics of primary RPE cells.

Although the ARPE-19 cell line is the most widely used RPE cell line (Dunn et al., 1996; Klettner et al., 2020), the expression patterns of ARPE-19 cells depend, not only on the origin of the cell line, but also on culture conditions (Samuel et al., 2017; Tian et al., 2004). Indeed, when cultured under conditions that promote differentiation, ARPE-19 cells are able to mimic many characteristics of primary human RPE, such as pigmentation, cobblestone-like appearance and polarization (Ahmado et al., 2011; Lynn et al., 2018; Hazim et al., 2019; Pfeffer and Fliesler, 2022). However, in the culture conditions used in our study, ARPE-19 are not fully differentiated. Our cells were not pigmented, did not present a hexagonal morphology and were not polarized. Indeed, we needed improved culture conditions to enhance the differentiation of ARPE-19 cells. Moreover, since TRAP1 expression is upregulated in tumours (Agorreta et al., 2014; Palladino et al., 2016 Xiao et al., 2021; Bruno et al., 2022; Matassa et al., 2022), it was important to confirm its expression in an RPE *in vitro* model that was not an immortalized or transformed cell line.

Thus, a more complex *in vitro* model that allows the obtention of fully differentiated RPE cells was needed.

In the last years, human induced pluripotent stem cells-derived RPE (iRPE) have emerged as additional source for the generation of fully mature and functional RPE cells (Ferrer et al., 2014; Maroutti et al.; 2015; Smith et al., 2019; Sharma et al., 2019 Miyagishima et al., 2021). In fact, the use of iRPE cells offers a promising alternative for further studies (Smith et al., 2019), enabling a better disease modelling. In this study we used an adaptation of the protocols by Maroutti *et al*., and Smith *et al*., altering and adjusting the cell plating densities and the CO_2 in the cell culture incubator. Using the small molecules nicotinamide (NIC) and chetomin (CTM) to promote the differentiation of hiPSC, we successfully obtained a pure and functional monolayer of RPE cells **(Fig. 13,14,15)**. After the end of the differentiation process, we collected the iRPE cells expressing the RPE specific markers retinal pigment epithelium-specific protein of 65 kDa (RPE65), the cellular retinaldehyde-binding protein (CRALBP) and the tight junction protein zonula occludens 1 (ZO-1) **(Fig. 15)**. Moreover, the cells showed the polarity expected of RPE cells, with ZO-1 showing predominant apical localization (Maroutti et al., 2015). Finally, we also demonstrated that TRAP1 protein is also expressed in the iRPE cells resultant from our differentiation protocol **(Fig. 15)**. The iRPE cells displayed many of the morphological and molecular characteristics of the primary RPE, confirming the robustness of the differentiation protocol. Moreover, since these cells exhibit similar characteristics to mature human RPE, this protocol has the potential to be cost-efficient to produce RPE cells with a high level of purity through a single passage of the culture. Indeed, the validation of iRPE cells often involves visually inspection of features such as confluency, hexagonality, and pigmentation, as well as analyzing gene expression in a subset of genes (Bharti et al., 2011). Although these assessments confirm the RPE phenotype, they lack the sensitivity required for comparing and validating cells across multiple laboratories and different patients with AMD. To address this limitation, researchers have employed scanning and transmission electron microscopy (TEM) to assess the structural characteristics of the RPE monolayer (Sharma et al., 2019). Through these techniques, it has been demonstrated that iRPE cells exhibit prominent pigment granules located apically, nuclei positioned basally, tight junctions connecting adjacent cells, and fully polarized and mature features evident in their confluent apical processes (Miyagishima et al., 2016; Sharma et al., 2019). Considering this, the optimization of the iRPE characterization made in our study will consist in using TEM analysis and in verifying if the obtained iRPE cells express another developmental (MITF, PAX6, TYRP1, TYR, GPNMB) and mature RPE markers (RLBP1, ALDH1A3, BEST1, CLDN19, EZRIN, MFRP) by quantitative PCR analysis (Maroutti et al., 2015; Sharma et al., 2019; Smith et al., 2019; Farnoodian et al., 2022). Additionally, we can perform a functional assessment of the tight junctions by measuring the transepithelial resistance

of cells grown in semi-permeable Transwell® filters (Miyagishima et al., 2016; Sharma et al., 2019). We can also assess the phagocytosis of photoreceptor outer segments (POS), a key task of the RPE (Miyagishima et al., 2016; Sharma et al., 2019; Bharti et al., 2022).

The implementation of this optimized protocol of iRPE differentiation holds potential as an effective model system for studying the role of TRAP1 in the RPE and to test the efficacy of a possible TRAP1-based therapy for AMD. In fact, as previously discussed, several authors have shown that iRPE cells can be used to model AMD *in vitro* (Garcia et al., 2015; Golestaneh et al., 2016; Saini et al., 2017; Dalvi et al., 2019; Peters et al., 2022). Further experiments in our study may include the generation of hiPSC from skin fibroblasts of AMD donors and age-matched healthy donors. After the establishment of the hiPSC lines, we can differentiate the hiPSC into RPE cells (iRPE). Indeed, iRPE derived from AMD human donors exhibit the disease relevant cellular phenotype and is a valuable tool for *in vitro* disease modelling in AMD (Golestaneh et al., 2016). Or we can use healthy iRPE cells and induce an AMD-like phenotype, by adding Bis-retinoid N-retinyl-N-retinylidene ethanolamine (A2E) a major component of lipofuscin, the main constituent of macular drusen (Parmar et al., 2018). We can also induce oxidative damage in the healthy iRPE by inhibiting the antioxidant response of the cells by silencing superoxide dismutase (SOD) proteins. To investigate the impact of the complete absence of TRAP1 in human RPE cells, we can also generate a TRAP1 knockout iRPE line, using technologies such as the system clustered regularly interspaced short palindromic repeats/Cas9 protein (CRISPR/Cas9).

Summing up, our findings about TRAP1 role in ARPE-19 cells and the implementation of a protocol for iRPE differentiation provide an unprecedented opportunity to understand the role of TRAP1 in the RPE, to better understand AMD disease mechanisms and to identify possible AMD novel therapeutics based in TRAP1 modulation.

5. Conclusion

5. Conclusion

Age-related macular degeneration (AMD) is the leading cause of severe vision loss and blindness in elderly people worldwide. Vision loss caused by advanced stages of AMD has profound human and socioeconomic consequences in all societies. The oxidative stress-induced damage of the retinal pigment epithelium (RPE) is thought to play a key role in the onset and progression of AMD. The RPE damage resultant from oxidative stress occurs due to the excessive accumulation of reactive oxygen species (ROS), primarily produced in the mitochondria under pathological conditions. Maintaining mitochondrial function homeostasis is crucial for keeping ROS at physiological levels and preventing the metabolic dysfunction observed in AMD pathology. Therefore, it is important to investigate proteins that are novel players in oxidative stress mechanisms within the RPE in the context of AMD.

Tumour necrosis factor receptor-associated protein 1 (TRAP1) is a mitochondrial chaperone that supports protein folding and contributes to the maintenance of mitochondrial integrity even under cellular stress. TRAP1 protects against mitophagy, mitochondrial apoptosis and dysfunction by decreasing the production and accumulation of ROS, thus, reducing oxidative stress. Considering the functions of TRAP1 described in other cell types, we propose that TRAP1 modulates mitochondrial metabolism in the RPE and plays a role in preventing the onset and progression of AMD. We hypothesize that TRAP1 mediates protection against oxidative stress in the RPE and therefore is a potential therapeutic target for AMD.

The objective of the present study was to assess the presence and function of TRAP1 in the human RPE and investigate whether TRAP1 provides protection against oxidative stress in RPE cells. To test our hypothesis, we studied the cellular functions of TRAP1 in the RPE, using the Human Adult Retinal Pigment Epithelial-19 (ARPE-19) cell line as *in vitro* model. We also aimed to optimize and implement an experimental protocol for the differentiation of RPE cells from human induced pluripotent stem cells (iRPE) to access the presence of TRAP1.

Our findings revealed that TRAP1 is expressed in human adult RPE cells and primarily localized in the mitochondria. Additionally, our study highlighted that silencing TRAP1 expression increased ROS production in human RPE cells, decreased mitochondrial respiratory capacity and lead to a quiescent metabolic state. The successful establishment of the iRPE model will also allow us to perform key experiments in the future, using a more complex human RPE *in vitro* model, that better replicates the characteristics of primary human RPE. Indeed, iRPE cultures are high-quality models for mechanistic RPE research, being a valuable resource in the investigation of the responsiveness to interventions and therapies, enabling personalized

treatment or preventive approaches for AMD patients or individuals at high risk of developing the disease.

Summing up, our findings about TRAP1 role in ARPE-19 cells and the implementation of a protocol for iRPE differentiation provide an unprecedented opportunity to understand the role of TRAP1 in the RPE, to better understand AMD disease mechanisms and to identify possible AMD novel therapeutics based in TRAP1 modulation.

6. Bibliography

6. Bibliography

Aboul Naga, S. H., Dithmer, M., Chitadze, G., Kabelitz, D., Lucius, R., Roider, J., & Klettner, A. Intracellular pathways following uptake of bevacizumab in RPE cells. *Exp. Eye Res.* **2015**, *131*, 29–41.

Agorreta, J., Hu, J., Liu, D., Delia, D., Turley, H., Ferguson, D. J., Iborra, F., Pajares, M. J., Larrayoz, M., Zudaire, I., Pio, R., Montuenga, L. M., Harris, A. L., Gatter, K., & Pezzella, F. TRAP1 regulates proliferation, mitochondrial function, and has prognostic significance in NSCLC. *Mol. Cancer Res*. **2014**, *12*(5), 660–669.

Aguilà, M., & Cheetham, M. E. Hsp90 as a Potential Therapeutic Target in Retinal Disease. *Adv. Exp. Med. Biol.* **2016**, *854*, 161–167.

Aguilà, M., Bevilacqua, D., McCulley, C., Schwarz, N., Athanasiou, D., Kanuga, N., Novoselov, S. S., Lange, C. A., Ali, R. R., Bainbridge, J. W., Gias, C., Coffey, P. J., Garriga, P., & Cheetham, M. E. Hsp90 Inhibition Protects against Inherited Retinal Degeneration. *Hum. Mol. Genet.* **2014**, *23*, 2164–2175.

Ahmado, A., Carr, A. J., Vugler, A. A., Semo, M., Gias, C., Lawrence, J. M., Chen, L. L., Chen, F. K., Turowski, P., da Cruz, L., & Coffey, P. J. Induction of differentiation by pyruvate and DMEM in the human retinal pigment epithelium cell line ARPE-19. *Inv. Ophthalm. Vis. Sci.* **2011**, *52*(10), 7148–7159.

Algvere, P. V., Kvanta, A., & Seregard, S. Drusen maculopathy: a risk factor for visual deterioration. *Acta ophthalmol.* **2016**, *94*(5), 427–433.

Alves, C. H., Fernandes, R., Santiago, A. R., & Ambrósio, A. F. Microglia Contribution to the Regulation of the Retinal and Choroidal Vasculature in Age-Related Macular Degeneration. *Cells.* **2020**, *9*(5), 1217.

Ambati, J., & Fowler, B. J. Mechanisms of age-related macular degeneration. *Neuron.* **2012**, *75*(1), 26–39.

Amoaku W.M., Chakravarthy U., Gale R., Gavin M., Ghanchi F., Gibson J., Harding S., Johnston R.L., Kelly S.P., Lotery A., Mahmood S., Menon G., Sivaprasad S., Talks J., Tufail A. & Yang Y. Defining response to anti-VEGF therapies in neovascular AMD. *Eye*. **2015**, *29(6)*, 721-31.

Amoroso, M. R., Matassa, D. S., Agliarulo, I., Avolio, R., Maddalena, F., Condelli, V., Landriscina, M., & Esposito, F. Stress-Adaptive Response in Ovarian Cancer Drug Resistance: Role of TRAP1 in Oxidative Metabolism-Driven Inflammation. *Adv. Protein Chem. Struct. Biol*. **2017**, *108*, 163–198.

Amoroso, M. R., Matassa, D. S., Laudiero, G., Egorova, A. V., Polishchuk, R. S., Maddalena, F., Piscazzi, A., Paladino, S., Sarnataro, D., Garbi, C., Landriscina, M., & Esposito, F. TRAP1 and the proteasome regulatory particle TBP7/Rpt3 interact in the endoplasmic reticulum and control cellular ubiquitination of specific mitochondrial proteins. *Cell Death Differ.* **2012**, *19*, 592–604.

Amoroso, M.R.; Matassa, D.S.; Sisinni, L.; Lettini, G.; Landriscina, M. & Esposito, F. TRAP1 Revisited: Novel Localizations and Functions of a "next-Generation" Biomarker. *Int. J. Oncol.* **2014**, *45*, 969–977.

Ao, J., Wood, J. P., Chidlow, G., Gillies, M. C., & Casson, R. J. Retinal pigment epithelium in the pathogenesis of age-related macular degeneration and photobiomodulation as a potential therapy?. *Clin. Exp. Ophthalm.* **2018**, *46*(6), 670–686.

Aryan, N., Betts-Obregon, B. S., Perry, G., & Tsin, A. T. Oxidative Stress Induces Senescence in Cultured RPE Cells. *Open Neurol. J*. **2016**, *10*, 83–87.

Avolio, R.; Matassa, D.S.; Criscuolo, D.; Landriscina, M. *&* Esposito, F. Modulation of Mitochondrial Metabolic Reprogramming and Oxidative Stress to Overcome Chemoresistance in Cancer. *Biomolecules.* **2020**, *10*, 135.

Baines, C. P., Kaiser, R. A., Purcell, N. H., Blair, N. S., Osinska, H., Hambleton, M. A., Brunskill, E. W., Sayen, M. R., Gottlieb, R. A., Dorn, G. W., Robbins, J., & Molkentin, J. D. Loss of Cyclophilin D Reveals a Critical Role for Mitochondrial Permeability Transition in Cell Death. *Nature.* **2005**, *434*, 658–662.

Bakri, S. J., Bektas, M., Sharp, D., Luo, R., Sarda, S. P., & Khan, S. Geographic atrophy: Mechanism of disease, pathophysiology, and role of the complement system. *J. Man. Care Spec. Pharm.* **2023**, *29*.

Bao, A., Nashine, S., Atilano, S., Chwa, M., Federoff, H., & Kenney, M. C. Differential responses of AMD mitochondrial DNA haplogroups to PU-91, a mitochondria-targeting drug. *Mitochondrion*. **2021**, *60*, 189–200.

Baqri, R.M.; Pietron, A.V.; Gokhale, R.H.; Turner, B.A.; Kaguni, L.S.; Shingleton, A.W.; Kunes, S. & Miller, K.E. Mitochondrial Chaperone TRAP1 Activates the Mitochondrial UPR and Extends Healthspan in Drosophila. *Mech. Ageing Dev.* **2014**, *141*, 35–45.

Barbosa, I. A., Vega-Naredo, I., Loureiro, R., Branco, A. F., Garcia, R., Scott, P. M., & Oliveira, P. J. TRAP1 regulates autophagy in lung cancer cells. *Eur. J. Clin. Invest.* **2018**, *48(4)*.

Bharti, K., den Hollander, A. I., Lakkaraju, A., Sinha, D., Williams, D. S., Finnemann, S. C., Bowes-Rickman, C., Malek, G., & D'Amore, P. A. Cell culture models to study retinal pigment

epithelium-related pathogenesis in age-related macular degeneration. *Exp*. Eye Res. **2022**, *222*, 109170.

Bharti, K., Miller, S. S., & Arnheiter, H. The new paradigm: retinal pigment epithelium cells generated from embryonic or induced pluripotent stem cells. *Pigm. Cell Melan. Res.* **2011**, *24*(1), 21–34.

Bhattacharya, B.; Mohd Omar, M.F.& Soong, R. The Warburg Effect and Drug Resistance. *Br. J. Pharmacol.* **2016**, *173*, 970–979.

Bilbao-Malavé, V., González-Zamora, J., de la Puente, M., Recalde, S., Fernandez-Robredo, P., Hernandez, M., Layana, A. G., & Saenz de Viteri, M. Mitochondrial Dysfunction and Endoplasmic Reticulum Stress in Age Related Macular Degeneration, Role in Pathophysiology, and Possible New Therapeutic Strategies. *Antiox*. **2021**, *10*(8), 1170.

Bodnar, A. G., Ouellette, M., Frolkis, M., Holt, S. E., Chiu, C. P., Morin, G. B., Harley, C. B., Shay, J. W., Lichtsteiner, S., & Wright, W. E. Extension of life-span by introduction of telomerase into normal human cells. *Science.* **1998**, *279*, 349–352.

Bradley, E.; Zhao, X.; Wang, R.; Brann, D.; Bieberich, E.& Wang, G. Low Dose Hsp90 Inhibitor 17AAG Protects Neural Progenitor Cells from Ischemia Induced Death. *J. Cell Commun. Signal.* **2014**, *8*, 353–362.

Brown, E. E., DeWeerd, A. J., Ildefonso, C. J., Lewin, A. S., & Ash, J. D. Mitochondrial oxidative stress in the retinal pigment epithelium (RPE) led to metabolic dysfunction in both the RPE and retinal photoreceptors. *Redox Biolog.* **2019**, *24*.

Bruno, G., Li Bergolis, V., Piscazzi, A., Crispo, F., Condelli, V., Zoppoli, P., Maddalena, F., Pietrafesa, M., Giordano, G., Matassa, D. S., Esposito, F., & Landriscina, M. TRAP1 regulates the response of colorectal cancer cells to hypoxia and inhibits ribosome biogenesis under conditions of oxygen deprivation. *Int. J. Onco.* **2022**, *60*(6), 79.

Burke J. M., Kaczara P., Skumatz C., Zareba M., Raciti M. W., Sarna T. Dynamic analyses reveal cytoprotection by RPE melanosomes against non-photic stress. *Mol. Vis.* **2011**, *17*, 2864–2877.

Butler, E.K.; Voigt, A.; Lutz, A.K.; Toegel, J.P.; Gerhardt, E.; Karsten, P.; Falkenburger, B.; Reinartz, A.; Winklhofer, K.F. & Schulz, J.B. The Mitochondrial Chaperone Protein TRAP1 Mitigates α-Synuclein Toxicity. *PLoS Genet.* **2012**, *8(2)*, 1002488.

Cabral de Guimaraes, T. A., Daich Varela, M., Georgiou, M., & Michaelides, M. Treatments for dry age-related macular degeneration: therapeutic avenues, clinical trials and future directions. *The British J. Ophthalm.* **2022**, *106*(3), 297–304.

Cannino, G., Urbani, A., Gaspari, M., Varano, M., Negro, A., Filippi, A., Ciscato, F., Masgras, I., Gerle, C., Tibaldi, E., Brunati, A. M., Colombo, G., Lippe, G., Bernardi, P., & Rasola, A. The mitochondrial chaperone TRAP1 regulates F-ATP synthase channel formation. *Cell Death Diff.* **2022**, *29*(12), 2335–2346.

Cechetto, J.D. & Gupta, R.S. Immunoelectron Microscopy Provides Evidence That Tumor Necrosis Factor Receptor-Associated Protein 1 (TRAP-1) Is a Mitochondrial Protein Which Also Localizes at Specific Extramitochondrial Sites. *Exp. Cell Res.* **2000**, *260*, 30–39.

Chae, Y. C., Caino, M. C., Lisanti, S., Ghosh, J. C., Dohi, T., Danial, N. N., Villanueva, J., Ferrero, S., Vaira, V., Santambrogio, L., Bosari, S., Languino, L. R., Herlyn, M., & Altieri, D. C. Control of Tumor Bioenergetics and Survival Stress Signaling by Mitochondrial HSP90s. *Cancer Cell.* **2012**, *22*, 331–344.

Chen, F. W., Davies, J. P., Calvo, R., Chaudhari, J., Dolios, G., Taylor, M. K., Patnaik, S., Dehdashti, J., Mull, R., Dranchack, P., Wang, A., Xu, X., Hughes, E., Southall, N., Ferrer, M., Wang, R., Marugan, J. J., & Ioannou, Y. A. Activation of mitochondrial TRAP1 stimulates mitochondria-lysosome crosstalk and correction of lysosomal dysfunction. *iScience.* **2022**, *25*(9), 104941.

Chen, Y.; Wang, B.; Liu, D.; Li, J.J.; Xue, Y.; Sakata, K.; Zhu, L.Q.; Heldt, S.A.; Xu, H. & Liao, F.F. Hsp90 Chaperone Inhibitor 17-AAG Attenuates Aβ-Induced Synaptic Toxicity and Memory Impairment. *J. Neurosci. Off. J. Soc. Neurosci.* **2014**, *34*, 2464–2470.

Chien, W.L.; Lee, T.R.; Hung, S.Y.; Kang, K.H.; Lee, M.J. & Fu, W.M. Impairment of Oxidative Stress-Induced Heme Oxygenase-1 Expression by the Defect of Parkinson-Related Gene of PINK1. *J. Neurochem.* **2011**, *117*, 643–653.

Chung, E. J., Efstathiou, N. E., Konstantinou, E. K., Maidana, D. E., Miller, J. W., Young, L. H., & Vavvas, D. G. AICAR suppresses TNF-α-induced complement factor B in RPE cells. *Sci. Rep.* **2017**, *7*(1), 17651.

Clarke, B. E., Kalmar, B., & Greensmith, L. Enhanced Expression of TRAP1 Protects Mitochondrial Function in Motor Neurons under Conditions of Oxidative Stress. *Int. J. Mol. Sci,* **2022**, *23*(3), 1789.

Costa, A.C.; Loh, S.H.Y. & Martins, L.M. Drosophila Trap1 Protects against Mitochondrial Dysfunction in a PINK1/Parkin Model of Parkinson's Disease. *Cell Death Dis.* **2013**, *4*, 467.

Costantino, E.; Maddalena, F.; Calise, S.; Piscazzi, A.; Tirino, V.; Fersini, A.; Ambrosi, A.; Neri, V.; Esposito, F. & Landriscina, M. TRAP1, a Novel Mitochondrial Chaperone Responsible for Multi-Drug Resistance and Protection from Apoptotis in Human Colorectal Carcinoma Cells.

Cancer Lett. **2009**, *279*, 39–46.

Dagda, R. K., Cherra, S. J., Kulich, S. M., Tandon, A., Park, D., & Chu, C. T. Loss of PINK1 function promotes mitophagy through effects on oxidative stress and mitochondrial fission. *J. Biol. Chem.* **2009**, *284(20)*, 13843–13855.

Dalvi, S., Galloway, C. A., Winschel, L., Hashim, A., Soto, C., Tang, C., MacDonald, L. A., & Singh, R. Environmental stress impairs photoreceptor outer segment (POS) phagocytosis and degradation and induces autofluorescent material accumulation in hiPSC-RPE cells. *Cell Death Dis.* **2019***, 5*, 96.

Dambrot, C., van de Pas, S., van Zijl, L., Brändl, B., Wang, J. W., Schalij, M. J., Hoeben, R. C., Atsma, D. E., Mikkers, H. M., Mummery, C. L., & Freund, C. Polycistronic lentivirus induced pluripotent stem cells from skin biopsies after long term storage, blood outgrowth endothelial cells and cells from milk teeth. *Diff. Res. Biol. Div.* **2013**, *85(3)*, 101–109.

Datta S., Cano M., Ebrahimi K., Wang L. & Handa J.T. The impact of oxidative stress and inflammation on RPE degeneration in non-neovascular AMD. *Prog. Retin. Eye Res*. **2017**, *60*, 201-218.

Davis, A. A., Bernstein, P. S., Bok, D., Turner, J., Nachtigal, M., & Hunt, R. C. A human retinal pigment epithelial cell line that retains epithelial characteristics after prolonged culture. *Inv. Ophthalm. Vis. Sci.* **1995**, *36*(5), 955–964.

Dean, D.O. & Tytell, M. Hsp25 and -90 Immunoreactivity in the Normal Rat Eye. *Inv. Ophthalmol. Vis. Sci.* **2001**, *42*, 3031–3040.

Dekker, F.A. & Rüdiger, S.G.D. The Mitochondrial Hsp90 TRAP1 and Alzheimer's Disease. *Front. Mol. Biosci.* **2021**, *8*, 6979138.

Deng, Y., Qiao, L., Du, M., Qu, C., Wan, L., Li, J., & Huang, L. Age-related macular degeneration: Epidemiology, genetics, pathophysiology, diagnosis, and targeted therapy. *Genes Dis.* **2021**, *9*(1), 62–79.

Dharaskar, S. P., & Amere Subbarao, S. The mitochondrial chaperone TRAP-1 regulates the glutamine metabolism in tumor cells. *Mitochondrion.* **2023b**, *69*, 159–170.

Dharaskar, S. P., Paithankar, K., & Amere Subbarao, S. Analysis and functional relevance of the chaperone TRAP-1 interactome in the metabolic regulation and mitochondrial integrity of cancer cells. *Sci. Rep.* **2023a**, *13(1)*, 7584.

Dunn, K. C., Aotaki-Keen, A. E., Putkey, F. R., & Hjelmeland, L. M. ARPE-19, a human retinal pigment epithelial cell line with differentiated properties. *Exp. Eye Res.* **1996**, *62*(2), 155–169.

Elnatan, D. & Agard, D.A. Calcium Binding to a Remote Site Can Replace Magnesium as Cofactor for Mitochondrial Hsp90 (TRAP1) ATPase Activity. *J. Biol. Chem.* **2018**, *293*, 13717–13724.

Elnatan, D.; Betegon, M. & Agard, D.A. Crystal structure of mitochondrial Hsp90 (TRAP1) with ATP in absence of Mg, fully hydrolyzed. **2016**. Available online at doi:10.2210/pdb5TVX/pdb (assessed on 6 June 2023).

Elnatan, D.; Betegon, M.; Liu, Y.; Ramelot, T.; Kennedy, M.A. & Agard, D.A. Symmetry broken and rebroken during the ATP hydrolysis cycle of the mitochondrial Hsp90 TRAP1. *Elife.* **2017**, *6*, 25235.

Faby, H., Hillenkamp, J., Roider, J., & Klettner, A. Hyperthermia-induced upregulation of vascular endothelial growth factor in retinal pigment epithelial cells is regulated by mitogen-activated protein kinases. *Gra. Arch. Clin. Exp. Ophtalm.* **2014**, *252*(11), 1737–1745.

Faienza, F.; Rizza, S.; Giglio, P. & Filomeni, G. TRAP1: A Metabolic Hub Linking Aging Pathophysiology to Mitochondrial S-Nitrosylation. *Front. Physiol.* **2020**, *11*, 340.

Farnoodian, M., Bose, D., Khristov, V., Susaimanickam, P. J., Maddileti, S., Mariappan, I., Abu-Asab, M., Campos, M., Villasmil, R., Wan, Q., Maminishkis, A., McGaughey, D., Barone, F., Gundry, R. L., Riordon, D. R., Boheler, K. R., Sharma, R., & Bharti, K. Cell-autonomous lipid-handling defects in Stargardt iPSC-derived retinal pigment epithelium cells. *Stem Cell Rep.* **2022**, *17*(11), 2438–2450.

Fasler-Kan E., Aliu N., Wunderlich K., Ketterer S., Ruggiero S., Berger S. & Meyer P. The Retinal Pigment Epithelial Cell Line (ARPE-19) Displays Mosaic Structural Chromosomal Aberrations. *Methods Mol, Biol*. **2018**,*1745*, 305-314.

Feher J., Kovacs I., Artico M., Cavallotti C., Papale A. & Balacco Gabrieli C. Mitochondrial alterations of retinal pigment epithelium in age-related macular degeneration. *Neurobiol. Aging*. **2006**, *27*, 983–993.

Felts, S. J., Owen, B. A., Nguyen, P., Trepel, J., Donner, D. B., & Toft, D. O. The hsp90-related protein TRAP1 is a mitochondrial protein with distinct functional properties. *J. Biol. Chem.* **2000**, *275(5)*, 3305–3312.

Fernandez-Godino, R., Bujakowska, K. M., & Pierce, E. A. Changes in extracellular matrix cause RPE cells to make basal deposits and activate the alternative complement pathway. *Hum. Mol. Gen.* **2018***, 27*(1), 147–159.

Fernandez-Godino, R., Garland, D. L., & Pierce, E. A. Isolation, culture and characterization of primary mouse RPE cells. *Nature Prot.* **2016**, *11*(7), 1206–1218.

Ferrer, M., Corneo, B., Davis, J., Wan, Q., Miyagishima, K. J., King, R., Maminishkis, A., Marugan, J., Sharma, R., Shure, M., Temple, S., Miller, S., & Bharti, K. A multiplex high-throughput gene expression assay to simultaneously detect disease and functional markers in induced pluripotent stem cell-derived retinal pigment epithelium. *Stem Cells Transl. Med.* **2014***,* *3*(8), 911–922.

Ferrington D.A., Ebeling M.C., Kapphahn R.J., Terluk M.R., Fisher C.R., Polanco J.R., Roehrich H., Leary M.M., Geng Z., Dutton J.R. & Montezuma S.R. Altered bioenergetics and enhanced resistance to oxidative stress in human retinal pigment epithelial cells from donors with age-related macular degeneration. *Redox Biol*. **2017**, *13*, 255–265.

Ferrington, D. A., Kenney, M. C., Atilano, S. R., Hurley, J. B., Brown, E. E., & Ash, J. D. Mitochondria: The Retina's Achilles' Heel in AMD. *Adv. Exp. Med. Biol.* **2021**, *1256*, 237–264.

Fields, M. A., Del Priore, L. V., Adelman, R. A., & Rizzolo, L. J. Interactions of the choroid, Bruch's membrane, retinal pigment epithelium, and neurosensory retina collaborate to form the outer blood-retinal-barrier. *Prog. Retin. Eye Res.* **2020**, *76*.

Fiesel, F.C.; James, E.D.; Hudec, R. *&* Springer, W. Mitochondrial Targeted HSP90 Inhibitor Gamitrinib-TPP (G-TPP) Induces PINK1/Parkin-Dependent Mitophagy. *Oncotarget.* **2017**, *8*, 106233–106248.

Finnemann, S. C., Bonilha, V. L., Marmorstein, A. D., & Rodriguez-Boulan, E. Phagocytosis of rod outer segments by retinal pigment epithelial cells requires alpha(v)beta5 integrin for binding but not for internalization. *Proc. Nat. Acad. Sci. USA.* **1997**, *94*(24), 12932–12937.

Fisher C.R. & Ferrington D.A. Perspective on AMD pathobiology: a bioenergetic crisis in the RPE. *Invest. Ophthalmol. Vis. Sci*. **2018**, *59*, 41–47.

Fleckenstein, M., Keenan, T. D. L., Guymer, R. H., Chakravarthy, U., Schmitz-Valckenberg, S., Klaver, C. C., Wong, W. T., & Chew, E. Y. Age-related macular degeneration. *Nature Rev. Dis. Prim.* **2021**, *7*(1), 31.

Fleckenstein, M., Mitchell, P., Freund, K. B., Sadda, S., Holz, F. G., Brittain, C., Henry, E. C., & Ferrara, D. The Progression of Geographic Atrophy Secondary to Age-Related Macular Degeneration. *Ophthalmology*. **2018**, *125*(3), 369–390.

Gaki, G.S. & Papavassiliou, A.G. Oxidative Stress-Induced Signaling Pathways Implicated in the Pathogenesis of Parkinson's Disease. *Neuromol. Med.* **2014**, *16*, 217–230.

Garcia, T. Y., Gutierrez, M., Reynolds, J., & Lamba, D. A. Modeling the Dynamic AMD-Associated Chronic Oxidative Stress Changes in Human ESC and iPSC-Derived RPE Cells. *Inv. Ophthalm. Vis. Sci.* **2015**, *56*(12), 7480–7488.

Gibbs, D., Kitamoto, J., & Williams, D. S. Abnormal phagocytosis by retinal pigmented epithelium that lacks myosin VIIa, the Usher syndrome 1B protein. *Proc. Nat. Acad. Sci. USA*. **2003**, *100*(11), 6481–6486.

Golestaneh N., Chu Y., Cheng S.K., Cao H., Poliakov E. & Berinstein D.M. Repressed SIRT1/PGC-1alpha pathway and mitochondrial disintegration in iPSC-derived RPE disease model of age-related macular degeneration. *J. Transl. Med*. **2016**, *14*, 344.

Golestaneh N., Chu Y., Xiao Y.Y., Stoleru G.L. & Theos A.C. Dysfunctional autophagy in RPE, a contributing factor in age-related macular degeneration. *Cell Death Dis*. **2017**, *8*, 2537

Guo, J.; Zhu, P.; Wu, C.; Yu, L.; Zhao, S. *&* Gu, X. In Silico Analysis Indicates a Similar Gene Expression Pattern between Human Brain and Testis. *Cytogenet. Genome Res.* **2003**, *103*, 58–62.

Guymer, R. H., & Campbell, T. G. Age-related macular degeneration. *Lancet.* **2023**, *401(10386)*, 1459–1472.

Guzzo, G.; Sciacovelli, M.; Bernardi, P. & Rasola, A. Inhibition of Succinate Dehydrogenase by the Mitochondrial Chaperone TRAP1 Has Anti-Oxidant and Anti-Apoptotic Effects on Tumor Cells. *Oncotarget.* **2014**, *5*, 11897–11908.

Hazim, R. A., Volland, S., Yen, A., Burgess, B. L., & Williams, D. S. Rapid differentiation of the human RPE cell line, ARPE-19, induced by nicotinamide. *Exp. Eye Res.* **2019**, *179*, 18–24.

Herrnstadt, C., Elson, J. L., Fahy, E., Preston, G., Turnbull, D. M., Anderson, C., Ghosh, S. S., Olefsky, J. M., Beal, M. F., Davis, R. E., & Howell, N. Reduced-median-network analysis of complete mitochondrial DNA coding-region sequences for the major African, Asian, and European haplogroups. *Amer. J. Hum. Gen.* **2002**, *70(5)*, 1152–1171.

Hetz, C. The Unfolded Protein Response: Controlling Cell Fate Decisions under ER Stress and Beyond. *Nature Rev. Mol. Cell Biol.* **2012**, *13*, 89–102.

Ho, S.W.; Tsui, Y.T.C.; Wong, T.T.; Cheung, S.K.K.; Goggins, W.B.; Yi, L.M.; Cheng, K.K. & Baum, L. Effects of 17-Allylamino-17-Demethoxygeldanamycin (17-AAG) in Transgenic Mouse Models of Frontotemporal Lobar Degeneration and Alzheimer's Disease. *Transl. Neurodegener.* **2013**, *2*, 24.

Holz, F. G., Schmitz-Valckenberg, S., & Fleckenstein, M. Recent developments in the treatment of age-related macular degeneration. *J. Clin. Inv.* **2014**, *124(4)*, 1430–1438.

Hoter, A.; El-Sabban, M.E. & Naim, H.Y. The HSP90 Family: Structure, Regulation, Function, and Implications in Health and Disease. *Int. J. Mol. Sci.* **2018**, *19*, 2560.

Hu, J., & Bok, D. A cell culture medium that supports the differentiation of human retinal pigment epithelium into functionally polarized monolayers. *Mol. Vis.* **2001***, 7*, 14–19.

Hu, S., Ferraro, M., Thomas, A. P., Chung, J. M., Yoon, N. G., Seol, J. H., Kim, S., Kim, H. U., An, M. Y., Ok, H., Jung, H. S., Ryu, J. H., Colombo, G., & Kang, B. H. Dual Binding to Orthosteric and Allosteric Sites Enhances the Anticancer Activity of a TRAP1-Targeting Drug. *J. Med. Chem.* **2020**, *63*, 2930–2940.

Hua, G.; Zhang, Q. & Fan, Z. Heat Shock Protein 75 (TRAP1) Antagonizes Reactive Oxygen Species Generation and Protects Cells from Granzyme M-Mediated Apoptosis. *J. Biol. Chem.* **2007**, *282*, 20553–20560.

Hurst, J., Schnichels, S., Spitzer, M. S., Bartz-Schmidt, K. U., Farecki, M. L., Szurman, P., & Januschowski, K. Negative Effects of Acid Violet-17 and MBB Dual In Vitro on Different Ocular Cell Lines. *Curr. Eye Res.* **2017***, 42*(8), 1209–1214.

Iacovelli, J., Zhao, C., Wolkow, N., Veldman, P., Gollomp, K., Ojha, P., Lukinova, N., King, A., Feiner, L., Esumi, N., Zack, D. J., Pierce, E. A., Vollrath, D., & Dunaief, J. L. Generation of Cre transgenic mice with postnatal RPE-specific ocular expression. *Inv. Ophthalmol.* **2011**, *52(3)*, 1378–1383.

Idelson, M., Alper, R., Obolensky, A., Ben-Shushan, E., Hemo, I., Yachimovich-Cohen, N., Khaner, H., Smith, Y., Wiser, O., Gropp, M., Cohen, M. A., Even-Ram, S., Berman-Zaken, Y., Matzrafi, L., Rechavi, G., Banin, E., & Reubinoff, B. Directed differentiation of human embryonic stem cells into functional retinal pigment epithelium cells. *Cell Stem Cell*. **2009**, *5*(4), 396–408.

Im, C.N.; Lee, J.S.; Zheng, Y. & Seo, J.S. Iron Chelation Study in a Normal Human Hepatocyte Cell Line Suggests That Tumor Necrosis Factor Receptor-Associated Protein 1 (TRAP1) Regulates Production of Reactive Oxygen Species. *J. Cell. Biochem.* **2007**, *100*, 474–486.

Jarrett, S. G., Lin, H., Godley, B. F., & Boulton, M. E. Mitochondrial DNA damage and its potential role in retinal degeneration. *Prog. Ret. Eye Res.* **2008**, *27*(6), 596–607.

Jiang, X. R., Jimenez, G., Chang, E., Frolkis, M., Kusler, B., Sage, M., Beeche, M., Bodnar, A. G., Wahl, G. M., Tlsty, T. D., & Chiu, C. P. Telomerase expression in human somatic cells does not induce changes associated with a transformed phenotype. *Nature Gen.* **1999***, 21*(1), 111–114.

Johansson I., Monsen V.T., Pettersen K., Mildenberger J., Misund K., Kaarniranta K., Schonberg S. & Bjorkoy G. The marine n-3 PUFA DHA evokes cytoprotection against oxidative stress and protein misfolding by inducing autophagy and NFE2L2 in human retinal pigment epithelial cells. *Autophagy*. **2015**, *11*, 1636–1651.

Joshi, A., Dai, L., Liu, Y., Lee, J., Ghahhari, N. M., Segala, G., Beebe, K., Jenkins, L. M., Lyons, G. C., Bernasconi, L., Tsai, F., Agard, D. A., Neckers, L., & Picard, D. The mitochondrial HSP90 paralog TRAP1 forms an OXPHOS-regulated tetramer and is involved in mitochondrial metabolic homeostasis. *BMC Biol.* **2020**, *18*(1), 10.

Kaarniranta K., Uusitalo H., Blasiak J., Felszeghy S., Kannan R., Kauppinen A., Salminen A., Sinha D. & Ferrington D. Mechanisms of mitochondrial dysfunction and their impact on age-related macular degeneration. *Prog. Retin. Eye Res*. **2020**, *79*, 100858.

Kaarniranta, K., Pawlowska, E., Szczepanska, J., Jablkowska, A., & Blasiak, J. Role of Mitochondrial DNA Damage in ROS-Mediated Pathogenesis of Age-Related Macular Degeneration (AMD). *Int. J. Mol. Sci.* **2019**, *20*(10), 2374.

Kanda A., Chen W., Othman M., Branham K.E., Brooks M., Khanna R., He S., Lyons R., Abecasis G.R. & Swaroop A. A variant of mitochondrial protein LOC387715/ARMS2, not HTRA1, is strongly associated with age-related macular degeneration. *Proc. Natl. Acad. Sci. USA*. **2007**,*104*,16227–16232.

Kang, B.H. TRAP1 regulation of mitochondrial life or death decision in cancer cells and mitochondria-targeted TRAP1 inhibitors. *BMB Rep.* **2012**, *45*, 1–6.

Kang, B.H.; Plescia, J.; Dohi, T.; Rosa, J.; Doxsey, S.J. & Altieri, D.C. Regulation of Tumor Cell Mitochondrial Homeostasis by an Organelle-Specific Hsp90 Chaperone Network. *Cell.* **2007**, *131*, 257–270.

Kanow, M. A., Giarmarco, M. M., Jankowski, C. S., Tsantilas, K., Engel, A. L., Du, J., Linton, J. D., Farnsworth, C. C., Sloat, S. R., Rountree, A., Sweet, I. R., Lindsay, K. J., Parker, E. D., Brockerhoff, S. E., Sadilek, M., Chao, J. R., & Hurley, J. B. Biochemical adaptations of the retina and retinal pigment epithelium support a metabolic ecosystem in the vertebrate eye. *Elife*. **2017**, *6*, 28899.

Karunadharma P.P., Nordgaard C.L., Olsen T.W. & Ferrington D.A. Mitochondrial DNA damage as a potential mechanism for age-related macular degeneration. *Inv. Ophthalmol. Vis. Sci*. **2010**, *51*, 5470–5479.

Kenney, M. C., Chwa, M., Atilano, S. R., Pavlis, J. M., Falatoonzadeh, P., Ramirez, C., Malik, D., Hsu, T., Woo, G., Soe, K., Nesburn, A. B., Boyer, D. S., Kuppermann, B. D., Jazwinski, S. M., Miceli, M. V., Wallace, D. C., & Udar, N. Mitochondrial DNA variants mediate energy production and expression levels for CFH, C3 and EFEMP1 genes: implications for age-related macular degeneration. *PloS one.* **2013**, *8*(1), 54339.

Khong, T. & Spencer, A. Targeting HSP 90 Induces Apoptosis and Inhibits Critical Survival and Proliferation Pathways in Multiple Myeloma. *Mol. Cancer Ther.* **2011**, *10*, 1909–1917.

Kim, H.; Yang, J.; Kim, M.J.; Choi, S.; Chung, J.-R.; Kim, J.-M.; Yoo, Y.H.; Chung, J. & Koh, H. Tumor Necrosis Factor Receptor-Associated Protein 1 (TRAP1) Mutation and TRAP1 Inhibitor Gamitrinib-Triphenylphosphonium (G-TPP) Induce a Forkhead Box O (FOXO)-Dependent Cell Protective Signal from Mitochondria. *J. Biol. Chem.* **2016**, *291*, 1841–1853.

Kim, S., Backe, S. J., Wengert, L. A., Johnson, A. E., Isakov, R. V., Bratslavsky, M. S., & Woodford, M. R. O-GlcNAcylation suppresses TRAP1 activity and promotes mitochondrial respiration. *Cell Stress Chap.* **2022**, *27(5)*, 573–585.

Kinnunen K., Petrovski G., Moe M.C., Berta A. & Kaarniranta K. Molecular mechanisms of retinal pigment epithelium damage and development of age-related macular degeneration. *Acta Ophthalmol*. **2012**, *90*, 299–309.

Kitagishi Y., Nakano N., Ogino M., Ichimura M., Minami A. & Matsuda S. PINK1 signaling in mitochondrial homeostasis and in aging. *Int. J. Mo.l Med*. **2017**, *39*, 3–8.

Klettner, A.K. Retinal Pigment Epithelium Cell Culture. Retinal Pigment Epithelium in Health and Disease. *Springer*. **2020**.

Klingeborn, M., Dismuke, W. M., Skiba, N. P., Kelly, U., Stamer, W. D., & Bowes Rickman, C. Directional Exosome Proteomes Reflect Polarity-Specific Functions in Retinal Pigmented Epithelium Monolayers. *Sci. Rep.* **2017**, *7*(1), 4901.

Kojima, M., Hoshimaru, M., Aoki, T., Takahashi, J. B., Ohtsuka, T., Asahi, M., Matsuura, N., & Kikuchi, H. Expression of heat shock proteins in the developing rat retina. *Neurosci. Lett.* **1996**, *205(3)*, 215–217.

Kroemer, G. & Blomgren, K. Mitochondrial Cell Death Control in Familial Parkinson Disease. *PLoS Biol.* **2007**, *5*, 1409–1411.

Kubota, K., Inoue, K., Hashimoto, R., Kumamoto, N., Kosuga, A., Tatsumi, M., Kamijima, K., Kunugi, H., Iwata, N., Ozaki, N., Takeda, M., & Tohyama, M. Tumor Necrosis Factor Receptor-Associated Protein 1 Regulates Cell Adhesion and Synaptic Morphology via Modulation of N-Cadherin Expression. *J. Neurochem.* **2009**, *110*, 496–508.

Kwon, Y. S., Zheng, M., Zhang, A. Y., & Han, Z. Melanin-like Nanoparticles as an Alternative to Natural Melanin in Retinal Pigment Epithelium Cells and Their Therapeutic Effects against Age-Related Macular Degeneration. *ACS Nano*. **2022**, *16*(11), 19412–19422.

Lakkaraju, A., Umapathy, A., Tan, L. X., Daniele, L., Philp, N. J., Boesze-Battaglia, K., & Williams, D. S. The cell biology of the retinal pigment epithelium. *Prog. Retin. Eye Res.* **2020**, 100846.

Laquatra, C., Sanchez-Martin, C., Dinarello, A., Cannino, G., Minervini, G., Moroni, E., Schiavone, M., Tosatto, S., Argenton, F., Colombo, G., Bernardi, P., Masgras, I., & Rasola, A. HIF1α-Dependent Induction of the Mitochondrial Chaperone TRAP1 Regulates Bioenergetic Adaptations to Hypoxia. *Cell Death Dis.* **2021**, *12*, 434.

Lavery, L.A.; Partridge, J.R.; Ramelot, T.A.; Elnatan, D.; Kennedy, M.A. & Agard, D.A. Structural Asymmetry in the Closed State of Mitochondrial Hsp90 (TRAP1) Supports a Two-Step ATP Hydrolysis Mechanism. *Mol. Cell.* **2014**, *53*, 330–343.

Lazarou M., Sliter D.A., Kane L.A., Sarraf S.A., Wang C., Burman J.L., Sideris D.P., Fogel A.I. & Youle R.J. The ubiquitin kinase PINK1 recruits autophagy receptors to induce mitophagy. *Nature*. **2015**, *524*, 309–314.

Lehmann, G. L., Benedicto, I., Philp, N. J., & Rodriguez-Boulan, E. Plasma membrane protein polarity and trafficking in RPE cells: past, present and future. *Exp. Eye Res.* **2014**, *126*, 5–15.

Leskovar, A.; Wegele, H.; Werbeck, N.D.; Buchner, J. & Reinstein, J. The ATPase Cycle of the Mitochondrial Hsp90 Analog Trap1. *J. Biol. Chem.* **2008**, *283*, 11677–11688.

Li, J.; Yang, F.; Guo, J.; Zhang, R.; Xing, X. & Qin, X. 17-AAG Post-Treatment Ameliorates Memory Impairment and Hippocampal CA1 Neuronal Autophagic Death Induced by Transient Global Cerebral Ischemia. *Brain Res.* **2015**, *1610*, 80–88.

Liao, D. S., Grossi, F. V., El Mehdi, D., Gerber, M. R., Brown, D. M., Heier, J. S., Wykoff, C. C., Singerman, L. J., Abraham, P., Grassmann, F., Nuernberg, P., Weber, B. H. F., Deschatelets, P., Kim, R. Y., Chung, C. Y., Ribeiro, R. M., Hamdani, M., Rosenfeld, P. J., Boyer, D. S., Slakter, J. S. & Francois, C. G. Complement C3 Inhibitor Pegcetacoplan for Geographic Atrophy Secondary to Age-Related Macular Degeneration: A Randomized Phase 2 Trial. *Ophthalmology*. **2020**, *127*(2), 186–195.

Lin H., Xu H., Liang F.Q., Liang H., Gupta P., Havey A.N., Boulton M.E. & Godley B.F. Mitochondrial DNA damage and repair in RPE associated with aging and age-related macular degeneration. *Inv. Ophthalmol. Vis. Sci*. **2011**, *52*, 3521–3529.

Lisanti, S.; Tavecchio, M.; Chae, Y.C.; Liu, Q.; Brice, A.K.; Thakur, M.L.; Languino, L.R. & Altieri, D.C. Deletion of the Mitochondrial Chaperone TRAP-1 Uncovers Global Reprogramming of Metabolic Networks. *Cell Rep.* **2014**, *8*, 671–677.

Liu, L.; Zhang, L.; Zhao, J.; Guo, X.; Luo, Y.; Hu, W. & Zhao, T. Tumor Necrosis Factor Receptor-Associated Protein 1 Protects against Mitochondrial Injury by Preventing High Glucose-Induced MPTP Opening in Diabetes. *Oxid. Med. Cell. Longev.* **2020**, *2020*, 6431517.

Liu, Y.X.; Wang, F. & Agard, D.A. Full-length human mitochondrial Hsp90 (TRAP1) with ADP-BeF3, **2020**. Available online at doi:10.2210/pdb6XG6/pdb (assessed on 6 June 2023).

Lopez-Crisosto. C.; Díaz-Vegas, A.; Castro, P.F.; Rothermel, B.A.; Bravo-Sagua, R. & Lavandero, S. Endoplasmic Reticulum-Mitochondria Coupling Increases during Doxycycline-Induced Mitochondrial Stress in HeLa Cells. *Cell Death Dis.* **2021**, *12*, 657.

Luo, Y., Zhuo, Y., Fukuhara, M., & Rizzolo, L. J. Effects of culture conditions on heterogeneity and the apical junctional complex of the ARPE-19 cell line. *Inv. Ophthalmol. Vis. Sci.* **2006**, *47*(8), 3644–3655.

Lynn, S. A., Keeling, E., Dewing, J. M., Johnston, D. A., Page, A., Cree, A. J., Tumbarello, D. A., Newman, T. A., Lotery, A. J., & Ratnayaka, J. A. A convenient protocol for establishing a human cell culture model of the outer retina. *F1000Research*. **2018**, *7*, 1107.

Maminishkis, A., Chen, S., Jalickee, S., Banzon, T., Shi, G., Wang, F. E., Ehalt, T., Hammer, J. A., & Miller, S. S. Confluent monolayers of cultured human fetal retinal pigment epithelium exhibit morphology and physiology of native tissue. *Inv. Ophthalmol. Vis. Sci.* **2006**, *47*(8), 3612–3624.

Maruotti, J., Sripathi, S. R., Bharti, K., Fuller, J., Wahlin, K. J., Ranganathan, V., Sluch, V. M., Berlinicke, C. A., Davis, J., Kim, C., Zhao, L., Wan, J., Qian, J., Corneo, B., Temple, S., Dubey, R., Olenyuk, B. Z., Bhutto, I., Lutty, G. A., & Zack, D. J. Small-molecule-directed, efficient generation of retinal pigment epithelium from human pluripotent stem cells. *Pro. Nat Acad. USA.* **2015***, 112*(35), 10950–10955.

Masgras, I., Ciscato, F., Brunati, A. M., Tibaldi, E., Indraccolo, S., Curtarello, M., Chiara, F., Cannino, G., Papaleo, E., Lambrughi, M., Guzzo, G., Gambalunga, A., Pizzi, M., Guzzardo, V., Rugge, M., Vuljan, S. E., Calabrese, F., Bernardi, P., & Rasola, A. Absence of Neurofibromin Induces an Oncogenic Metabolic Switch via Mitochondrial ERK-Mediated Phosphorylation of the Chaperone TRAP1. *Cell Rep.* **2017a**, *18*, 659–672.

Masgras, I.; Laquatra, C.; Cannino, G.; Serapian, S.A.; Colombo, G. & Rasola, A. The Molecular Chaperone TRAP1 in Cancer: From the Basics of Biology to Pharmacological Targeting. *Semin. Cancer Biol.* **2021**, *76*, 45-53.

Masgras, I.; Sanchez-Martin, C.; Colombo, G. & Rasola, A. The Chaperone TRAP1 As a Modulator of the Mitochondrial Adaptations in Cancer Cells. *Front. Oncol.* **2017b**, *7*, 58.

Matassa, D. S., Criscuolo, D., Avolio, R., Agliarulo, I., Sarnataro, D., Pacelli, C., Scrima, R., Colamatteo, A., Matarese, G., Capitanio, N., Landriscina, M., & Esposito, F. Regulation of mitochondrial complex III activity and assembly by TRAP1 in cancer cells. *Cancer Cell Int.* **2022**, *22(1)*, 402.

Matassa, D.S.; Agliarulo, I.; Avolio, R.; Landriscina, M. & Esposito, F. Trap1 Regulation of Cancer Metabolism: Dual Role as Oncogene or Tumor Suppressor. *Genes.* **2018**, *9*, 195.

Matassa, D. S., Amoroso, M. R., Agliarulo, I., Maddalena, F., Sisinni, L., Paladino, S., Romano, S., Romano, M. F., Sagar, V., Loreni, F., Landriscina, M., & Esposito, F. Translational Control in the Stress Adaptive Response of Cancer Cells: A Novel Role for the Heat Shock Protein TRAP1. *Cell Death Dis.* **2013**, *4*, 851.

May-Simera, H. L., Wan, Q., Jha, B. S., Hartford, J., Khristov, V., Dejene, R., Chang, J., Patnaik, S., Lu, Q., Banerjee, P., Silver, J., Insinna-Kettenhofen, C., Patel, D., Lotfi, M., Malicdan, M., Hotaling, N., Maminishkis, A., Sridharan, R., Brooks, B., Miyagishima, K. & Bharti, K. Primary Cilium-Mediated Retinal Pigment Epithelium Maturation Is Disrupted in Ciliopathy Patient Cells. *Cell Rep.* **2018**, *22*(1), 189–205.

McClellan, A. J., Xia, Y., Deutschbauer, A. M., Davis, R. W., Gerstein, M., & Frydman, J. Diverse cellular functions of the Hsp90 molecular chaperone uncovered using systems approaches. *Cell.* **2007**, *131*(1), 121–135.

Mehrzadi, S., Hemati, K., Reiter, R. J., & Hosseinzadeh, A. Mitochondrial dysfunction in age-related macular degeneration: melatonin as a potential treatment. *Exp. Opin. Therap. Targets*. **2020**, *24*(4), 359–378.

Mendes, H.F. & Cheetham, M.E. Pharmacological Manipulation of Gain-of-Function and Dominant-Negative Mechanisms in Rhodopsin Retinitis Pigmentosa. *Hum. Mol. Genet.* **2008**, *17*, 3043–3054.

Mettu, P. S., Allingham, M. J., & Cousins, S. W. Incomplete response to Anti-VEGF therapy in neovascular AMD: Exploring disease mechanisms and therapeutic opportunities. *Prog. Retin. Eye Res.* **2021**, *82*, 100906.

Minasyan L., Sreekumar P.G., Hinton D.R. & Kannan R. Protective Mechanisms of the Mitochondrial-Derived Peptide Humanin in Oxidative and Endoplasmic Reticulum Stress in RPE Cells. *Oxid. Med. Cell Longev*. **2017**, 1675230.

Mitchell, P., Liew, G., Gopinath, B., & Wong, T. Y. Age-related macular degeneration. *Lancet*. **2018**, *392*, 1147–1159.

Mitter, S. K., Song, C., Qi, X., Mao, H., Rao, H., Akin, D., Lewin, A., Grant, M., Dunn, W., Jr, Ding, J., Bowes Rickman, C., & Boulton, M. Dysregulated autophagy in the RPE is associated with increased susceptibility to oxidative stress and AMD. *Autophagy*. **2014**, *10*(11), 1989–2005.

Miyagishima, K. J., Sharma, R., Nimmagadda, M., Clore-Gronenborn, K., Qureshy, Z., Ortolan, D., Bose, D., Farnoodian, M., Zhang, C., Fausey, A., Sergeev, Y. V., Abu-Asab, M., Jun, B., Do, K. V., Kautzman Guerin, M. A., Calandria, J., George, A., Guan, B., Wan, Q., Sharp, R. C. & Bharti, K. AMPK modulation ameliorates dominant disease phenotypes of CTRP5 variant in retinal degeneration. *Commun. Biol.* **2021**, *4*(1), 1360.

Miyagishima, K. J., Wan, Q., Corneo, B., Sharma, R., Lotfi, M. R., Boles, N. C., Hua, F., Maminishkis, A., Zhang, C., Blenkinsop, T., Khristov, V., Jha, B. S., Memon, O. S., D'Souza, S., Temple, S., Miller, S. S., & Bharti, K. In Pursuit of Authenticity: Induced Pluripotent Stem Cell-Derived Retinal Pigment Epithelium for Clinical Applications. *Stem Cells Transl. Med.* **2016**, *5*(11), 1562–1574.

Miyazaki, T.; Neff, L.; Tanaka, S.; Horne, W.C. & Baron, R. Regulation of Cytochrome c Oxidase Activity by C-Src in Osteoclasts. *J. Cell Biol.* **2003**, *160*, 709–718.

Montesano, G.N.; Chirico, G.; Pirozzi, G.; Costantino, E.; Landriscina, M. & Esposito, F. Tumor necrosis factor-associated protein 1 (TRAP-1) protects cells from oxidative stress and apoptosis. *Stress.* **2007**, *10*, 342–350.

Mueller, E. E., Schaier, E., Brunner, S. M., Eder, W., Mayr, J. A., Egger, S. F., Nischler, C., Oberkofler, H., Reitsamer, H. A., Patsch, W., Sperl, W., & Kofler, B. Mitochondrial haplogroups and control region polymorphisms in age-related macular degeneration: a case-control study. *PloS one*. **2012**, *7*(2), 30874.

Munezero, D., Aliff, H., Salido, E., Saravanan, T., Sanzhaeva, U., Guan, T., & Ramamurthy, V. HSP90α is needed for the survival of rod photoreceptors and regulates the expression of rod PDE6 subunits. *J. Biol. Chem*. **2023**, *299*(6), 104809.

Nabi, I. R., Mathews, A. P., Cohen-Gould, L., Gundersen, D., & Rodriguez-Boulan, E. Immortalization of polarized rat retinal pigment epithelium. *J. Cell Sci.* **1993**, *104 (1)*, 37–49.

Nittala, M. G., Metlapally, R., Ip, M., Chakravarthy, U., Holz, F. G., Staurenghi, G., Waheed, N., Velaga, S. B., Lindenberg, S., Karamat, A., Koester, J., Ribeiro, R., & Sadda, S. Association of Pegcetacoplan With Progression of Incomplete Retinal Pigment Epithelium and Outer Retinal Atrophy in Age-Related Macular Degeneration: A Post Hoc Analysis of the FILLY Randomized Clinical Trial. *JAMA Ophtalmol.* **2022**. 1*40*(3), 243–249

Nordgaard C.L., Berg K.M., Kapphahn R.J., Reilly C., Feng X., Olsen T.W. & Ferrington D.A. Proteomics of the retinal pigment epithelium reveals altered protein expression at progressive stages of age-related macular degeneration. *Invest. Ophthalmol. Vis. Sci*. **2006**, *47*, 815–822

Nordgaard C.L., Karunadharma P.P., Feng X., Olsen T.W. &Ferrington D.A. Mitochondrial proteomics of the retinal pigment epithelium at progressive stages of age-related macular degeneration. *Inv. Ophthalmol. Vis. Sci*. **2008**, *49*, 2848–2855

Ogura, M.; Yamaki, J.; Homma, M.K. & Homma, Y. Mitochondrial C-Src Regulates Cell Survival through Phosphorylation of Respiratory Chain Components. *Biochem. J.* **2012**, *447*, 281–289.

Osakada, F., Ikeda, H., Sasai, Y., & Takahashi, M. Stepwise differentiation of pluripotent stem cells into retinal cells. *Nature Prot.* **2009**, *4*(6), 811–824.

Palladino, G., Notarangelo, T., Pannone, G., Piscazzi, A., Lamacchia, O., Sisinni, L., Spagnoletti, G., Toti, P., Santoro, A., Storto, G., Bufo, P., Cignarelli, M., Esposito, F., & Landriscina, M. TRAP1 regulates cell cycle and apoptosis in thyroid carcinoma cells. *Endocr. Relat. Cancer*. **2016**, *23(9)*, 699–709.

Panvini, A. R., Gvritishvili, A., Galvan, H., Nashine, S., Atilano, S. R., Kenney, M. C., & Tombran-Tink, J. Differential mitochondrial and cellular responses between H vs. J mtDNA haplogroup-containing human RPE transmitochondrial cybrid cells. *Exp. Eye Res.* **2022**, *219*, 109013.

Park K.H., Cozier F., Ong O.C. & Caprioli J. Induction of heat shock protein 72 protects retinal ganglion cells in a rat glaucoma model. *Inv. Ophthalmol. Vis. Sci*. **2001**, *42*, 1522–1530.

Parmar, V. M., Parmar, T., Arai, E., Perusek, L., & Maeda, A. A2E-associated cell death and inflammation in retinal pigmented epithelial cells from human induced pluripotent stem cells. *Stem cell Res*. **2018**, *27*, 95–104

Parodi, M. B., Iacono, P., & Da Pozzo, S. Anti-VEGF and Retinal Dystrophies. *Curr. Drug. Targets* **2020**, *21*(12), 1201–1207.

Peters, F., Ebner, L. J. A., Atac, D., Maggi, J., Berger, W., den Hollander, A. I., & Grimm, C. Regulation of ABCA1 by AMD-Associated Genetic Variants and Hypoxia in iPSC-RPE. *Int. J. Mol. Sci.* **2022**, *23*(6), 3194.

Pfau, M., Schmitz-Valckenberg, S., Ribeiro, R., Safaei, R., McKeown, A., Fleckenstein, M., & Holz, F. G. Association of complement C3 inhibitor pegcetacoplan with reduced photoreceptor degeneration beyond areas of geographic atrophy. *Sci. Rep.* **2022**, *12*(1), 17870.

Pfeffer, B. A., & Fliesler, S. J. Reassessing the suitability of ARPE-19 cells as a valid model of native RPE biology. *Exp. Eye Res.* **2022**, *219*, 109046.

Piri, N., Kwong, J. M., Gu, L., & Caprioli, J. Heat shock proteins in the retina: Focus on HSP70 and alpha crystallins in ganglion cell survival. *Prog. Ret. Eye Res.* **2016**, *52*, 22–46.

Pridgeon, J.W.; Olzmann, J.A.; Chin, L-S.S. & Li, L. PINK1 Protects against Oxidative Stress by Phosphorylating Mitochondrial Chaperone TRAP1. *PLoS Biol.* **2007**, *5*, 1494–1503.

Purushottam Dharaskar, S., Paithankar, K., Kanugovi Vijayavittal, A., Shabbir Kara, H., & Amere Subbarao, S. Mitochondrial chaperone, TRAP1 modulates mitochondrial dynamics and promotes tumor metastasis. *Mitochondrion*. **2020**, *54*, 92–101.

Quinn, P.M.J.; Moreira, P.I.; Ambrósio, A.F. & Alves, C.H. PINK1/PARKIN Signalling in Neurodegeneration and Neuroinflammation. *Acta Neuropathol. Commun.* **2020**, *8*, 189.

Ramos Rego, I., Santos Cruz, B., Ambrósio, A. F., & Alves, C. H. TRAP1 in Oxidative Stress and Neurodegeneration. *Antioxidants*. **2021**, *10(11)*.

Rasola, A. & Bernardi, P. The Mitochondrial Permeability Transition Pore and Its Involvement in Cell Death and in Disease Pathogenesis. *Apoptosis Int. J. Program. Cell Death.* **2007**, *12*, 815–833.

Rasola, A.; Neckers, L. & Picard, D. Mitochondrial Oxidative Phosphorylation TRAP(1)Ped in Tumor Cells. *Trends Cell Biol.* **2014**, *24*, 455–463.

Rottenberg H. & Hoek J.B. The path from mitochondrial ROS to aging runs through the mitochondrial permeability transition pore. *Aging Cell.* **2017**, *16*, 943–955.

Rub C., Wilkening A. & Voos W. Mitochondrial quality control by the Pink1/Parkin system. *Cell Tissue Res*. **2017**, *367*, 111–123.

Saini, J. S., Corneo, B., Miller, J. D., Kiehl, T. R., Wang, Q., Boles, N. C., Blenkinsop, T. A., Stern, J. H., & Temple, S. Nicotinamide Ameliorates Disease Phenotypes in a Human iPSC Model of Age-Related Macular Degeneration. *Cell stem cell*. **2017**, *20*(5), 635–647

Samuel, W., Jaworski, C., Postnikova, O. A., Kutty, R. K., Duncan, T., Tan, L. X., Poliakov, E., Lakkaraju, A., & Redmond, T. M. Appropriately differentiated ARPE-19 cells regain phenotype and gene expression profiles similar to those of native RPE cells. *Mol. Vis.* **2017**, *23*, 60–89.

Sanchez-Martin, C.; Moroni, E.; Ferraro, M.; Laquatra, C.; Cannino, G.; Masgras, I.; Negro, A.; Quadrelli, P.; Rasola, A. & Colombo, G. Rational Design of Allosteric and Selective Inhibitors of the Molecular Chaperone TRAP1. *Cell Rep.* **2020**, *31*, 107531.

Santarelli, M., Diplotti, L., Samassa, F., Veritti, D., Kuppermann, B. D., & Lanzetta, P. Advances in pharmacotherapy for wet age-related macular degeneration. *Exp. Opinion. Pharm.* **2015**, *16*(12), 1769–1781.

Schnichels, S., Hagemann, U., Januschowski, K., Hofmann, J., Bartz-Schmidt, K. U., Szurman, P., Spitzer, M. S., & Aisenbrey, S. Comparative toxicity and proliferation testing of aflibercept, bevacizumab and ranibizumab on different ocular cells. *British J. Ophthalm.* **2013**, *97*(7), 917–923.

Schnichels, S., Schultheiss, M., Hofmann, J., Szurman, P., Bartz-Schmidt, K. U., & Spitzer, M. S. Trichostatin A induces cell death at the concentration recommended to differentiate the RGC-5 cell line. *Neurochem. Inter.* **2012**, *60*(6), 581–591.

Sciacovelli, M.; Guzzo, G.; Morello, V.; Frezza, C.; Zheng, L.; Nannini, N.; Calabrese, F.; Laudiero, G.; Esposito, F. & Landriscina, M. The Mitochondrial Chaperone TRAP1 Promotes Neoplastic Growth by Inhibiting Succinate Dehydrogenase. *Cell Metab.* **2013**, *17*, 988–999.

Serapian, S.A.; Sanchez-Martín, C.; Moroni, E.; Rasola, A. & Colombo, G. Targeting the Mitochondrial Chaperone TRAP1: Strategies and Therapeutic Perspectives. *Trends Pharmacol. Sci.* **2021**, *42*, 566–576.

Sessa, C., Shapiro, G. I., Bhalla, K. N., Britten, C., Jacks, K. S., Mita, M., Papadimitrakopoulou, V., Pluard, T., Samuel, T. A., Akimov, M., Quadt, C., Fernandez-Ibarra, C., Lu, H., Bailey, S., Chica, S., & Banerji, U. First-in-human phase I dose-escalation study of the HSP90 inhibitor AUY922 in patients with advanced solid tumors. *Clinical Cancer Research.* **2013***, 19*(13), 3671–3680.

Sharma, R., Bose, D., Maminishkis, A., & Bharti, K. Retinal Pigment Epithelium Replacement Therapy for Age-Related Macular Degeneration: Are We There Yet?. *Annual Rev. Pharm. Toxicol.* **2020**, *60*, 553–572.

Sharma, R., Khristov, V., Rising, A., Jha, B. S., Dejene, R., Hotaling, N., Li, Y., Stoddard, J., Stankewicz, C., Wan, Q., Zhang, C., Campos, M. M., Miyagishima, K. J., McGaughey, D., Villasmil, R., Mattapallil, M., Stanzel, B., Qian, H., Wong, W., Chase, L. & Bharti, K. Clinical-grade stem cell-derived retinal pigment epithelium patch rescues retinal degeneration in rodents and pigs. *Sci. Transl. Med.* **2019**, *11*(475), 5580.

Shiau, A.K.; Harris, S.F.; Southworth, D.R. & Agard, D.A. Structural Analysis of E. Coli Hsp90 Reveals Dramatic Nucleotide-Dependent Conformational Rearrangements. *Cell.* **2006**, *127*, 329–340.

Siegelin, M.D. Inhibition of the Mitochondrial Hsp90 Chaperone Network: A Novel, Efficient Treatment Strategy for Cancer? *Cancer Lett.* **2013**, *333*, 133–146.

Sima, S. & Richter, K. Regulation of the Hsp90 System. *Biochim. Biophys. Acta. Mol. Cell Res.* **2018**, *1865*, 889–897.

Singh, D.; Arora, R.; Kaur, P.; Singh, B.; Mannan, R. & Arora, S. Overexpression of Hypoxia-Inducible Factor and Metabolic Pathways: Possible Targets of Cancer. *Cell Biosci.* **2017**, *7*, 1–9.

Smith, E. N., D'Antonio-Chronowska, A., Greenwald, W. W., Borja, V., Aguiar, L. R., Pogue, R., Matsui, H., Benaglio, P., Borooah, S., D'Antonio, M., Ayyagari, R., & Frazer, K. A. Human iPSC-Derived Retinal Pigment Epithelium: A Model System for Prioritizing and Functionally Characterizing Causal Variants at AMD Risk Loci. *Stem Cell Rep.* **2019***, 12*(6), 1342–1353.

Song, H. Y., Dunbar, J. D., Zhang, Y. X., Guo, D., & Donner, D. B. Identification of a protein with homology to hsp90 that binds the type 1 tumor necrosis factor receptor. *J. Biol. Chem*. **1995**, *270(8)*, 3574–3581.

Sonoda, S., Spee, C., Barron, E., Ryan, S. J., Kannan, R., & Hinton, D. R. A protocol for the culture and differentiation of highly polarized human retinal pigment epithelial cells. *Nature Protoc.* **2009**, *4(5)*, 662–673.

Sorkio, A., Hongisto, H., Kaarniranta, K., Uusitalo, H., Juuti-Uusitalo, K., & Skottman, H. Structure and barrier properties of human embryonic stem cell-derived retinal pigment epithelial cells are affected by extracellular matrix protein coating. *Tissue Eng.* **2014**, *20*(3-4), 622–634.

Spitzer, M. S., Mlynczak, T., Schultheiss, M., Rinker, K., Yoeruek, E., Petermeier, K., Januschowski, K., & Szurman, P. Preservative-free triamcinolone acetonide injectable suspension versus "traditional" triamcinolone preparations: impact of aggregate size on retinal biocompatibility. *Retina.* **2011**, *31*(10), 2050–2057.

Spitzer, M. S., Yoeruek, E., Sierra, A., Wallenfels-Thilo, B., Schraermeyer, U., Spitzer, B., Bartz-Schmidt, K. U., & Szurman, P. Comparative antiproliferative and cytotoxic profile of bevacizumab (Avastin), pegaptanib (Macugen) and ranibizumab (Lucentis) on different ocular cells. *Graefe Arch. Clin. Exp. Ophtalmol.* **2007***, 245*(12), 1837–1842.

Standing, A.S.I.; Hong, Y.; Paisan-Ruiz, C.; Omoyinmi, E.; Medlar, A.; Stanescu, H.; Kleta, R.; Rowcenzio, D.; Hawkins, P. & Lachmann, H. TRAP1 Chaperone Protein Mutations and Autoinflammation. *Life Sci. Alliance.* **2020**, *3*, 201900376.

Strunnikova, N. V., Maminishkis, A., Barb, J. J., Wang, F., Zhi, C., Sergeev, Y., Chen, W., Edwards, A. O., Stambolian, D., Abecasis, G., Swaroop, A., Munson, P. J., & Miller, S. S.. Transcriptome analysis and molecular signature of human retinal pigment epithelium. *Hum. Mol. Gen.* **2010**, *19*(12), 2468–2486.

Sung, N.; Lee, J.; Kim, J.H.; Chang, C.; Tsai, F.T. & Lee, S. 2.4 Å Resolution Crystal Structure of Human TRAP1NM, the Hsp90 Paralog in the Mitochondrial Matrix. *Acta Crystallogr.* **2016**, *72*, 904–911.

Süsskind, D., Hagemann, U., Schrader, M., Januschowski, K., Schnichels, S., & Aisenbrey, S. Toxic effects of melphalan, topotecan and carboplatin on retinal pigment epithelial cells. *Acta Ophthalm*. **2016**, *94*(5), 471–478.

Takamura, H.; Koyama, Y.; Matsuzaki, S.; Yamada, K.; Hattori, T.; Miyata, S.; Takemoto, K.; Tohyama, M. & Katayama, T. TRAP1 Controls Mitochondrial Fusion/Fission Balance through Drp1 and Mff Expression. *PLoS ONE.* **2012**, *7*, 51912.

Takemoto, K.; Miyata, S.; Takamura, H.; Katayama, T. & Tohyama, M. Mitochondrial TRAP1 Regulates the Unfolded Protein Response in the Endoplasmic Reticulum. *Neurochem. Int.* **2011**, *58*, 880–887.

Terluk M.R., Kapphahn R.J., Soukup L.M., Gong H., Gallardo C., Montezuma S.R. & Ferrington D.A. Investigating mitochondria as a target for treating age-related macular degeneration. *J. Neurosci.* **2015**, *35*, 7304–7311.

Tian, J., Ishibashi, K., & Handa, J. T. The expression of native and cultured RPE grown on different matrices. *Physiol. Gen.* **2004**, *17*(2), 170–182.

Toops, K. A., Tan, L. X., & Lakkaraju, A. A detailed three-step protocol for live imaging of intracellular traffic in polarized primary porcine RPE monolayers. *Exp. Eye Res.* **2014**, *124*, 74–85.

Tseng, W. A., Thein, T., Kinnunen, K., Lashkari, K., Gregory, M. S., D'Amore, P. A., & Ksander, B. R. NLRP3 inflammasome activation in retinal pigment epithelial cells by lysosomal destabilization: implications for age-related macular degeneration. *Inv. Ophthalm. Vis. Sci.* **2013**, *54*(1), 110–120.

Tso, A., Costa, B.L.D., Fehnel, A., Levi, S.R., Jenny, L.A., Ragi, S.D., Li, Y. & Quinn, P.M.J. Generation of Human iPSC-Derived Retinal Organoids for Assessment of AAV-Mediated Gene Delivery. In *Molecular and therapeutic strategies for Retinitis Pigmentosa. Methods in Molecular Biology: Humana Press*, New York, USA, **2022**, *2560*.

Tsujimoto, Y.; Shimizu, S. Role of the Mitochondrial Membrane Permeability Transition in Cell Death. *Apoptosis Int. J. Program. Cell Death.* **2007**, *12*, 835–840.

Verba, K.A.; Wang, R.Y.-R.; Arakawa, A.; Liu, Y.; Shirouzu, M.; Yokoyama, S. & Agard, D.A. Atomic structure of Hsp90-Cdc37-Cdk4 reveals that Hsp90 traps and stabilizes an unfolded kinase. *Science.* **2016**, *352*, 1542–1547.

Volobouеva, L.A.; Duan, M.; Ouyang, Y.; Emery, J.F.; Stoy, C. & Giffard, R.G. Overexpression of Mitochondrial Hsp70/Hsp75 Protects Astrocytes against Ischemic Injury in Vitro. *J. Cereb. Blood Flow Metab. Off. J. Int. Soc. Cereb. Blood Flow Metab.* **2008**, *28*, 1009–1016.

Wakakura, M., & Foulds, W. S. Heat shock response and thermal resistance in cultured human retinal pigment epithelium. Exp. Eye Res. **1993**, *56*(1), 17–24.

Wang A.L., Lukas T.J., Yuan M., Du N., Tso M.O. & Neufeld AH. Autophagy, exosomes and drusen formation in age-related macular degeneration. *Autophagy*. **2009**, *5*, 563–564.

Wang L., Cano M. & Handa J.T. p62 provides dual cytoprotection against oxidative stress in the retinal pigment epithelium. *Biochim. Biophys. Acta*. **2014**, *1843*, 1248–1258.

Wang, P., Xing, Y., Chen, C., Chen, Z., & Qian, Z. Advanced glycation end-product (AGE) induces apoptosis in human retinal ARPE-19 cells via promoting mitochondrial dysfunction and activating the Fas-FasL signaling. *Biosci. Biotech. Biochem.* **2016**, *80*(2), 250–256.

Wang, R.; Shao, F.; Liu, Z.; Zhang, J.; Wang, S.; Liu, J.; Liu, H.; Chen, H.; Liu, K. & Xia, M. The Hsp90 Inhibitor SNX-2112, Induces Apoptosis in Multidrug Resistant K562/ADR Cells through Suppression of Akt/NF-KB and Disruption of Mitochondria-Dependent Pathways. *Chem. Biol. Interact.* **2013**, *205*, 1–10.

Wang, Y.; Lin, J.; Chen, Q.Z.; Zhu, N.; Jiang, D.Q.; Li, M.X. & Wang, Y. Overexpression of Mitochondrial Hsp75 Protects Neural Stem Cells against Microglia-Derived Soluble Factor-Induced Neurotoxicity by Regulating Mitochondrial Permeability Transition Pore Opening in Vitro. *Int. J. Mol. Med.* **2015**, *36*, 1487–1496.

Westermann B. Mitochondrial fusion and fission in cell life and death. *Nat. Rev. Mol. Cell Biol*. **2010**, *11*, 872–884.

Wykoff, C. C., Rosenfeld, P. J., Waheed, N. K., Singh, R. P., Ronca, N., Slakter, J. S., Staurenghi, G., Monés, J., Baumal, C. R., Saroj, N., Metlapally, R., & Ribeiro, R. Characterizing New-Onset Exudation in the Randomized Phase 2 FILLY Trial of Complement Inhibitor Pegcetacoplan for Geographic Atrophy. *Ophthalm.* **2021**, *128*(9), 1325–1336.

Xiang, F.; Huang, Y.S.; Shi, X.H. & Zhang, Q. Mitochondrial Chaperone Tumour Necrosis Factor Receptor-Associated Protein 1 Protects Cardiomyocytes from Hypoxic Injury by Regulating Mitochondrial Permeability Transition Pore Opening. *FEBS J.* **2010**, *277*, 1929–1938.

Xiang, F.; Ma, S.; Lv, Y.; Zhang, D.; Song, H. & Huang, Y. Tumor Necrosis Factor Receptor-Associated Protein 1 Regulates Hypoxia-Induced Apoptosis through a Mitochondria-Dependent Pathway Mediated by Cytochrome c Oxidase Subunit II. *Burn. Trauma.* **2019**, *7*, 16.

Xiao, L., Hu, Q., Peng, Y., Zheng, K., Zhang, T., Yang, L., Wang, Z., Tang, W., Yu, J., Xiao, Q., Zhang, D., Zhang, W., He, C., Wu, D., Zheng, Y., & Liu, Y. TRAP1 suppresses oral squamous cell carcinoma progression by reducing oxidative phosphorylation metabolism of Cancer-associated fibroblasts. *BMC Cancer.* **2021**, *21(1)*.

Xie, S.; Wang, X.; Gan, S.; Tang, X.; Kang, X. & Zhu, S. The Mitochondrial Chaperone TRAP1 as a Candidate Target of Oncotherapy. *Front. Oncol.* **2021**, *10*, 585047.

Xu, L.; Volobouеva, L.A.; Ouyang, Y.B.; Emery, J.F.; Giffard, R.G.; Emery, J.F. & Giffard, R.G. Overexpression of Mitochondrial Hsp70/Hsp75 in Rat Brain Protects Mitochondria, Reduces Oxidative Stress, and Protects from Focal Ischemia. *J. Cereb. Blood Flow Metab.* **2009**, *29*, 365–374.

Xu, Y. T., Wang, Y., Chen, P., & Xu, H. F. Age-related maculopathy susceptibility 2 participates in the phagocytosis functions of the retinal pigment epithelium. *Int. J. Ophthalm.* **2012**, *5*(2), 125–132.

Yamaguchi, A.; Ishikawa, K.; Inoshita, T.; Shiba-Fukushima, K.; Saiki, S.; Hatano, T.; Mori, A.; Oji, Y.; Okuzumi, A. & Li, Y. Identifying Therapeutic Agents for Amelioration of Mitochondrial Clearance Disorder in Neurons of Familial Parkinson Disease. *Stem Cell Rep.* **2020**, *14*, 1060–1075.

Yang, J., Yang, K., Meng, X., Liu, P., Fu, Y., & Wang, Y. Silenced SNHG1 Inhibited Epithelial-Mesenchymal Transition and Inflammatory Response of ARPE-19 Cells Induced by High Glucose. *J. Inflamm. Res.* **2021**, *14*, 1563–1573.

Yao J., Jia L., Khan N., Lin C., Mitter S.K., Boulton M.E., Dunaief J.L., Klionsky D.J., Guan J.L., Thompson D.A. & Zacks D.N. Deletion of autophagy inducer RB1CC1 results in degeneration of the retinal pigment epithelium. *Autophagy*. **2015**, *11*, 939–953

Yoshida, S., Tsutsumi, S., Muhlebach, G., Sourbier, C., Lee, M. J., Lee, S., Vartholomaiou, E., Tatokoro, M., Beebe, K., Miyajima, N., Mohney, R. P., Chen, Y., Hasumi, H., Xu, W., Fukushima, H., Nakamura, K., Koga, F., Kihara, K., Trepel, J., Picard, D. & Neckers, L.

Molecular chaperone TRAP1 regulates a metabolic switch between mitochondrial respiration and aerobic glycolysis. *Proc. Natl. Acad. Sci.* **2013**, *110(17)*, 1604–1612.

Zhang, L.; Karsten, P.; Hamm, S.; Pogson, J.H.; Müller-Rischart, A.K.; Exner, N.; Haass, C.; Whitworth, A.J.; Winklhofer, K.F. & Schulz, J.B.TRAP1 rescues PINK1 loss-of-function phenotypes. *Hum. Mol. Genet.* **2013**, *22*, 2829–2841.

Zhang, L.; Liu, L.; Li, X.; Zhang, X.; Zhao, J.; Luo, Y.; Guo, X. & Zhao, T. TRAP1 Attenuates H9C2 Myocardial Cell Injury Induced by Extracellular Acidification via the Inhibition of MPTP Opening. *Int. J. Mol. Med.* **2020**, *46*, 663–674.

Zhang, M., Jiang, N., Chu, Y., Postnikova, O., Varghese, R., Horvath, A., Cheema, A. K., & Golestaneh, N. Dysregulated metabolic pathways in age-related macular degeneration. *Sci. Rep.* **2020**, *10*(1), 2464.

Zhang, P.; Lu, Y.; Yu, D.; Zhang, D. & Hu, W. TRAP1 Provides Protection Against Myocardial Ischemia-Reperfusion Injury by Ameliorating Mitochondrial Dysfunction. *Cell. Physiol. Biochem.* **2015**, *36*, 2072–2082.

Zhang, X., Zhong, Z., & Li, W. Downregulation of TRAP1 aggravates injury of H9c2 cardiomyocytes in a hyperglycemic state. *Exp. Ther. Med.* **2019**, *18(4)*, 2681–2686.

Zheng, T. & Zhang, Z. Activated Microglia Facilitate the Transmission of α-Synuclein in Parkinson's Disease. *Neurochem. Int.* **2021**, *148*, 105094.

Zhou, D.; Liu, Y.; Ye, J.; Ying, W.; Ogawa, L.S.; Inoue, T.; Tatsuta, N.; Wada, Y.; Koya, K. & Huang, Q. A Rat Retinal Damage Model Predicts for Potential Clinical Visual Disturbances Induced by Hsp90 Inhibitors. *Toxicol. Appl. Pharmacol.* **2013**, *273*, 401–409.

Zuehlke, A. & Johnson, J.L. Hsp90 and Co-Chaperones Twist the Functions of Diverse Client Proteins. *Biopolymers.* **2010**, *93*, 211–217.

7. Supplementary Material

7. Supplementary Material

7.1. Differentiation and Characterization of iRPE Cells

Detailed Protocol

Reagents

- hESC-grade Matrigel (Catalog number 354277; Corning, New York, USA);
- TrypLE select enzyme (Catalog number 12563029; Gibco, Waltham, USA);
- mTeSR1 (Catalog number 05850; STEMCELL Technologies, Vancouver, Canada);
- DMEM (Catalog number 11965; Invitrogen, Waltham, USA);
- F12 (Catalog number 111765; Invitrogen, Waltham, USA);
- DMEM/F12 (Catalog number 11330; Invitrogen, Waltham, USA);
- KO SR (Catalog number 10828; Invitrogen, Waltham, USA);
- B27, 50x (Catalog number 17504; Invitrogen, Waltham, USA);
- NEAA 100X (Catalog number 11140; Invitrogen, Waltham, USA);
- Glutamine 100X (Catalog number 25030; Invitrogen, Waltham, USA);
- Anti-Anti 100X (Catalog number 15240; Invitrogen, Waltham, USA);
- Nicotinamide (NIC) (Catalog number N3376; Sigma-Aldrich, St. Louis, USA);
  Note: NIC 1 M stock (100×; 1 mL in 100 mL): to 50 mL of cell culture water, add 6.1 g of NIC, filter sterilize. Keep at 4 °C for up to 1 month;
- Chetomin (CTM) (Catalog number C9623; Sigma-Aldrich, St. Louis, USA);
  Note: CTM 1 mM stock (20,000x; 5 µl in 100 mL): dilute 1 mg of CTM into 1.4 mL of cell culture-tested DMSO (Catalog number D2650; Sigma-Aldrich, St. Louis, USA). Aliquot and store at −80 °C. Note: After thawing, keep CTM aliquots at room temperature in desiccator for up to 1 week. It is also possible to freeze/thaw CTM at least two or three times without affecting its efficiency in driving RPE differentiation;
- β-mercaptoethanol (Catalog number M3148; Sigma-Aldrich, St. Louis, USA);
  Note: β-mercaptoethanol 1M stock can be prepared with sterile distilled water. Store it at room temperature for a couple of months. Do not attempt to filter-sterilize pure β-mercaptoethanol as it will dissolve materials out of the filter.

Medium Composition

RPE Differentiation Medium (RPE DM Medium)		
Medium and supplements	**Concentration**	**500 mL**
DMEM/F12	85% (vol/vol)	410 mL
KO SR	15% (vol/vol)	75 mL
Glutamine 100X	2 mM	5 mL
NEAA 100X	0.1 mM	5 mL
Anti-Anti 100X	1%	5 mL
β-mercaptoethanol (Stock: 14.3M)	0.1 mM	3.5 µL

RPE Medium		
Medium and supplements	**Concentration**	**500 mL**
DMEM	70 % (vol/vol)	335 mL
F12	30% (vol/vol)	150 mL
B27, 50x	2%	10 mL
Anti-Anti 100X	1%	5 mL

Experimental Procedures

Differentiation Day -5

- Remove the medium and add 500 µL of TrypLE express per well in 6-well plates (6 WP), incubate 5 min at 37 °C, collect the cells and add 6 ml of mTesR plus medium and count them.
- Centrifuge the cells at 300 xg during 5 min.
- Plate hiPSC cells at high density (20,000 cells per cm^2, i.e., 192,000 cells per well (6 WP)) on Matrigel.
- Culture cells in 2 ml mTesR plus medium with 2 µl of Y-27632 in 5% CO_2.

Differentiation Day -4

- Replace the medium by mTesR plus medium (without Y-27632).

Differentiation Day -2

- Replace the medium by mTesR plus medium (without Y-27632).

Differentiation Day 0

- Once cells reached the desired confluency (>80%, approximately 5 days, replace mTesR plus medium with RPE differentiation medium (RPE DM) (2 ml/6 WP).

Differentiation Day 1 (RPE differentiation induction with DM + NIC and CTM)

- Replace medium with RPE DM supplemented with 10 mM Nicotinamide (NIC) and 50 nM Chetomin (RPE DM + NIC + CTM).
- Change medium every day, adding fresh NIC and CTM.

Differentiation Day 14 (RPE Differentiation Induction with DM + NIC)

- Culture cells in RPE DM medium supplemented with 10mM NIC (RPE DM + NIC). Use 2 mL per well (6 WP).
- Feed cultures daily until day 28.

Differentiation Day 28 (Amplification and RPE Maturation with RPE Medium)

- Remove medium and add 1 mL of TrypLE select enzyme.
- Incubate for 12 min at 37 °C, 5% CO_2 until most cells look rounded.
- Vigorously dissociate cells in TrypLE select enzyme until most or all clumps have disappeared.

- Add 2 mL of **RPE medium** and transfer to 15 mL tube.
- Centrifuge, 130 ×g, for 5 min.
- Remove supernatant and resuspend cell solution in **RPE medium**.
- Filter through a 40-µm nylon mesh (BD Falcon) and count the cells.
- On dishes precoated with Matrigel, plate RPE cells at a density of 250–300,000 cells per cm^2 ($2.4x10^6$ – $2.9x10^6$ cells per well (6 WP)).

  Note: About one week after each passage, the polygonal cells formed a very tight, fully pigmented monolayer.

Differentiation Day 56 (Amplification and RPE Maturation with RPE Medium)

- Remove RPE medium and add 1 mL of TrypLE select enzyme.
- Incubate for 12 min at 37 °C, 5% CO_2 until most cells look rounded.
- Vigorously dissociate cells in TrypLE select enzyme until most or all clumps have disappeared.
- Add 2 mL of RPE medium and transfer to 15 mL tube.
- Centrifuge, 130 ×g, for 5 min.
- Remove supernatant and resuspend cell solution in RPE medium.
- Filter through a 40-µm nylon mesh (BD Falcon) and count the cells.
- On dishes precoated with Matrigel, plate RPE cells at a density of 100,000 cells per cm^2 ($1x10^6$ cells per well (6 WP)).

Differentiation Day 84 (Harvest)

- Harvest and/or cryopreserve the cells.